

Development of Dissipative Supramolecular Materials - From Concept to Application

Caren Wanzke

Vollständiger Abdruck der von der Fakultät für Chemie der Technischen Universität München zur Erlangung des akademischen Grades eines

Doktors der Naturwissenschaften (Dr. rer. nat.)

genehmigten Dissertation.

Vorsitzender: Prof. Dr. Matthias Feige
Prüfer der Dissertation: 1. Prof. Dr. Job Boekhoven
2. Prof. Dr. Oliver Lieleg
3. Prof. Dr. Max von Delius

Die Dissertation wurde am 12.03.2020 bei der Technischen Universität München eingereicht und durch die Fakultät für Chemie am 12.05.2020 angenommen.

" Es war einmal, (what) vor etlichen Jahren
Ein Typ, der in Harvard Professor war, namens Edward Clarke (yeah)
Und wie es damals üblich war, trug er ein swaggy Bart
Et cetera, et cetera auf jeden Fall schrieb er einen Bestseller (aha)
Und der war sowas wie sein Lebenswerk
Für die damals junge Emanzipation, sowas wie die Gegenwehr
Denn in dem ganzen Buch, sagte er lediglich
Die Frau sollte nicht studieren, weil es für sie schädlich ist (aha)
Denn dafür, so viele Informationen aufzunehmen (what)
Sei das weibliche Gehirn einfach nicht ausgelegt (aha)
Und außerdem, Frauen die zu viel denken
Würden dadurch nur ihr Blut verschwenden (aha)
Und so ihre Gebärmutter zerstören
Mädchen könnten entweder lernen oder Mutter werden (yeah)
Frauen mit Kinderwunsch
Stellen ihre kognitive Leistung also lieber in den Hintergrund (sheesh)
Nur nicht so kompliziert denken und so (aha)
Vor allem nicht während der Menstruation
Von diesem Buch hat er eine Menge verkauft
Noch lange nach seinem Tod haben ihm die Menschen geglaubt (yo) "

Fatoni

Abstract

Dissipative or out-of-equilibrium supramolecular self-assembly is a new strategy to design novel materials. Inspired by nature, where a diversity of assembled structures is found in energy dissipating states, scientists try to adapt this concept and generate functional supramolecular materials with the sophistication and complexity of biological materials. The main strategy towards this concept is to develop a supramolecular assembly process that function exclusively under the input of energy. That means, a precursor molecule is activated by a chemical fuel and the yielded product is able to self-assemble. The product is designed to be intrinsically unstable and spontaneously revert to its precursor state. Consequently, the assemblies emerge in response to chemical energy and without energy the self-assembled structure decays. The overall aim of this thesis is to create new self-assembled structures based on out-of-equilibrium self-assembly. More specifically, the aim was to study the assembly's unique properties and design relevant materials around these assemblies.

Materials like vesicles, colloids, or emulsions are from particular interest because they create compartments that can be used to enrich or encapsulate a molecular payload. Using peptide-based precursors and an acid-anhydride-based reaction cycle, vesicles (Chapter 4) and colloids (Chapter 5) could be realized. The colloids serve as a hydrophobic pocket, protect the product species, as well as accumulate hydrophobic material. Excitingly, the kinetics of the deactivation reaction change from first- to zero-order. This new mechanism is particularly interesting and could successfully implemented in emulsions (Chapter 6). For the emulsions, simple aliphatic-based precursors are used that self-assemble upon fuel addition. As soon as oil droplets are formed, the kinetics of the deactivation change to a zero-order decay. In these droplets, hydrophobic drugs were encapsulated. Due to the zero-order kinetics and linear shrinkage of the droplet volume, the drug is release with a constant rate.

Simplifying the system can result in an interesting drug delivery vehicle since systems with zero-order release profiles are highly desirable in the pharmaceutical industry.

Zusammenfassung

Dissipative, supramolekulare Selbstassemblierung ist eine neue Strategie, um innovative Materialien zu designen. Inspiriert von der Natur, in der viele Strukturen im dissipativen, selbstassemblierten Zustand zu finden sind, versuchen Wissenschaftler dieses Konzept zu adaptieren, um funktionale, supramolekulare Materialien zu generieren. Eine Hauptstrategie ist einen supramolekularen Assemblierungsprozess zu entwickeln, der exklusiv unter Energiezugabe funktioniert. Das bedeutet, ein Edukt wird durch einen chemischen Treibstoff aktiviert und das erhaltene Produkt ist in der Lage zu assemblieren. Das Produkt ist dabei intrinsisch instabil und fällt spontan zurück in seinen Ausgangszustand, dem Edukt. Die assemblierten Strukturen sind also direkt an die Zufuhr von chemischer Energie gekoppelt und zerfallen ohne diese. Das Hauptziel dieser Arbeit ist neue selbstassemblierte Materialien basierend auf diesem Konzept zu kreieren. Im Speziellen ist das Ziel die neuartigen Eigenschaften der Materialien zu studieren und in relevanten Anwendungsbereichen einzusetzen.

Vesikel, Kolloide oder Emulsionen sind als Strukturen besonders interessant. Sie bilden Kompartimente aus, die verwendet werden können, um molekulare Ladungen anzureichern oder einzuschließen. Unter Verwendung von Peptid-basierten Edukten und einem Säure-Anhydride Reaktionszyklus können Vesikel (Kapitel 4) und Kolloide (Kapitel 5) realisiert werden. Kolloide, als hydrophobe Kompartimente, können die Produkt-Spezies beschützen und hydrophobe Moleküle anreichern. Außerdem verändert sich dabei die Kinetik der Rückreaktion von erster zu nullter Ordnung. Dieser interessante, neue Mechanismus konnte auch erfolgreich in Emulsionen implementiert werden (Kapitel 6). Diese Emulsionen werden aus einfachen aliphatischen Molekülen durch Zufuhr chemischer Energie gebildet. Durch Bildung der hydrophoben Öl-Tröpfchen entsteht ebenfalls eine Reaktionskinetik nullter Ordnung. In dieser hydrophoben Matrix werden hydrophobe Medikamente eingeschlossen. Aufgrund der neuen Reaktionskinetik und der darauffolgenden gleichmäßigen Verringerung des Tröpfchen Volumens werden diese Medikamente mit konstanter Geschwindigkeit freigesetzt.

Eine vereinfachte Version dieses Systems kann für die pharmazeutische Industrie interessant sein, da dort therapeutische Systeme mit kontrollierter Wirkstoffabgabe sehr erwünscht sind.

Abbreviations

| | |
|---------------|--|
| A | Alanine |
| AA | Acrylic acid |
| Am | Acrylamide |
| Ag | Silver |
| Au | Gold |
| a.u. | arbitrary units |
| ADP | Adenosine diphosphate |
| AMP | Adenosine monophosphate |
| ATP | Adenosine triphosphate |
| BCS | biopharmaceutics classification system |
| CAC | Critical aggregation concentration |
| D | Aspartic acid |
| DBC | dibenzoyl-(L)-cystine |
| DMS | Dimethyl sulfate |
| DSA | dissipative self-assembly |
| E | Glutamic acid |
| e.e. | enantiomeric excess |
| EDC | 1-Ethyl-3-(3-dimethylaminopropyl) carbodiimide |
| e.g. | exempli gratia, for example |
| et al. | et alii/aliae, and others |
| F | Phenylalanine |
| Fmoc | Fluoren-9-ylmethoxycarbonyl |
| G | Glycine |
| GTP | Guanosine triphosphate |
| GDP | Guanosine diphosphate |
| HIV | human immunodeficiency viruses |
| HPLC | high pressure liquid chromatography |
| hr | hour |
| i.e. | id est, that is |
| L | Leucine |
| LCD | liquid-crystal display |
| min | minute |

| | |
|----------------------|-----------------------|
| Nap | naphthoxyacetyl |
| PEG | Polyethylene glycol |
| P_i | Orthophosphate |
| PKA | protein kinase A |
| λPP | λ-protein phosphatase |
| R | Arginine |
| S | Serine |
| sCT | Salomon calcitonin |
| TA | Tannic acid |
| TFA | Trifluoroacetic acid |
| UV | ultraviolet |
| V | Valine |
| Vis | visible |
| Y | Tyrosine |

| | | |
|------------|---|------------|
| 1. | Molecular Self-Assembly | 1 |
| | 1.1 Energy Landscapes | 3 |
| | 1.1.1 In-Equilibrium Self-Assembly | 3 |
| | 1.1.2 Out-of-Equilibrium Self-Assembly | 4 |
| | 1.1.3 Dissipative Out-of-Equilibrium Self-Assembly | 5 |
| | 1.2 Man-Made Reaction Cycles | 7 |
| | 1.2.1 Methylation | 7 |
| | 1.2.2 Phosphorylation | 8 |
| | 1.2.3 Acid-Anhydride Chemistry | 9 |
| | 1.3 Outlook | 11 |
| 2. | Materials Formed by Dissipative Self-Assembly | 12 |
| | 2.1 Transient Supramolecular Materials | 13 |
| | 2.1.1 Self-Erasing Inks..... | 15 |
| | 2.1.2 Catalytic Reaction Control | 17 |
| | 2.1.3 Transient Hydrogels..... | 20 |
| | 2.1.4 Dissipative Materials for Controlled Release | 24 |
| | 2.2 Controlled Drug Delivery | 28 |
| | 2.3 Outlook | 32 |
| 3. | Aims of the Thesis | 33 |
| 4. | Dynamic Vesicles Formed by Dissipative Self-Assembly | 35 |
| 5. | Dissipative Assemblies that Inhibit Their Deactivation | 55 |
| 6. | Active Droplets in a Hydrogel Release Drugs with a Constant and Tunable Rate | 74 |
| 7. | Conclusion and Outlook | 92 |
| 8. | Materials and Methods | 94 |
| 9. | Further Publications | 101 |
| 10. | Acknowledgments | 103 |
| 11. | References | 105 |

1. Molecular Self-Assembly

'Is anything not self-assembly?',

a bold question that was asked by Whiteside and Grzybowski in their *Science Viewpoint* in 2002. Until today, there is no concrete definition of the term 'self-assembly' but the authors suggest that the term is limited to processes with pre-existing components, that are reversible and can be controlled by the design of components.^[1] Above all, self-assembly describes a process by which isolated components organize spontaneously and autonomously in an ordered structure without any human interaction.^[2-3] In general, this process is not limited to molecules but can occur with components of any size in an appropriate environment, ranging from molecules to galaxies.^[4-5] However, the basic concepts were developed with molecules and the assembling process is best understood and highly developed in this area.^[4]

Molecular self-assembly is a result of molecules that interact with each other with generally weak and non-covalent interactions. Typical examples are van der Waals or Coulomb interactions, and, hydrophobic interactions or hydrogen bonds, as well as relatively weak covalent bonds like coordination bonds.^[4, 6-7] Importantly, the interaction leads from a less ordered state to a final more ordered state, *e.g.*, a crystal structure. Another key aspect is the reversibility of the system. The components need the possibility to adjust their position within the generated self-assembled structure. That means, the forces for disruption should be comparable to the strength of the interaction. The environment of the components has also a strong influence on the process since the molecules need to be mobile to assemble with another. In solution, the major part of that mobility is provided by thermal motion.^[1, 4]

With these conceptual insights in the process, one of the remaining questions is: 'Why should we be interested in self-assembled systems?'. Molecular self-assembly is omnipresent in various fields, *e.g.*, chemistry, material science, or biology. Peering in biology and life itself, lipid bilayers,^[8] folding of polypeptide chains into proteins,^[9] or folding of nucleic acids into their functional forms^[10] are just a few examples of complex

self-assembled structures.^[11] That shows, molecular self-assembly has been there long before it developed in a main topic of scientific interest.^[12] In nature, an exceptional diversity of structure and function is found in self-assembled systems that can be used flexible, efficient, and dynamic.^[12-13] If we want to adapt this complexity for new smart materials and nanotechnology, or if we want to understand life, understanding molecular self-assembly is required.^[1]

The main focus in the following sections is on different types of self-assembly according to their energy landscapes, from in-equilibrium to dissipative non-equilibrium self-assembly. Furthermore, I discuss various approaches to create synthetic man-made reaction cycles that try to mimic biological behavior.

1.1 Energy Landscapes

Molecular self-assembly can occur through several processes based on thermodynamic and kinetic stability of molecules, building blocks, or the self-assembled state itself. A comparison of their thermodynamic and kinetic properties, as well as their energy landscapes of the Gibbs free energy, helps to understand the differences between possible types of self-assembly. The main classes that can be observed are in-equilibrium that is controlled thermodynamically and kinetically controlled out-of-equilibrium self-assembly. Furthermore, the latter can be divided in kinetically trapped or metastable states, and dissipative out-of-equilibrium.^[14-17]

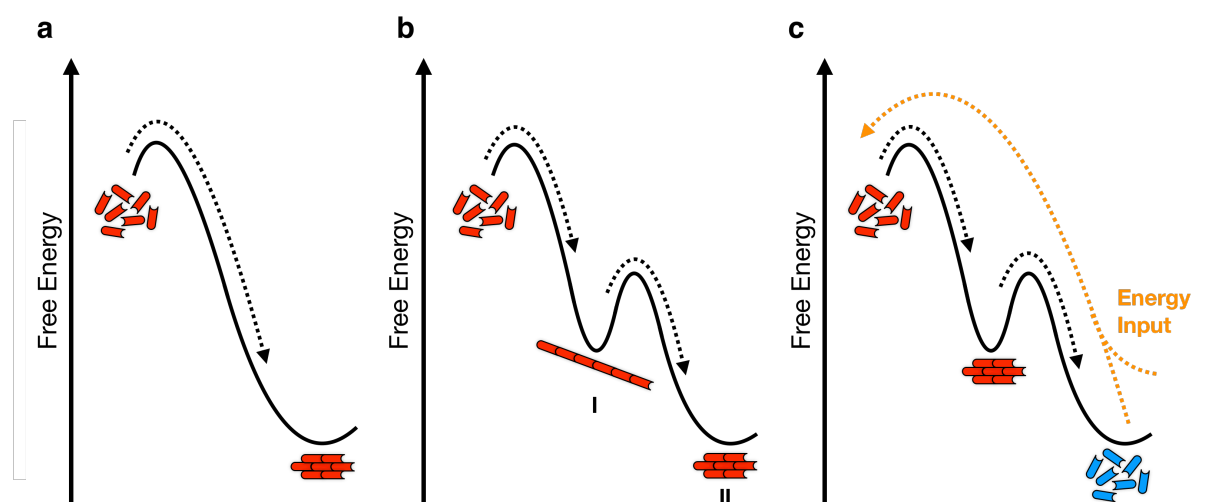


Figure 1: Schematic free energy landscape of different self-assembly processes. **a)** In-equilibrium; **b)** Out-of-equilibrium kinetically trapped (I) and metastable (II); **c)** Dissipative out-of-equilibrium self-assembly.

Details of the energy landscapes depicted in figure 1 are described in the following sections with a focus on the concept of dissipative out-of-equilibrium self-assembly.

1.1.1 In-Equilibrium Self-Assembly

Characteristic of in-equilibrium self-assembly is that the self-assembled structure resides in the global minimum of the energy landscape (Figure 1a). The unassembled building block is in a state that is endowed with more free energy.^[4] Thus, the assembly process is linked to a gain in free energy which is thermodynamically favored. Reversibility plays an important role as well since self-assembled building blocks need to be able to exchange with those that are in solution. The exchange occurs with equal

rates such that there is no net flow of energy, *i.e.*, the assembly is in equilibrium with its environment.^[14] The exchange of building blocks with its environment allows for a dynamic system that can self-correct to find the energetic minima and therefore, the thermodynamically most-favored state.^[13, 17] The rate of exchange between the two states is directly connected to the strength of the dominating non-covalent interaction. For example, small spherical micelles have relatively weak interactions so that the dynamics of the system are high and the exchange rates are fast.^[18] In comparison, the bilayer of phospholipids is cohered by stronger non-covalent interactions resulting in lower dynamics and exchange rates that are orders of magnitude slower.^[8, 11, 19] Self-assembly in equilibrium has been studied extensively and there are countless examples of published man-made materials that are well-understood and tunable within every detail.^[20-22] That is one reason why self-assembled supramolecular materials are already popular and commonly used in the industry.^[23-24]

1.1.2 Out-of-Equilibrium Self-Assembly

Out-of-equilibrium self-assembly occurs when the structure resides higher in the energy landscape not in the global but a local minimum (Figure 1b). Reaching the thermodynamic global minimum would be still favored. That leads to two possible scenarios, *i.e.*, kinetically trapped assemblies or metastable assemblies. Their difference is in height of the activation barrier between the local minimum in which the assembly resides and the global minimum.^[14-15]

In the kinetically trapped assemblies, the self-assembled structure remains in the local minimum, because the activation barrier is too high to transition to the global minimum (Figure 1b, state I). In other words, the building blocks are not able to exchange with the surrounding environment and can thus not reach the global minimum. The structures are kinetically trapped and have an infinite lifetime in this state. The second pathway results in a so-called metastable state (Figure 1b, state II). Here, the energy barrier is relatively low, so that building blocks can exchange with the surrounding. They can slowly convert to the thermodynamic state at the global minimum. The local minimum is an intermediate step with a finite lifetime and is thus metastable. Within the minimum, the system has really low dynamics and slow to no exchange rates which means this state is thermodynamically out-of-equilibrium.^[16, 25]

1.1.3 Dissipative Out-of-Equilibrium Self-Assembly

The final class of self-assembly, I discuss, is dissipative self-assembly (DSA) and the focus of this thesis. Dissipative self-assembly is also a process that occurs out-of-equilibrium. In this process, the global thermodynamic minimum is represented by a precursor (Figure 1c, blue) that does not assemble. In an irreversible chemical reaction, this precursor can react with a fuel to be converted to an activated building block for the assembly. That building block has absorbed energy from the chemical fuel and is thus represented by a local minimum higher in the energy landscape. From that position, the activated building block can self-assemble since the assembled structure is in a lower local minimum of the free energy landscape. However, the self-assembled structures are thermodynamically labile, and this state is thus an out-of-equilibrium state. A second irreversible chemical reaction reverts the building blocks to their original state in the global minimum. In this step, the energy that the building block gains in the first reaction is dissipated in the environment. If the energy input is constant, the self-assembled state can be maintained in a steady-state, but the system continuously absorbs and dissipates energy. Stopping the energy influx results in the complete disassembly of the structure.^[14-15, 26]

The concept of dissipative self-assembly plays a central role in biology and life, *e.g.*, in bacteria swarms, or the replication of the cell components and the following assembly into another cell during mitosis. Life is a dynamic process: If the energy influx stops, the cell dies.^[1, 27] Actin filaments, histones, and chromatin, protein aggregates in signaling pathways as well as microtubules are just a few examples of critical structures that use dissipative self-assembly.^[11, 19, 28-30] These dynamic materials have unique properties and are made to possess specific functions. Especially interesting, besides the possibility to control them in space and time, is that they can adapt towards environmental changes. For example, if the chemical reaction cycle remains intact the assemblies can repair themselves after externally applied damage.^[14]

Nature has always been an inspiration for scientists and, since most synthetic materials function in equilibrium,^[22] studying dissipative out-of-equilibrium analogs opens up new strategies to unique materials. Synthetic approaches towards self-assembled structures coupled to reaction cycles have indeed been made.^[14, 31] In these minimalist designs, a non-assembling precursor becomes activated using a fuel

(Figure 2). That activated product is designed to assemble after reaching a critical aggregation concentration (CAC), *i.e.*, the self-assembly process cannot proceed below this threshold concentration of the product. Importantly, the product and thus the self-assembled structure is inherently unstable such that it reverts to its original precursor state in a deactivation reaction. The deactivation can be caused by a reaction with an abundant species or spontaneously through energy dissipation to the environment.^[32-33]

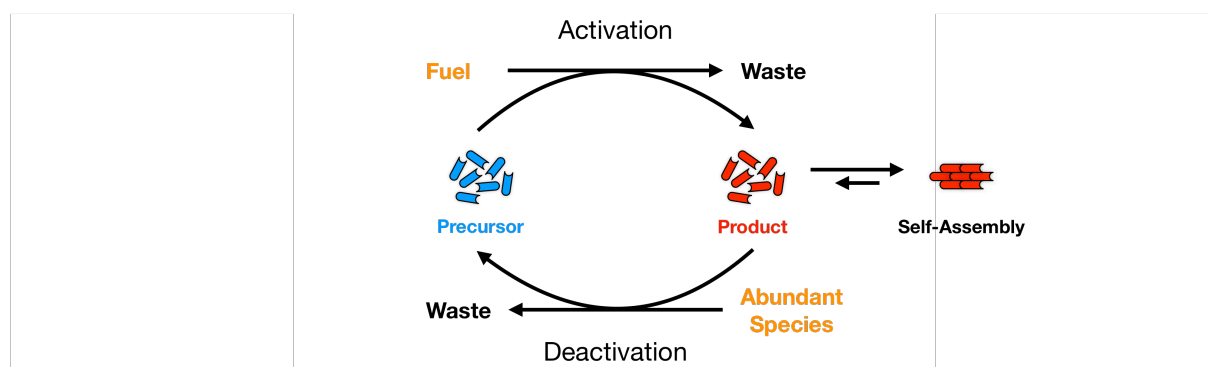


Figure 2: Schematic reaction cycle coupled to a self-assembly process.

While the focus of this thesis is on dissipative self-assembly driven by chemical fuels, light can also be used as an energy source. To that extent, UV-light was successfully used in many dissipative systems, *e.g.*, gelators^[34] or the assembly of nanoparticles.^[35] Commonly used is the UV-induced isomerization of *trans*-azobenzene derivatives to the instable *cis*-form. Over time, the *cis*-form reverted to the more stable *trans*-form by thermal relaxation. The UV-induced activation and spontaneous deactivation both generate no waste molecules, *i.e.*, in the back reaction all dissipated energy is released in the form of heat. That offers a great advantage compared to the chemically fueled system because many dissipative cycles can be performed and no waste accumulates.^[36] In chapter 2.1.1 I discuss a detailed example. Another category that I discuss in more detail is fuel-driven chemical reaction networks. Here, a high-energy molecule is used to activate the precursor while producing a waste product. That waste product tends to accumulate in the reaction mixture and can also result in failure of the dissipative system.^[37-38] In the next section, I highlight several types of reactions that have been used to create diverse chemical reaction networks that can induce dissipative self-assembly.

1.2 Man-Made Reaction Cycles

The prerequisites for a synthetic chemical reaction cycles that can drive DSA are rather stringent which could explain why examples remain relatively rare. For example, the activation and deactivation have to take place in the same environment and under the same conditions, so external influences like temperature or solvent cannot be changed. Furthermore, both reactions should work with independent and irreversible pathways. Additionally, interactions between the different reagents of the reactions should be avoided to eliminate possible background reactions.^[14, 31] Despite these concrete requirements, researchers were able to find functioning chemical reaction cycles. I will review three exemplary cycles that are based on different chemical reactions in the next section.

1.2.1 Methylation

The first example of a chemically fueled reaction cycle designed to drive dissipative self-assembly was published by van Esch, Eelkema and coworkers.^[32] A methylating agent as a fuel in the activation reaction to convert carboxylate precursors to their corresponding methyl esters. The energy dissipating or deactivation reaction is an alkaline hydrolysis that occurs spontaneously in water and is leading to the acid precursor (Figure 3).

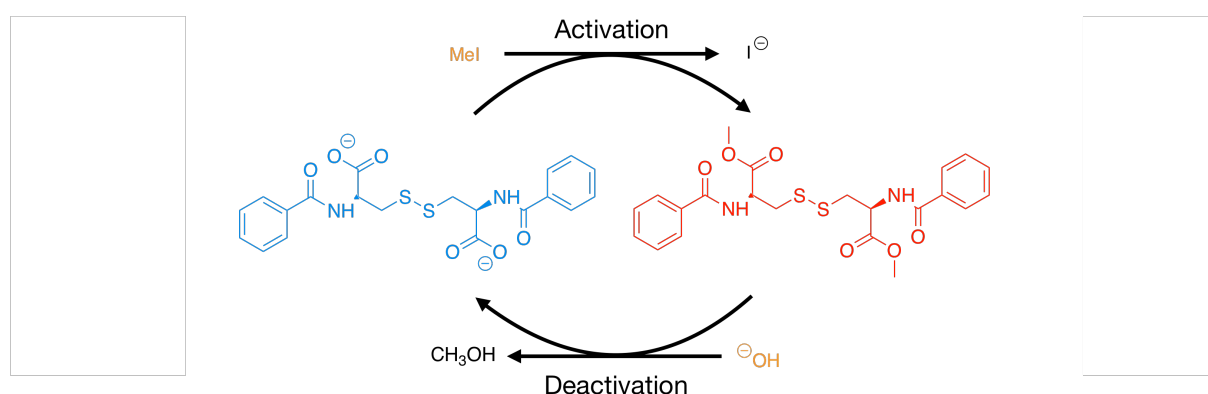


Figure 3: Schematic representation of the reaction cycle. DBC (blue) reacts with two MeI (orange) in the activation reaction to the corresponding dimethyl ester (red) and two iodide. The deactivation reaction occurs spontaneously within the alkaline environment producing methanol as waste.

The precursor in the reaction cycle is based on dibenzoyl-(L)-cystine (DBC, figure 3, blue), which is known to be a pH-responsive self-assembler.^[39] In contrast, the esters

of DBC showed self-assembling behavior independent of the pH,^[40] which gave the idea to combine the soluble DBC with an esterification reaction to induce a self-assembly process. Indeed, in a pH-stat setup at pH 7 and 35 °C, the methylation with the alkylation agent methyl iodide (MeI) was sufficiently fast to create a self-assembled gel. The abolishment of the two negative charges and thus, the increased hydrophobicity of the product (Figure 3, red) was the major driving force of the assembly. Furthermore, intermolecular hydrogen-bonding stabilized fiber formation. The alkaline hydrolysis was slower than the formation reaction which is an important requirement to accumulate sufficient product for self-assembly. As the fuel was depleting, the hydrolysis rate was higher than the esterification rate and resulted in a total recovery of the DBC, as well as the complete disassembly of the structure after 350 hours. Excitingly, the gelation could be repeated by adding another batch of fuel.^[32]

1.2.2 Phosphorylation

Hermans *et al.* used a biocatalytic approach to design chemical reaction cycles. Supramolecular polymers were built from a symmetric peptide derivative as a precursor. Adenosine triphosphate (ATP) as a fuel and the enzyme protein kinase A (PKA) were used to phosphorylate the peptide, creating adenosine diphosphate (ADP) as side product. In an aqueous solution, another enzyme, λ -protein phosphatase (λ PP), catalyzes the deactivation to the precursor producing two equivalents of orthophosphate (P_i) (Figure 4).^[41]

The symmetric peptide derivative (PDI, figure 4, blue) is based on 3,4,9,10-perylenediimide with the consensus sequence LRRASL (L: Leucine, R: Arginine, A: Alanine, S: Serine) for PKA. Perylenediimide derivatives are known to self-assemble due to aromatic stacking interactions, the hydrophobic effect and electrostatic interactions.^[42-43] The precursor PDI can be phosphorylated on both serine residues resulting in p-PDI first and then in p2-PDI (Figure 4, red). The dynamic phosphorylation and dephosphorylation of serine is ubiquitously present in living systems, *e.g.*, to control chromatin structures or signal transduction and was already successfully implemented in the design of artificial systems.^[44-46] The introduction of two phosphate groups reduced the overall charge of the molecule and resulted in an almost zwitterionic p2-PDI which impacted the supramolecular polymer structure. Important for this dissipative cycle is that the species (Figure 4) are not in chemical equilibrium.

The activation and deactivation reactions are possible through the enzyme-catalyzed reactions which are two different chemical pathways. The terminal triethylene glycol groups assure water solubility and increase the accessibility of the target sides for the enzymes. PDI and p2-PDI are both self-assembling into supramolecular polymers but with different chirality. With the described reaction network, the group was able to switch the polymers and their chirality for a defined time period by adding a batch of fuel. Moreover, they showed a first continuously fueled example with non-equilibrium steady states. The state of the mole fractions of the different species was sustained in a continuous stirred tank reactor by a constant influx of fuel.^[41]

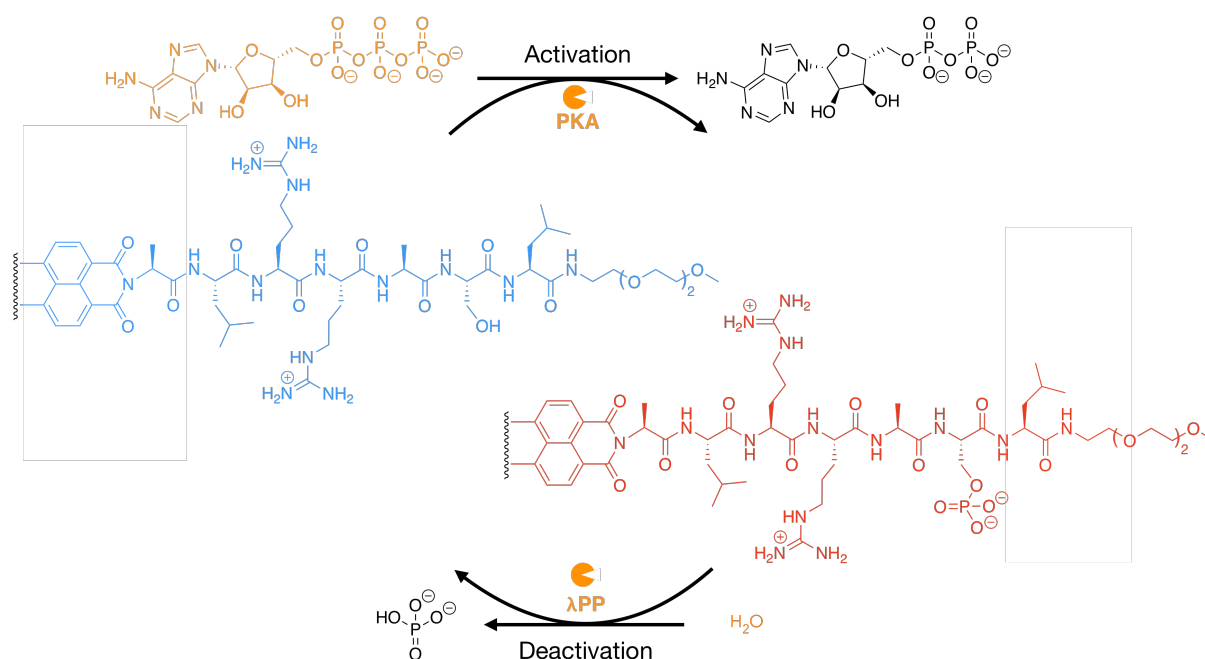


Figure 4: Schematic representation of the reaction cycle. PDI (blue, depicted half) reacts with PKA and two ATP (orange) in an enzyme-catalyzed activation reaction to p2-PDI (red) and two ADP molecules as waste. The deactivation is as well an enzyme-catalyzed reaction with λPP and water back to the precursor and two orthophosphate molecules as waste.

1.2.3 Acid-Anhydride Chemistry

The last reaction network I mention is based on acid-anhydride chemistry and was first shown by Boekhoven *et al.*^[47] and Hartley *et al.*^[48] An carboxylic acid-based precursor is condensed to its corresponding anhydride by a carbodiimide. Since the anhydride is intrinsically unstable in an aqueous solution it spontaneously hydrolysis to the acid precursor (Figure 5).

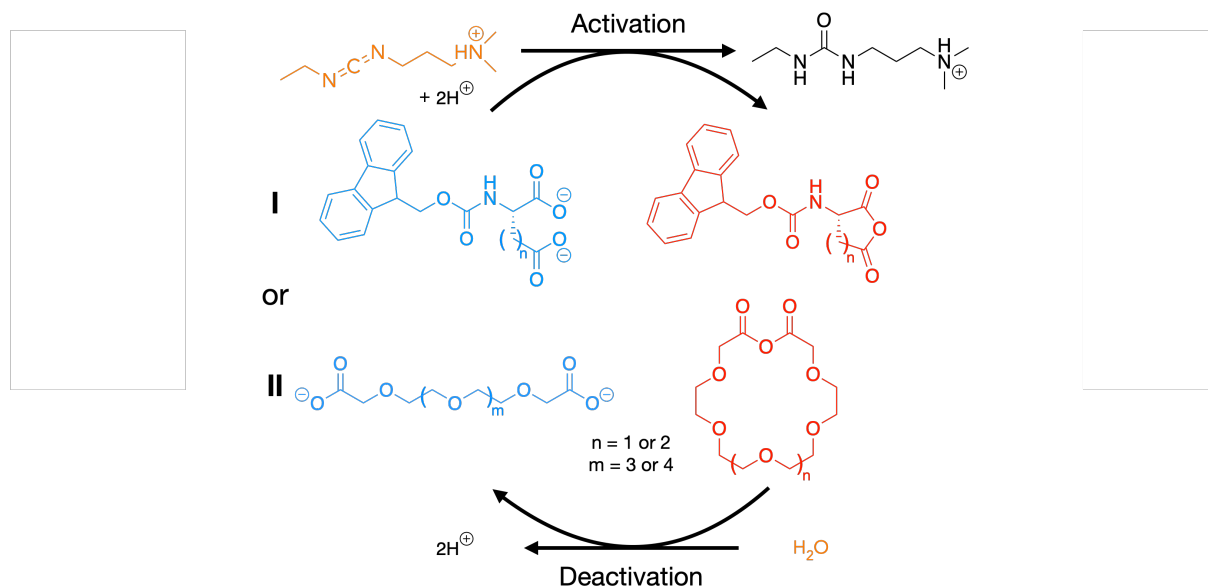


Figure 5: Schematic representation of the acid-anhydride-based reaction cycle. Fmoc-protected peptides (I, blue) or oligo(ethylene glycol) derivatives (II, blue) are fuel with EDC (orange) during the activation reaction to result in the corresponding anhydrides (red). In the deactivation reaction they spontaneously react with the solvent water back to the precursor state.

Boekhoven et al. designed a dissipative self-assembly system based on peptide precursors, e.g., Fluoren-9-ylmethoxycarbonyl-protected (Fmoc-) aspartic (D, $n=1$) or glutamic (E, $n=2$) acid (Figure 5, I, blue). EDC, 1-ethyl-3-(3-dimethylaminopropyl) carbodiimide (Figure 5, orange), activated the carboxylate precursor and converted them to their corresponding anhydrides (Figure 5, I, red). The reaction produces one equivalent of the water-soluble urea (EDU) as waste. In its finite lifetime, the anhydride is able to self-assemble because of its increased hydrophobicity compared to the precursor. Stacking interactions of the Fmoc-groups and possible hydrogen bonding between the peptide chains support the self-assembled structure. As mentioned, the anhydride product can spontaneously hydrolyze in the aqueous solution or even in the assembly which leads back to the precursor solution. The group showed several self-assembled structures depending on the amino acid sequence of their precursor.^[47]

The same approach was used by Hartley and coworkers. The precursors TEG-Ac ($m=1$) and PEG-Ac ($m=2$) (Figure 5, II, blue) were fueled with EDC to form a macrocycle (Figure 5, II, red). The macrocycles were not able to self-assemble into a larger structure but similar to crown ethers they could be used to capture different ions in solution.^[48]

1.3 Outlook

Molecular self-assembly has been studied extensively in the last decades and scientists gained vast understanding concerning different concepts and possible applications. Consequently, static or in-equilibrium self-assembly is commonly used in material science. But inspired by nature, the focus recently shifted towards dynamic or non-equilibrium self-assembled systems. Interesting new concepts that mimic biological non-equilibrium self-assembly were discovered and different chemical reaction cycles have been described. The approaches, either completely synthetic or using components from biology like enzymes, brought a great variety of different structures and materials. Until now, the link between transient man-made materials and a distinct and unique function as we see it in biology is still missing. A few groups investigate possible applications that I discuss in the next chapter, as well as potential areas wherein transient materials would be advantageous.

2. Materials Formed by Dissipative Self-Assembly

The concept of dissipative, non-equilibrium self-assembly that I discussed in the previous chapters opens up interesting strategies to design supramolecular materials with unique properties. In this chapter, I will discuss biological examples of dissipative supramolecular materials in more detail as a blueprint for supramolecular chemists. Then I will discuss the possible features of transient materials made by dissipative self-assembly. I will describe in which areas the concept could be already applied and give reported examples. Furthermore, I will briefly outline the state of the art of controlled drug delivery platforms focusing on zero-order release profiles and show its advantages.

2.1 Transient Supramolecular Materials

Supramolecular materials have become popular in material science in recent times. Using molecular building blocks that interact with each other via non-covalent bonds offer a promising strategy to create functional materials.^[22] Established design rules^[23, 49-54] and new synthetic methods allowed that it could be included in interesting applications.^[21, 24, 55] One prominent example are the liquid crystals^[56] in LCDs, but also block copolymer micelles^[57] to deliver drugs,^[58-59] or supramolecular polymers^[20] that can help the body regenerate lost tissue^[15, 60] can already be applied in the pharmaceutical industry.

At the thermodynamic equilibrium, we have an astonishing understanding and ability to control these materials. We could further exploit this knowledge and attain the attractive features that we see in the supramolecular materials biology produces.^[22] For example, some biological supramolecular materials are able to self-heal or self-replicate.^[11] A crucial difference between synthetic and natural systems is that biological materials often exist out-of-equilibrium. That means, that the function of these materials is directly related to a constant energy uptake from their environment.^[61] The source of energy in *e.g.*, living cells is an irreversible chemical reaction with the high energy molecules nucleoside triphosphates (ATP or GTP). The cytoskeleton of eukaryotic cells offers several demonstrative examples of a complex network that are regulated by such higher energy molecules. It contains three types of fibrillar structures that are constantly polymerizing and depolymerizing at the expense of chemical energy, *i.e.*, microtubules, actin filaments, and intermediate filaments.^[19, 61]

Microtubules are hollow, tubular polymers that are formed by laterally assembled protofilaments. These protofilaments consist of α/β -tubulin dimers bound to GDP or GTP (Figure 6a). They are the largest assembly in the cytoskeleton and mechanically stiff but extremely dynamic. Their assembly and disassembly dynamics are regulated by the chemical activation and deactivation of the tubulin dimers. In the activation step GTP binds to tubulin to form GTP-bound tubulin as a new building block for polymerization. The metastable GTP-bound tubulin is able to self-assemble. However, its self-assembly also catalyzes the hydrolysis to GDP-tubulin soon after incorporation in the filament. The released energy of the hydrolysis reaction is stored as a

mechanical strain in the GDP-bound tubulin self-assembly (Figure 6a, blue/green). The endcap of the microtubule that still contains GTP-bound tubulin acts as a stabilizer for the microtubule (blue/red). If the microtubules lose the endcap, be it stochastically or through external stimuli, it rapidly disassembles and releases the stored mechanical strain, which is referred to as the catastrophe.^[28-29]

The dynamic instabilities of microtubules are essential for a quick reorientation and a fast search of cellular space, which would be impossible using in-equilibrium self-assembly. Due to their non-equilibrium nature, the microtubules and their features are only functional under a constant supply of energy, e.g. the hydrolysis of GTP. Once the fuel is consumed the microtubules decay completely.^[61]

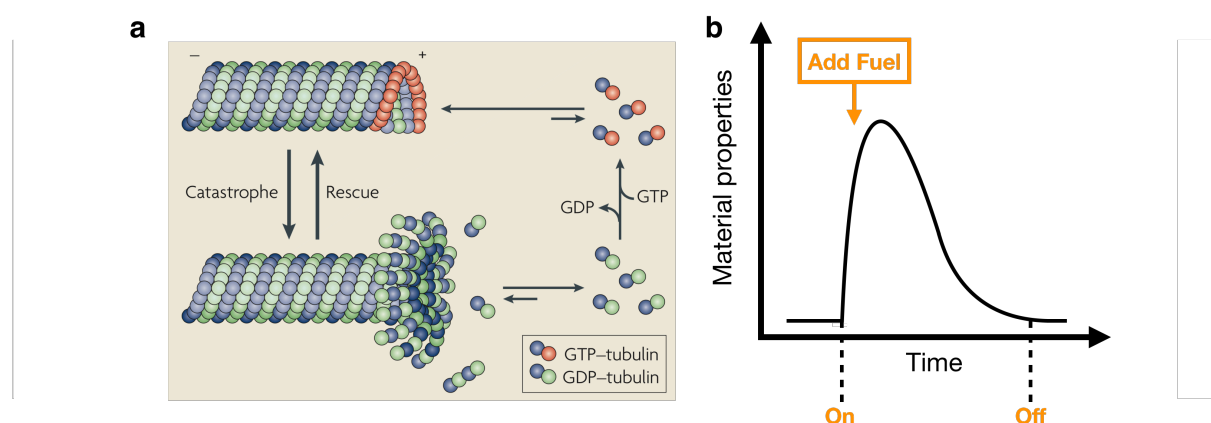


Figure 6: a) Schematic representation of microtubule formation^[28] b) Concept of dissipative materials; Properties are directly connected with the addition of fuel.

While assembly and disassembly here coexist, they show the ideal concept of a chemically fueled, dissipative self-assembly with adaptive properties.^[30] Transient supramolecular materials are designed to adapt this concept and create controlled, dynamic, functional materials. By adding a chemical fuel, molecular building blocks become activated and self-assemble into the desired material with specific properties (Figure 6b). That means the material properties can be switched on by adding fuel. Moreover, the material remains functional as long as fuel is present. However, it decays after all fuel is consumed such that the material properties are switched off. The molecular building blocks can be recovered and reused in a new cycle. Being conceptually new, only a few examples of dissipative supramolecular materials exist. In the following section, I will give an overview of reported systems with interesting and promising features.

2.1.1 Self-Erasing Inks

Materials or inks that store information over a predefined time period are not only interesting in secure communications but might also be used to reduce the consumption of traditional paper because it makes it rewriteable. Self-erasing paper or tickets of public transportation that autonomously erase after their expiration are some potential applications.^[35, 62-64] Until today, the research for such media is focused on photochromic molecules. Exposed to light of a suitable wavelength these molecules isomerize and change color.^[65-67] Embedded in a polymer or gel matrix the writing with light can be rapid and accurate, as well as works within a suitable timeframe from 16 to 24 hours until it self-erases.^[35, 65, 67-68] Disadvantages of these materials are that color-variations are not possible because of only two colors corresponding to the two states of photoisomerization and a relatively low extinction coefficient. Furthermore, their tendency to quickly photo bleach is a huge drawback for the reusability.^[35, 69]

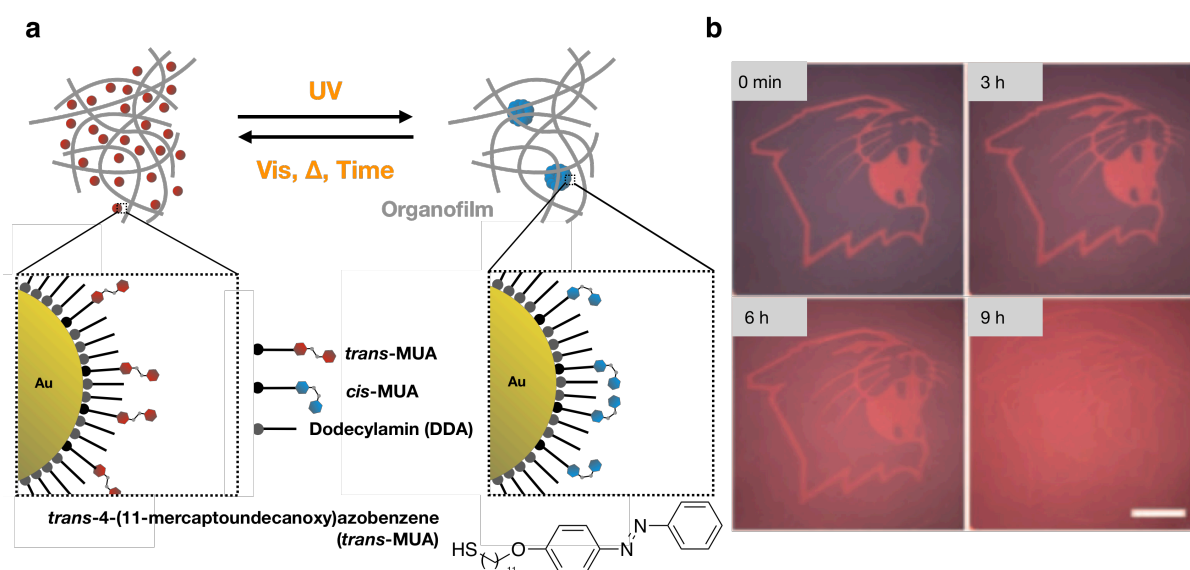


Figure 7: **a)** Single Au-Nanoparticles (red) with a mixed monolayer consisting of DDA and *trans*-MUA on the surface embedded in an organofilm. Upon UV-irradiation *cis*-MUA is formed and Nanoparticles form metastable aggregates with a supraspherical shape (blue). **b)** The image written on the Au-Nanoparticle film self-erases in daylight within 9 hrs (exposure through a transparency photomask).^[35]

A conceptually new approach, using dissipative supramolecular materials was shown by Grzybowski and coworkers using gold (Au) and silver (Ag) nanoparticles that assemble into aggregates upon UV irradiation.^[2, 35] The surface of the nanoparticles is coated with a photo-switchable azobenzene group and the single particles are

embedded in a thin, flexible orangefilm (Figure 7a). UV-light triggers the isomerization from the *trans*- to the *cis*-azobenzene with a significantly larger dipole-moment.^[70] As a result, metastable, supraspherical aggregates are formed of which the color depends on the exposure time.^[35, 70-73] In the absence of UV irradiation, the metastable assemblies fall apart spontaneously and the written image self-erase (Figure 7b). The erasure time can be controlled by the amount of induced dipole-moments and accelerated by visible light and heat. Excitingly, the material could be reused several times.^[35]

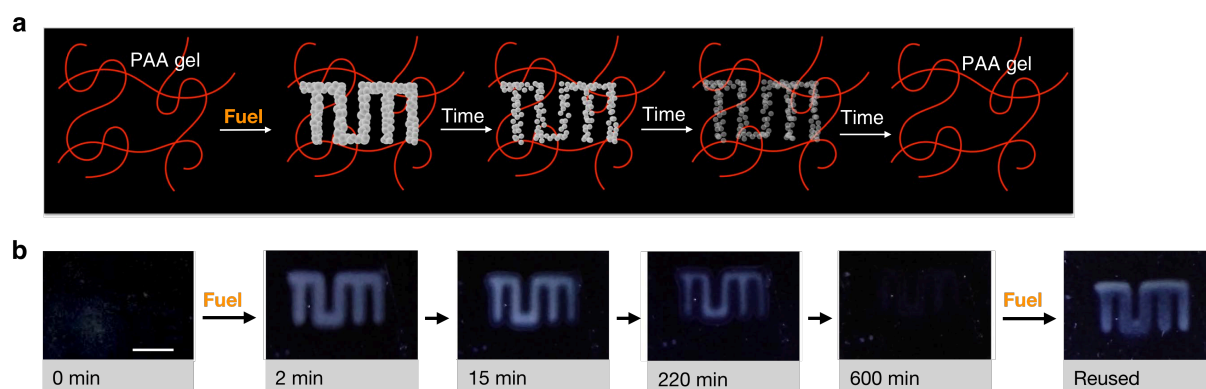


Figure 8: a) Schematic representation of the self-erasing medium; Fmoc-D-OH is dissolved in a polyacrylamide hydrogel. b) Photographs of gel over time. After 600 minutes the gel was rinsed and reused. The scale bar represents 1 cm.^[47]

Another example of such a self-erasing ink is shown by Boekhoven *et al.* The peptide-based system operates with similar principles as described above but is driven by the consumption of a chemical fuel. Fmoc-D-OH was converted to the corresponding anhydride by the consumption of a chemical fuel, a carbodiimide (see chapter 1.2.3). Due to the increased hydrophobicity, the anhydride was able to self-assemble into large spherulites which change the turbidity of the sample from optically clear to milky. Embedded in a polymeric hydrogel, the fuel could be applied on the surface of this polymer material which resulted in a local increase in turbidity (Figure 8a). By the use of templates, a sharp image could be “written”. Because the spherulites were a dissipative assembly, the messages would spontaneously self-erase, and the material could be reused for several cycles, which opens the door for the development of, e.g., reusable paper (Figure 8b).^[47]

2.1.2 Catalytic Reaction Control

Nature often impresses us with elegant and efficient ways to synthesize complex molecules,^[74-75] perform reactions with high selectivity,^[76] and accelerated rates,^[77-78] or stabilize volatile molecules.^[79] Complex self-assembled structures as mentioned in chapter 2.1, nucleic acid templates to accelerate reaction rates^[80-81] or creating a specific chirality through an enzyme-catalysis,^[82-83] are just a few examples. Until today, it is a huge inspiration for researchers that is never dwindling.

A fundamental difference between man-made reactions and biological systems is that chemists typically use molecules free in solution or on an interface while biology uses the effect of nanoscale confinements. Especially supramolecular chemists were interested if they can mimic structures that serve as a supramolecular host and bind smaller molecules in their cavities.^[84] The use of self-assembled materials to serve as a nano-reactor has been studied elaborately, and successful examples include nanoporous materials,^[85-86] emulsion microdroplets,^[87] hydrogels,^[88] or coacervate droplets.^[89] The reversible dynamic nature of dissipative self-assembly offers new possibilities to combine temporary materials that allow the accumulation of small molecules. That would enable dynamic control over chemical reactions and their catalytic activity. First examples have already been shown.

As an early example of a nano-reactor created by dissipative self-assembly, the group of Rafal Klajn developed dynamic self-assembling nanoflasks from nanoparticles based on gold, silica, and magnetite, and a photochemical fuel. The mechanism is identical to the example of chapter 2.1.1. The surface of the nanoparticles is coated with a photo-switchable azobenzene group and a UV-trigger leads to the isomerization from *trans*- to *cis*-azobenzene. Due to the larger dipole-moment aggregates are formed, creating a polar environment in a nonpolar solvent. Polar molecules, like water or hydrophilic additives, accumulate in this new environment to reduce repulsive interactions with the solvent (Figure 9a). The dimension of the flask can be tuned by different diameters of used nanoparticles ranging from 6 nm for gold to 17 nm for silica. Interestingly, the group showed that it is possible to increase reaction rates and improve selection within the flask. Several model reactions were tested, *e.g.*, the hydrolysis of acetal (Figure 9b) or the stereoselective UV-induced dimerization of anthracene (Figure 9d). Moreover, adding a chiral ligand to the nanoparticles enabled

the possibility of enantioselective trap phenyl ethanol (Figure 9c). While the acceleration of the hydrolysis of acetal was modest (Figure 9b, graph), the dimerization of anthracene showed an impressive two orders of magnitude higher rate in the presence of dissipative self-assembled nanoparticles (Figure 9d, graph). Crucially, removing the energy source or applying visible light led to the disassembly of the nanoflasks and a solution of single nanoparticles. The disassembly process destroyed the polar environment within the nanoflasks, interrupted the ongoing chemical reaction in the cavities and confirmed the dynamic control over the chemical reactions.^[14, 84]

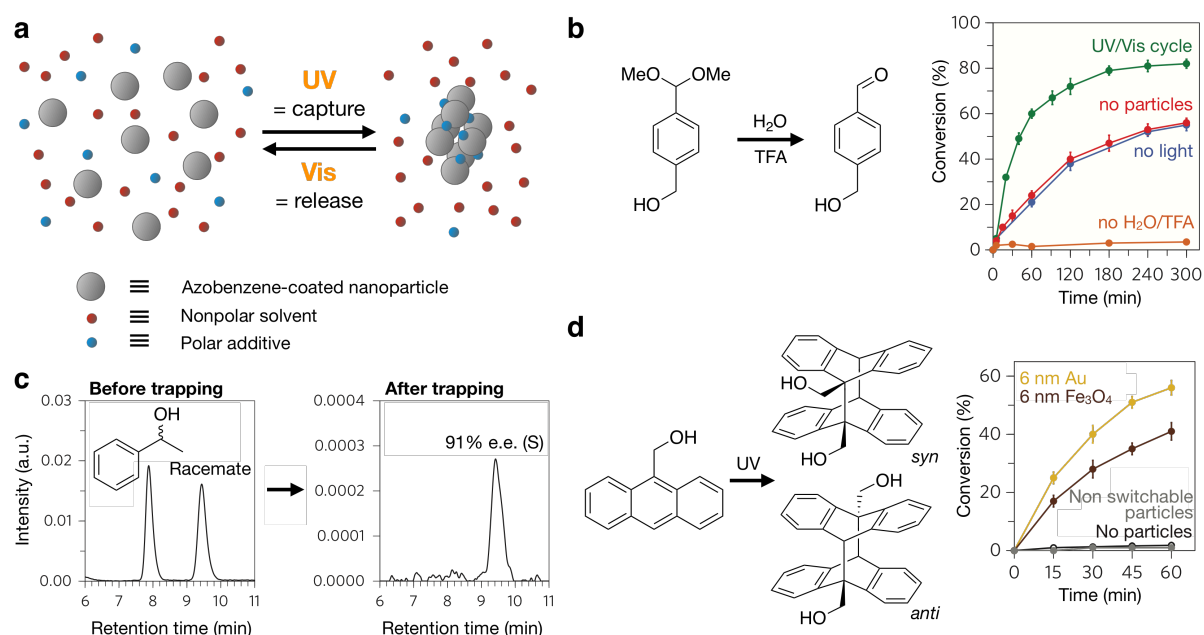


Figure 9: **a)** Schematic representation of the reversible trapping of polar molecules during the light induced self-assembly of nanoparticles. **b)** Hydrolysis of acetal; Light-accelerated hydrolysis (green) in comparison to no particles (red), no light (blue) and no reagent (orange). **c)** Enantioselective light-induced trapping of 1-phenylethanol; HPLC traces before (left) and after (right) the trapping. **d)** UV-induced dimerization of anthracene derivatives; Light-accelerated dimerization with Au-nanoparticles (yellow) and Fe₃O₄-nanoparticles (brown) in comparison to no particles (black) and non-switchable particles (grey).^[84]

Another example of using dissipative self-assembly to create a transient reactor was shown by Prins and Coworkers. In the example, the authors were able to design a dissipative vesicular nanoreactor. C₁₆TACN·Zn²⁺ was used as a precursor (Figure 10a, blue), consisting of 1,4,7-triazacyclononane with a positively charged Zinc cation as a headgroup and an aliphatic C₁₆ chain as an apolar tail. Solutions with a high concentration of the precursor already showed micelle formation but in the presence of ATP as a fuel, the critical aggregation concentration dropped significantly, and the

surfactant assembled into stable vesicles with a diameter of 50 to 100 nm. Since the interactions of $C_{16}TACN^+Zn^{2+}$ with ATP were strong, the vesicles cannot disassemble spontaneously. However, potato apyrase, an enzyme that can rapidly hydrolyze ATP to AMP and two molecules of orthophosphate, could be used to induce the disassembly process.^[90] AMP and P_i were not able to stabilize the vesicles resulting in the desired dissociation and completing the transient vesicle formation with a controlled lifetime. The described cycle (Figure 10a) could be repeated several times by addition of a new batch of ATP. Furthermore, the apolar vesicle bilayer could serve as a medium for chemical reactions that typically occur at a low rate in water. For example, the nucleophilic aromatic substitution between 4-chloro-7-nitrobenzofurazan (NBD-Cl) and 1-octanethiol (C_8-SH) was chosen because of the expectation to enrich the reactants within the vesicle bilayer (Figure 10b). The yields of the substitution were noticeably higher when the self-assembled vesicles are present. Moreover, higher ATP concentrations showed increased product formation (Figure 10c).^[38]

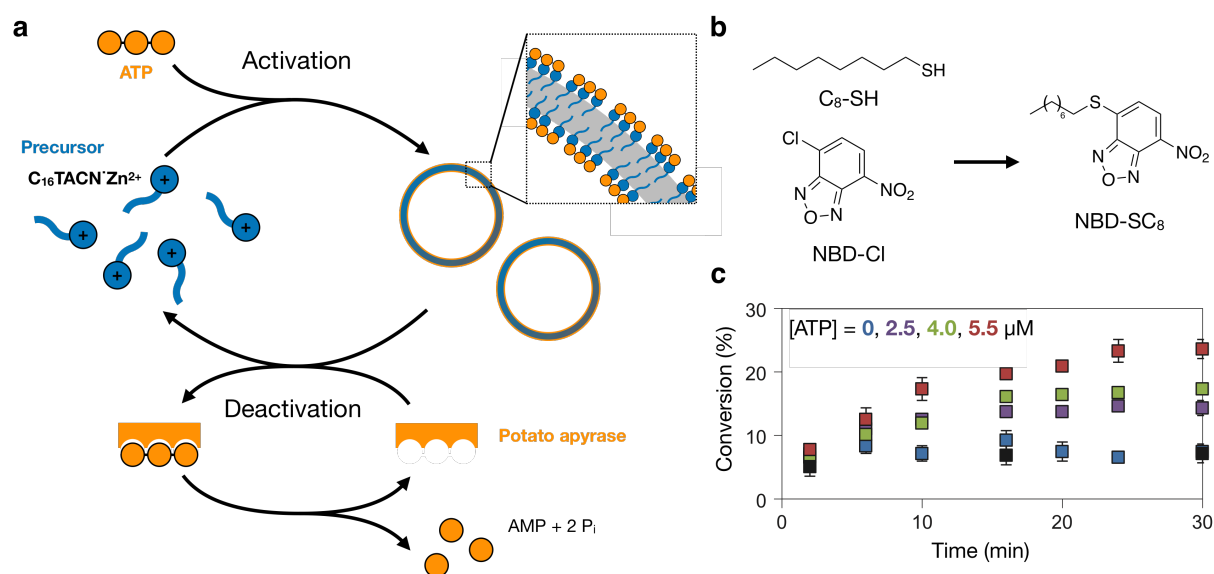


Figure 10: a) Schematic representation of the dissipative self-assembly of vesicles. b) Model reaction of C_8-SH and NBD-Cl to NBD- SC_8 . c) Conversion over time for the same conditions but varying ATP concentrations. Black markers show the control experiment without the self-assembled structure.^[38]

These are impressive examples of dissipative nanoreactors that require a (photo)chemical fuel to maintain their non-equilibrium functionality. Moreover, that are novel strategies that mimic biological systems and facilitate new possibilities to synthesize materials or small molecules.

2.1.3 Transient Hydrogels

Hydrogels are cross-linked three-dimensional polymer networks that can absorb and contain high percentages of water (up to 90%).^[91] They can swell, but do not dissolve in water. Hydrophilic groups, like amino, carboxyl, and hydroxyl, attached to a polymer backbone give the water-holding capacity while a crosslinked network is fundamental to retain a solid-like structure, despite being mostly composed of in water. This combination leads to high flexibility and similarities to natural tissues, which brought them significant attention for a wide range of applications including healthcare, food industry, and cosmetics.^[92] Especially, the high water content and the resulting biocompatibility is favorable over other types of polymeric scaffold and they are thus frequently applied in the biomedical field.^[93] Furthermore, permeability for incursion of nutrients and excretion of metabolites emphasize the biological character and inspire researchers for novel biomaterials and bioapplications.^[92, 94] Scaffolds for tissue engineering,^[95] soft tissue engineering,^[96] targeted delivery,^[97-98] wound healing,^[99] or soft contact lenses^[100] are just a few examples for the use of hydrogels in this area.

Hydrogel-based materials could benefit from the temporal control of dissipative systems. For example, a hydrogel with defined material properties over a certain lifetime can aid the body in the regeneration of tissue. The material could be programmed to disassemble in its small molecular building blocks and be disposed of by the body after a predetermined time. Moreover, the ability of dissipative assemblies to self-heal would allow the material to repair small damages.^[14, 64, 101] Because of the abovementioned advantages, fundamental studies to develop dissipative hydrogels have shown promising results. While these examples may still be far from clinical application, it does demonstrate progress and the potential of such materials.

The first synthetic example of a transient material based on a chemically fueled non-equilibrium self-assembly process was a hydrogel.^[32] Van Esch, Eelkema and coworkers investigated molecular gelators with one to three anionic carboxylate groups in combination with an ester-forming alkylation reaction (see chapter 1.2.1). First methyl iodide,^[32] but then dimethyl sulfate (DMS)^[33] a commonly used, strong methylation agent and different gelators formed an active hydrogel-based material. Looking at the results for DBC as a precursor, rheology revealed a rapid increase in gel stiffness and the lifetime of the assemblies depending on the added fuel

concentration (Figure 11a). Kinetics measurements using HPLC (Figure 11b) demonstrated the presence of the anhydride during the complete cycle and the dependence of the product yield on the amount of fuel added. Moreover, gels of the DBC anhydride showed a self-regenerating behavior after mechanical destruction and could regain their material properties (Figure 11c).

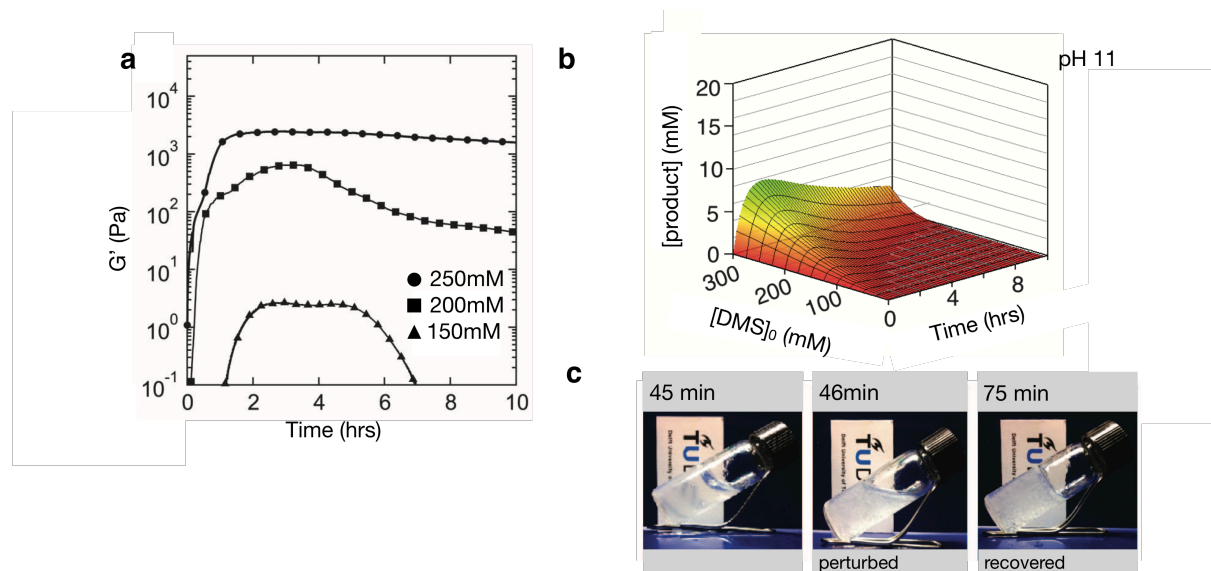


Figure 11: **a)** Rheology time sweeps of a DBC solution at varying concentrations DMS. **b)** Transient kinetics of the anhydride product measured by HPLC with different initial concentrations of DMS. **c)** Fuel-driven gel regeneration, photographs before (45 min) and directly after (46 min) a mechanical perturbation of the gel as well as the regenerated gel (75 min).^[33]

A similar concept to design dissipative hydrogels was used by Ulijn *et al.* In this example, a methyl-ester was converted to a peptide bond catalyzed by an enzyme.^[37, 102] As a precursor, the authors used an amide that reacted with a methylated amino acid in a short peptide sequence (Figure 12a). The inspiration here was that already short peptide compositions are known for a high sequence-dependent self-assembling process into functional materials.^[103-107] The peptide-fuel (Figure 12a, orange) included an aromatic amino acid residue (F: Phenylalanine, I)^[102] or a naphthoxyacetyl-functionalization (Nap, II).^[37] That increases the likelihood of self-assembly driven by aromatic π -stacking additionally to the hydrogen bonding between the peptide-backbones.^[104, 108-109] The activation of the precursor (Figure 12a, blue) was a transacylation catalyzed by α -Chymotrypsin, a well-known enzyme for the catalysis of peptide synthesis. The conversion to the short peptide product (red) giving rise to the hydrogel product. Simultaneously, the deactivation, a hydrolysis reaction, took place

resulting in the origin precursor and waste product.^[110-111] Interestingly, both reactions were catalyzed by the enzyme. Problematic in this approach was controlling the lifetime of the assemblies since the enzyme catalyzed the forward as well as the backward reaction.^[14]

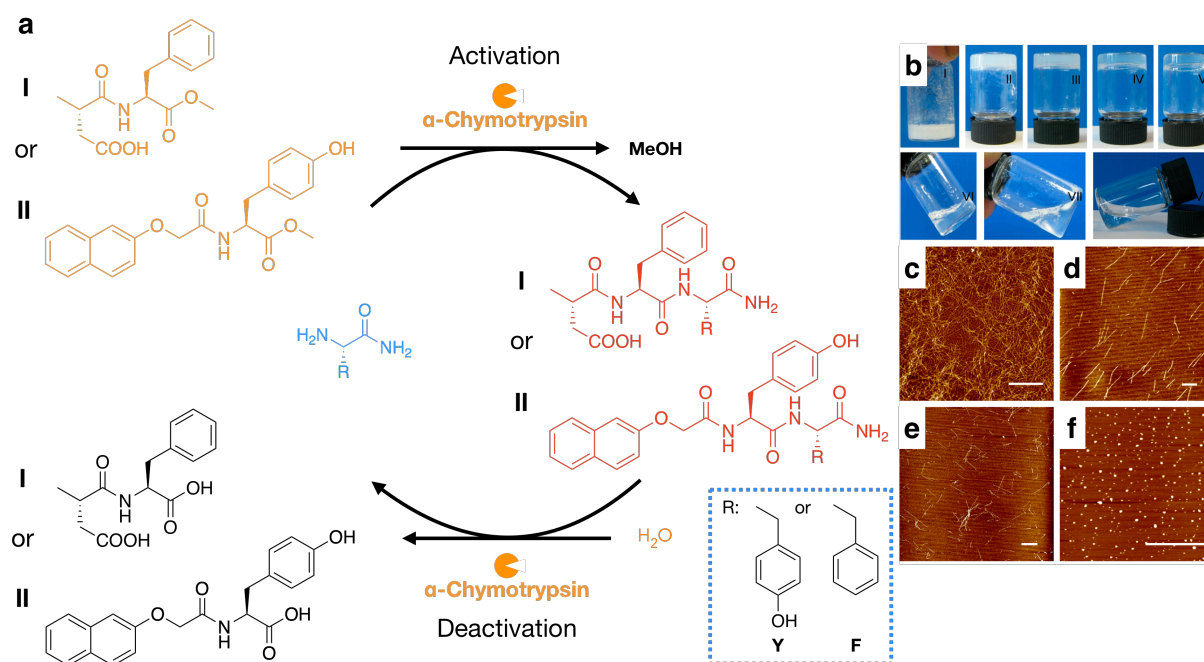


Figure 12: **a)** Enzyme catalyzed chemical reaction cycle with an amide precursor (blue) that converts to the short dipeptide (red) using a peptide fuel with an aromatic residue (I) or a Nap-functionalization (II). **b)** Photographs of the Nap-YY-NH₂ gel at different timepoints (1 min, 5 min, 1 h, 2h, 3h, 4h, 5h and after the reaction at 8h). AFM images of Nap-YY-NH₂ at **c)** 30 min, **d)** 3 h, **e)** 5h and **f)** 8h.

An example of a purely synthetic peptide-based dissipative assembly was recently published by Boekhoven *et al.* An acid-anhydride chemical reaction cycle (see chapter 2.1.3) with Fmoc-protected tripeptides (Fmoc-AAD-OH, -AAE-OH, -AVD-OH, and -AVE-OH, V: Valine) as precursors was used to induce hydrogel formation after fuel addition. The lifetimes of these hydrogels could be extended by increasing the amount of fuel that was added. Moreover, these lifetimes could be predicted by kinetic models. Such predictability would render them useful for protentional applications. However, a drawback for high fuel concentration was that the system tends to kinetically trap. Kinetically trapped means here that the product indeed reacts back to the precursor over time but is not able to disassemble afterward so that it remains in the hydrogel state.^[47]

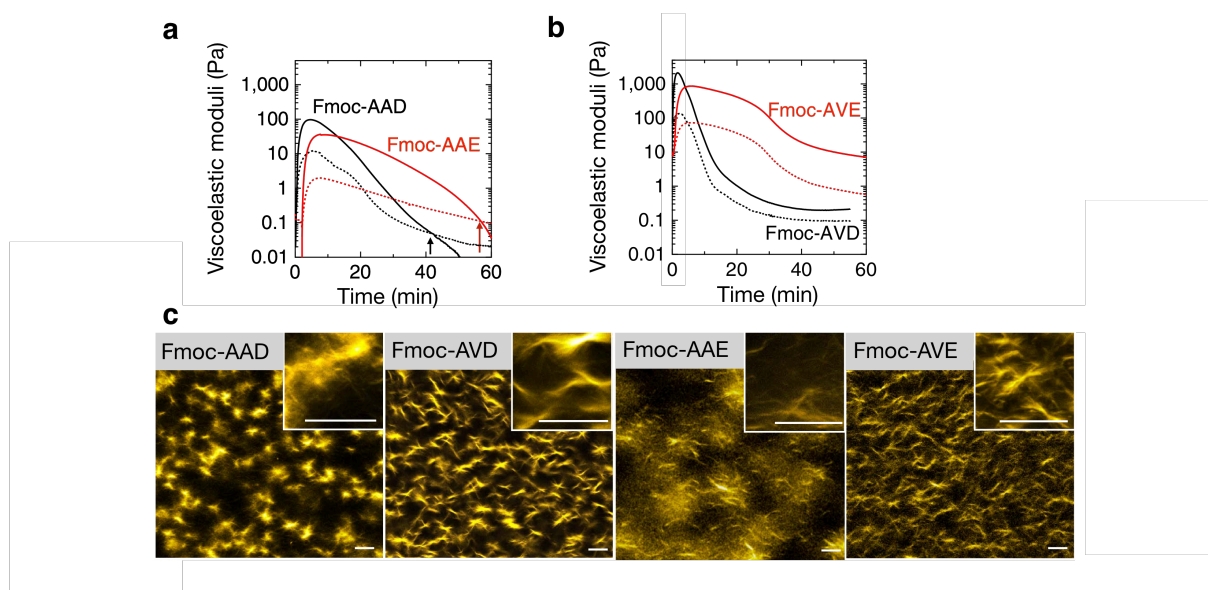


Figure 13: Rheological time sweeps of gels formed by **a)** Fmoc-AAD-OH and Fmoc-AAE-OH as well as **b)** Fmoc-AVD-OH and Fmoc-AVE-OH. **c)** Confocal microscopy of different gels after 10 min.

A final example, I highlight, was introduced by Hartley and Konkolewicz and results in the formation of transient polymer gels.^[112] Copolymers with different ratios of acrylamide (Am) and acrylic acid (AA) were synthesized by a controlled polymerization reaction (Figure 14a). These copolymers were used as precursor molecules in the chemical reaction cycle. The free acrylic acid side chains were able to crosslink upon fuel addition and promote rapid gelation (Figure 14b). The de-crosslinking and consequent de-gelation time is correlated to the percentage of possible crosslinks and subsequently the stiffness of the gel. A copolymer with 35% of acrylic acid remained in the hydrogel state for ca. 9.5 hours while a copolymer with just 15% acrylic acid lasted for only 3.5 hours (Figure 14c).

Even though these hydrogel-based transient materials have no real applications yet, the concepts have great potential and the observed lifetimes are interesting for medical use. In this area, *e.g.*, new controlled release mechanisms are highly desirable and dissipative materials push already towards this direction, as described in the next section.

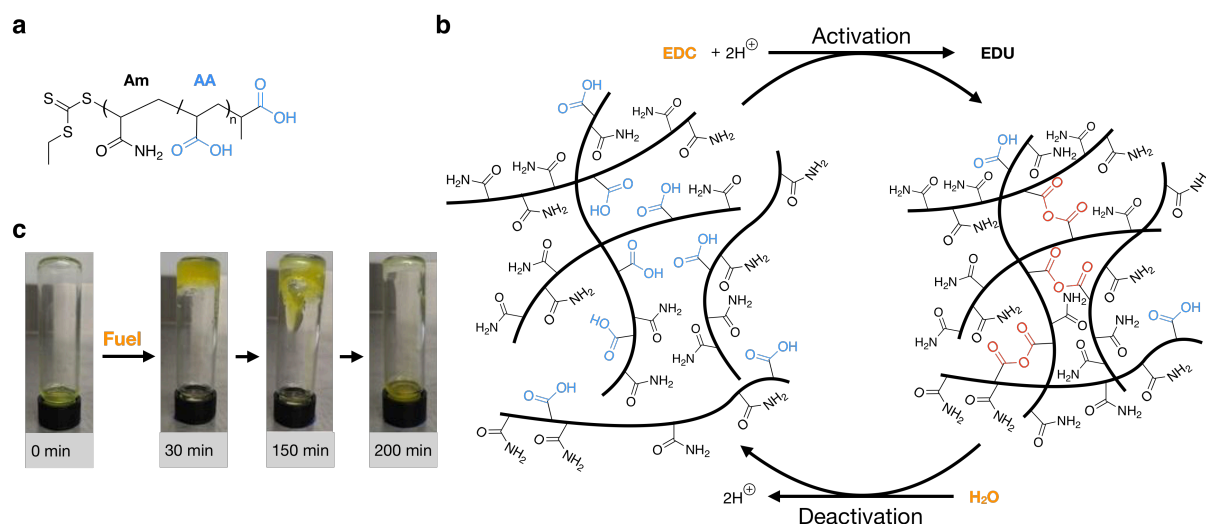


Figure 14: a) Chemical structure of the used polymer, poly(Am₈₅-r-AA₁₅) or poly(Am₆₅-r-AA₃₅); $n = 100$. b) Scheme of the EDC-fueled Am-AA copolymer crosslinking cycle. c) Photographs of an inverted tube test of poly(Am₈₅-r-AA₁₅) with EDC over time.

2.1.4 Dissipative Materials for Controlled Release

Controlled release, a research field that was established in the early 1950s, aims at the tunable delivery of compounds at an effective level in a reasonable time period. External stimuli like pH, UV light, temperature, enzymes, or osmosis have been investigated to establish new methods that regulate release.^[113] The first developed system was polymer-based and able to release oral drugs in a customized profile.^[114-115] Until today, the controlled release of active ingredients in the pharmaceutical industry is a relevant and still studied application area, which I will discuss in more detail later on.

The huge potential of controlled release was quickly realized in other areas too, *e.g.*, in the fields of cosmetics, pesticides, agriculture, or food science.^[113] Further early examples were the controlled release of marine antifoulants^[116] or fertilizers.^[117-118] A strategy for the release of fertilizer can be based on lifetime-control of the materials by using biodegradable polymers like starch-polyurethane^[119] or starch-polyvinyl-alcohol^[120] mixtures. Another concept, these fields could thus benefit from, are dissipative supramolecular materials because of their intrinsic ability to control their lifetime. Indeed, examples of transient materials that regulate the delivery of small molecules exist, which I will highlight below.

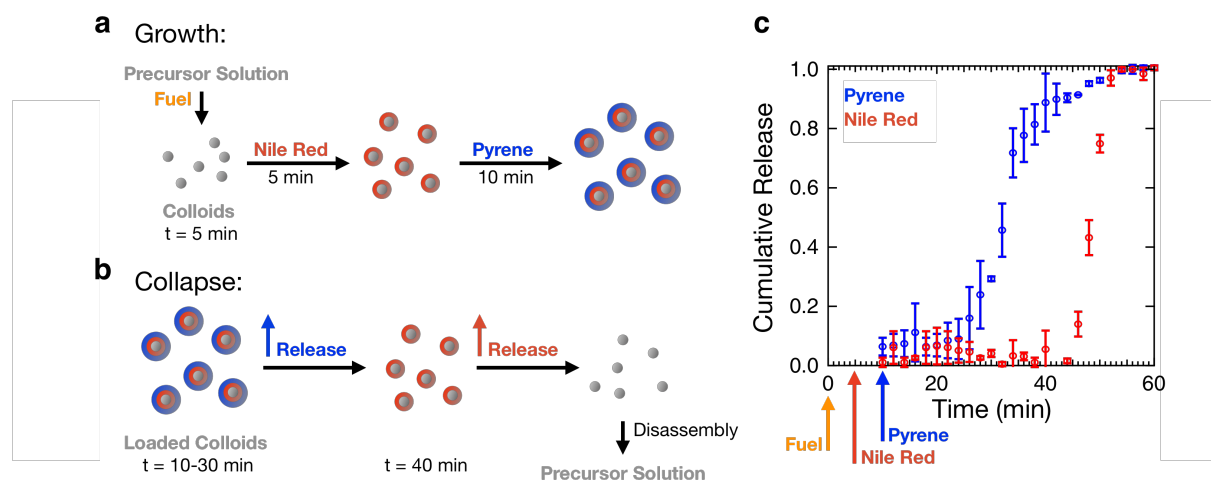


Figure 15: Schematic representation of **a**) the growth process of the colloids with the addition of dyes and **b**) the collapse after fuel depletion with the sequential release of the dyes, Pyrene (blue) and Nile Red (red). **c**) Cumulative release profile of the dyes over time; The arrows mark the addition of fuel (orange), Nile Red (red) and Pyrene (blue).^[47]

Boekhoven *et al.* described dissipative colloids that can store and release hydrophobic molecules in a controlled manner. The underlying process of this non-equilibrium self-assembly is a chemically fueled acid-anhydride-reaction cycle (see chapter 1.2.3) with a Fmoc-protected peptide-based precursor (Fmoc-E-OH). In comparison to the very similar precursor Fmoc-D-OH (see chapter 2.1.1), Fmoc-E-OH self-assembles into spherical colloids upon fuel addition. The lifetime of these colloids can be tuned from 30 to 120 minutes depending on the amount of fuel. Because the colloids have a finite and tunable lifetime, their ability to set free hydrophobic molecules was investigated. The colloids were first loaded with two different hydrophobic dyes, Nile Red (Figure 15, red) and Pyrene (blue). These dyes were loaded in the colloids by adding the dyes during the formation of the colloids, early in the cycle, with a 5 minutes time difference (Figure 15a). When the fuel was running low, the loaded colloids start collapsing collectively and releasing the dyes sequentially vice versa (Figure 15b). The cumulative release profile (Figure 15c) showed that pyrene (blue trace) was released first, starting at 30 minutes, and only now the pyrene release was completed, the Nile Red release (red trace) started.^[47]

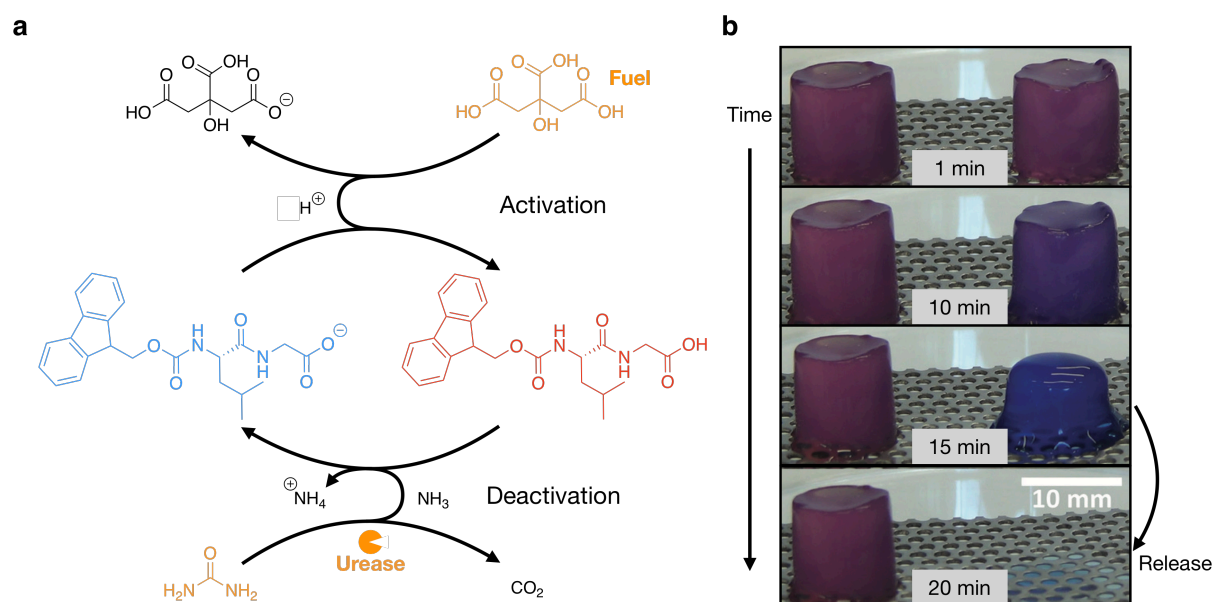


Figure 16: a) Coupled reaction cycles to create the dissipative hydrogel. b) Photographs of a stable hydrogel (left) in comparison to the dissipative hydrogel with burst release (right).^[121]

The idea of controlled release using dissipative supramolecular materials was further explored by Walther and coworkers. They used reaction cycles that resulted in a release of a dye. The authors used a hydrogelator that is based on a Fmoc-protected dipeptide (Fmoc-LG-OH) that is highly soluble at alkaline pH but tends to form self-assembled hydrogels at acidic pH. The chemical reactions that indirectly control the self-assembly process is a combination of citric acid as fuel and the enzyme urease (Figure 16a). Starting with well-soluble solutions at pH 10, the addition of citric acid rapidly decreases the pH which protonates the hydrogelator. The protonation induced the self-assembly into a fiber network due to the removal of electrostatic repulsion. Simultaneously, the enzyme urease decomposes urea to carbon dioxide gas and ammonia that slowly increases the pH. Hence, the temporal control of the system can be tuned from minutes to hours by the amount of urease in the system. Back at alkaline pH, the hydrogelator disassembles completely reverting the precursor solution.^[121] As already shown in thermodynamically controlled self-assembled hydrogels, these materials are able to store and release hydrophilic molecules.^[91, 97-98, 122] Using the described dynamic hydrogel, the storage time can be controlled by the lifetime of the gel because the hydrophilic cargo is released in one burst synchronized with the disassembly of the material (Figure 16b).^[121]

The examples discussed above show the sequential and burst release of molecules. However, different industries and applications require various release profiles and a wider range of delivery vehicles. Especially in the pharmaceutical industry, controlled release has large potential but also the standards are high. In the next section, I will discuss in detail strategies, possibilities and advantages for controlled drug release.

2.2 Controlled Drug Delivery

The goal of drug delivery devices is to ensure that the concentration of an active pharmaceutical ingredient in the blood plasma is at a concentration where it is most efficient. If the concentration is too low, there are no therapeutic effects. If it is too high, the drug can be toxic (Figure 17).^[123-124] The goal of drug delivery vehicles is thus to maintain a drug concentration within this therapeutic window for a predefined period of time. These devices are particularly useful for drugs with low solubility and bioavailability (BCS class II drugs).^[125]

The materials used to deliver drugs are, *e.g.*, hydrogels or emulsions that have the ability to increase the solubility of these drugs.^[126-128] These materials help to solubilize the hydrophobic drug, for example, by incorporation in oil droplets. The drug delivery device releases the drug to the surrounding tissue, which mostly results in diffusion-controlled drug release, *i.e.*, the release kinetics follow first-order. In first-order processes, typically following Higuchi's kinetics,^[129-130] the drug initially releases fast but slows down as time progresses. Consequently, the corresponding concentration of the drug in the plasma is first high, but then quickly falls out of the therapeutic window. In other words, initially, there is a risk of over-dosage and after, it rapidly loses efficacy. A solution to overcome this problem is the use of multiple dosing, *e.g.*, a dose in the morning, afternoon and evening (Figure 17).^[113, 123-124]

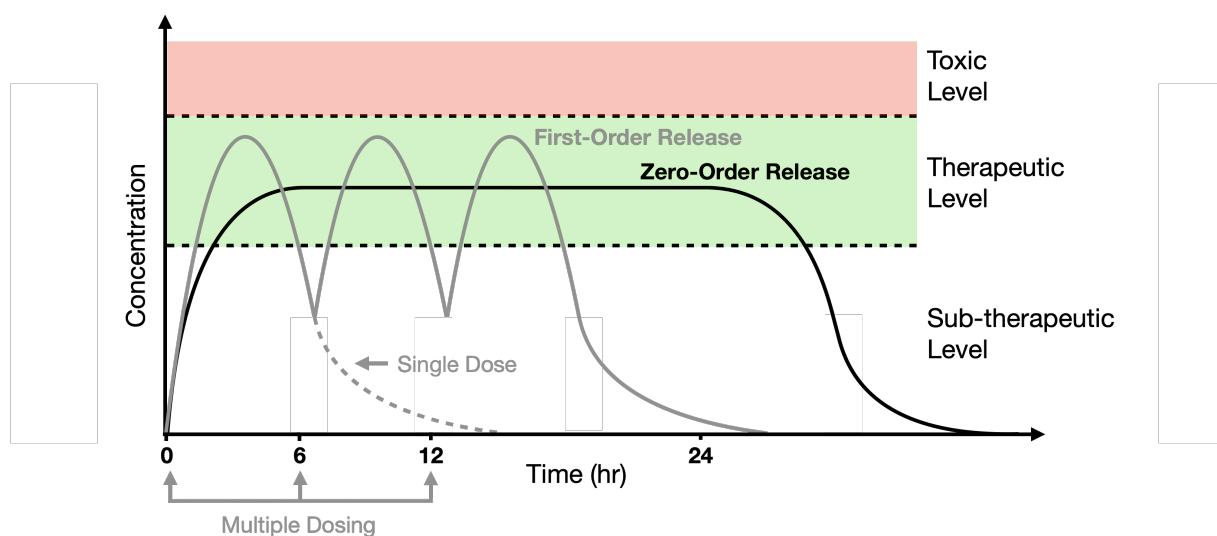


Figure 17: Drug concentration in the blood plasma using vehicles with different release profiles.

Another solution to overcome the drawback of first-order release vehicles is by using materials that release drugs with zero-order. These materials have a constant rate of drug release over the entire release period. That means the release rate is independent of the amount of drug that has been released. Consequently, the fluctuation of drug concentration in the plasma will be minimized and can be optimized to stay within the therapeutic window over the entire release period. Such materials could decrease the risk of over- or under-dosage leading to higher therapeutic efficiency compared to first-order delivery devices. Moreover, only one dosage per day would be required (Figure 17).^[129, 131]

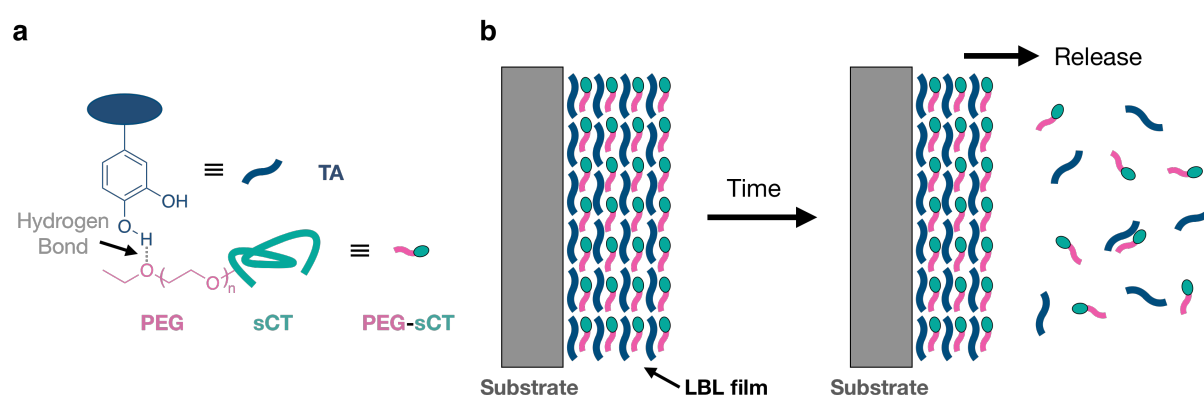


Figure 18: a) Hydrogen bonding between PEG-sCT and TA; b) Surface-erosion mechanism from the LBL film.

Examples of zero-order delivery vehicles exist but are relatively rare. The method by which these materials operate is to transition diffusion-controlled kinetics to concentration-independent kinetics. One strategy is to use a surface erosion mechanism, in which the release rate does not depend on the concentration in the surrounding medium but on the surface area of the container. For example, recently Zhang and Liu *et al.* showed that a peptide therapeutic could be released with zero-order kinetics over a time frame of 24 hours. The authors made use of a water-soluble polymer covalently bound to a peptide-based drug. PEGylated salmon calcitonin (PEG-sCT) is an attractive therapeutic against bone disorders. In the work, the polyphenol tannic acid (TA) is used to develop a hydrogen-bonded layer-by-layer (LBL) film (Figure 18a). Applying the PEG-sCT and TA on a substrate by alternately dipping in aqueous solutions of both, creates a high surface-area to volume ratio. Thus, the limiting factor for dissolution and consequent release of the drug is the surface area of the film. In other words, the drug release (v) linearly depends on the surface area of

the material ($v = k \cdot \text{Surface Area}$). Since the material was a film, the surface area did not decrease significantly as the material decomposed, and thus the rate of drug release did not change as a function of time (Figure 18b).^[129]

Langer, a pioneer in the field of drug delivery, developed with his coworkers many interesting strategies for controlled release system in the last decades.^[132-136] For example, an approach to overcome the drawbacks of first-order release was to improve the polymer matrix geometry.^[133] The authors of the study found that changing the shape from a commonly used rectangular slab to a hemispheric matrix led to a constant zero-order release of micro- and macromolecules over a time period of up to 50 days (Figure 19a). More recently, the focus on engineering new defined platforms for specific drugs and diseases to find efficient treatment methods and resolving current widespread issues like *e.g.*, HIV therapy. For example, an oral once-weekly drug delivery system for HIV antiretroviral treatment was developed. It consists of six surrounding arms attached to a central core (Figure 19b). The core offers stability to the construction which can be folded into a capsule. Meanwhile, the arms offer mechanical rigidity and can be loaded with drugs. This design is able to be loaded with different drug-polymer matrices each having defined release profiles and can be tuned to have desired drug release rates and specific plasma pharmacokinetics (Figure 19c).^[136]

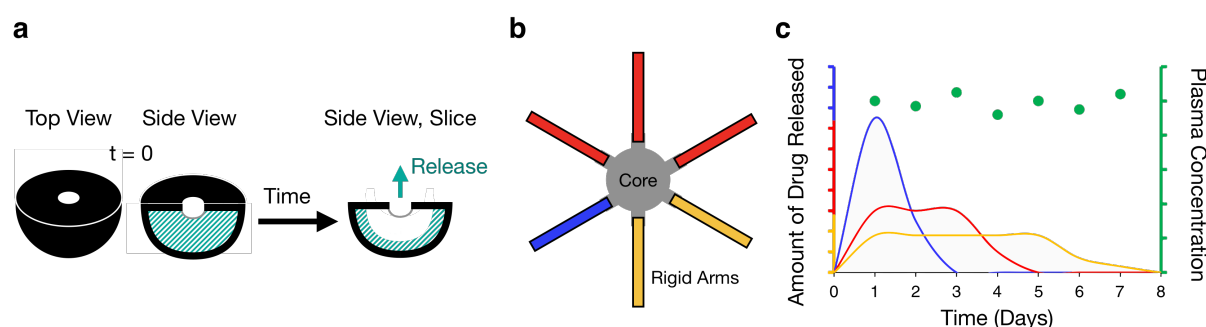


Figure 19: **a)** Scheme of a hemispheric matrix with a polymer-drug-blend inside; The top hole allows release.^[133] **b)** Design of the HIV treatment device; The rigid arms are filled with different drug-polymer matrices (blue, red and yellow). **c)** Schematic representation of an ideal system with a constant plasma concentration of the drug (green) over several days. The colored traces show possible release profiles from the different drug-polymer-matrices.^[136]

Taken together, several concepts exist for the controlled release of active agents. Especially delivery vehicles with zero-order release profiles are very desirable because

of their high therapeutic efficiency during the entire release period. Fluctuation and toxic effects can be minimized while the plasma drug concentration stays constant.^[131, 137] However, achieving zero-order kinetics continues to be a big challenge in today's research. Most of the developed solutions only match with one specific drug and cannot be generalized to broad classes of drugs. Moreover, they are frequently hard to formulate, complex and can be expensive.^[138-145] Thus, the field could benefit from fundamentally new strategies.^[113]

2.3 Outlook

Dissipative supramolecular materials are a new concept that can be used in many fields. Recent examples show that exciting proof of principle examples ranging from self-erasing and reusable inks, self-healing hydrogels, and materials with controlled release profiles. Especially the last example could be interesting for pharmaceutical applications. The industry could benefit from fundamentally new strategies to control the release of drugs. Burst and sequential release profiles can be exciting for delivery vehicles, but the advantages of zero-order kinetics are obvious because of their high therapeutic efficiency. The transient nature of dissipative supramolecular self-assembly could offer solutions to the problem. As the field of dissipative supramolecular materials matures, design rules to control the lifetime of materials become clear. Moreover, methods to convert first-order to zero-order decay have also been described. Peptides are already commonly used in delivery vehicles and therapeutics because of their high bioavailability. Interestingly, peptide-based precursors for dissipative materials have already been explored.^[47] Furthermore, transient emulsions could be developed which is ideal for the solubility of hydrophobic molecules.^[146] Taken together, there is a good foundation for the further development of a material based on dissipative self-assembly that can be applied as a delivery platform. A simple and versatile system, which is easy to synthesize and shows zero-order release would be optimal.

3. Aims of the Thesis

The overarching aim of this thesis was to push the field of dissipative self-assembly beyond exploratory basic science and search for their application in relevant materials. As mentioned, dissipative supramolecular materials could be useful in different areas, but I was specifically interested in developing a material that can deliver drugs in a controlled manner.

Initially, peptide-based precursors in a known fuel-driven reaction cycle were explored to search for interesting structures and features. Peptides were chosen, because of their vast library of self-assembled structures known and their shown potential to be coupled to energy dissipating chemical reaction cycles. Furthermore, the target was to explore how changes in a peptide design would affect the structure that would form upon self-assembly and its material properties. The aim was to create self-assembled structures like vesicles or colloids and further exploited them as materials. These structures would be particularly interesting as materials because of their ability to compartmentalize and enrich molecules with specific properties. The acid-anhydride based reaction cycle using EDC as a chemical fuel, established by the Boekhoven group, was the base of the studies.

In the first steps, I describe in chapter 4, a peptide sequence was discovered that self-assembled into vesicles upon fuel addition. Deeper insights in the structure and its composition showed the defined characteristics that are needed to form a stable membrane. Specific conditions, short lifetimes, and high dynamics were not the ideal requirements to expand this towards a drug delivery vehicle. Besides that, a colloid-former was found with a similar but shorter peptide sequence. In that work, which I discuss in chapter 5, we discovered a new mechanism by which the assembly can regulate its decay profile and transition it to constant zero-order kinetics. Understanding and controlling the mechanism was a key point to develop materials with a defined release profile. That prompted me to implement that mechanism in simple, versatile materials that could deliver drugs with zero-order kinetics.

The material I aimed for the zero-order drug delivery was an emulsion. Emulsions are already frequently used in the pharmaceutical industry. In chapter 6, I thus develop a simple precursor that forms an emulsion after the addition of EDC. As expected, the same self-protection mechanism leads to a decay profile with zero-order kinetics. As the emulsion decays with zero order, I used it as a drug delivery material with a controlled constant release profile.

In conclusion, I aimed to adapt a known chemical reaction network to new precursors that self-assemble into structures that can be applied in relevant materials. The temporal control of transient materials and an implemented feedback mechanism, as we see it in biology, can be useful for functional materials. Converting zero-order kinetics of a system to controlled zero-order release of an active agent is the ultimate goal. Especially in the field of drug delivery understanding and controlling the release mechanism is key for the application of novel and smart delivery vehicles.

4. Dynamic Vesicles Formed by Dissipative Self-Assembly

Abstract.

In this work, we coupled the acid-anhydride-based reaction cycle, described in chapter 1.2.3, to new peptide precursors in order to achieve dissipative self-assembly of vesicles. Terminal aspartic (D) or glutamic acid (E) can be condensed to the corresponding anhydrides by an intramolecular reaction with a carbodiimide. The anhydrides are not stable in an aqueous solution and rapidly hydrolyze back to the acids. With this concept, Fmoc-protected tripeptides (Fmoc-GGD-OH and -GGE-OH) are used as precursors and 1-ethyl-3-(3-dimethylaminopropyl) carbodiimide (EDC) is used as fuel. The peptides are water soluble but this changes with the addition of EDC. The formed anhydride-product is inducing a self-assembly process upon its increased hydrophobicity. We encountered that the emerging vesicles are highly dynamic and remodel through several morphologies in their limited lifetime. Moreover, experiments show that the vesicles are a mixture of precursor and product during the entire process which is supported by molecular simulations. That reveals a subtle balance between the two components is necessary to form a stable membrane. As soon as the fuel runs low, the assembled vesicles start to decay, and the equilibrium is been reinstated. This dynamic formation of vesicles offers a novel model platform to study membrane remodeling or to create artificial compartments.

This work has been published:

Title: Dynamic Vesicles Formed by Dissipative Self-Assembly
Authors: Caren Wanzke, Alexander Jussupow, Fabian Kohler, Prof. Dr. Hendrik Dietz, Prof. Dr. Ville R. I. Kaila, Prof. Dr. Job Boekhoven
First published: 07. November 2019
Journal: *ChemSystemsChem* **2020**, 2, e1900044.
Publisher: WILEY-VCH
DOI: 10.1002/syst.201900044

Reprinted with permission of John Wiley and Sons.

This section states the individual work of each author in the publication above. C. Wanzke designed and conducted all experiments. A. Jussupow and V. R. I. Kaila performed and analyzed the molecular simulations and wrote the simulation part in the manuscript and supporting information. F. Kohler and H. Dietz helped with cryogenic transmission electron microscopy. C. Wanzke and J. Boekhoven wrote the manuscript. The work was performed under the supervision and guidance of J. Boekhoven.

Special
Collection

Dynamic Vesicles Formed By Dissipative Self-Assembly

Caren Wanzke,^[a] Alexander Jussupow,^[a] Fabian Kohler,^[b] Hendrik Dietz,^[b, c] Ville R. I. Kaila,^[a] and Job Boekhoven^{*(a, c)}

Synthetic lipid membranes have served as important models for cellular membranes. However, these static membranes do not recapitulate the dynamic nature of the biological membranes which are frequently remodeled to support cellular function. An ideal membrane model would thus also display dynamic exchange of lipids. In this work, we achieve such a system by coupling the self-assembly of peptides into membranes with a chemical reaction cycle. The reaction cycle activates and deactivates the peptides for self-assembly at the expense of a chemical fuel. The resulting membranes are dynamically remodeled, and, over their 40 min lifetime, they emerge, grow, and are torn apart before they eventually decay.

Phospholipids are the main component of biological membranes.^[1] Synthetic analogues of these phospholipids have gained significant attention over the past decades as they are ideal model systems for the biological cell membranes.^[2,3] However, a crucial difference between synthetic phospholipid membranes and biological ones lies in their dynamics, *i.e.*, synthetic phospholipid membranes are static with low lipid-exchange rates in part due to the low solubility of phospholipids, whereas biological membranes are dynamic. In the cell, new phospholipids are continuously synthesized in the Kennedy pathway while reactions in the Lands cycle remodel existing lipids.^[4] Both cycles are non-equilibrium processes that allow the cell to control its membrane morphology, to sustain its asymmetry, and remodel it on demand. A better model system for membranes would thus also include some degree of the dynamics in the building block activation and deactivation. Such a model could be used to explore fundamental mecha-

nisms in biological membrane remodeling or serve as the basis for synthetic cells.

To reconstitute the dynamic behavior of biological assemblies, researchers have previously coupled chemical reactions with a dynamic equilibrium to the activation and deactivation of membrane-forming surfactants yielding so-called dynamic covalent surfactants. For example, the dynamic imine formation from aldehydes and amines was explored to create double-tailed cationic surfactants, *in situ*. This approach resulted in the formation of dynamic micelles, vesicles, and vesicle gels.^[5–8] The dynamics were recapitulated in the rapid response of the membranes to changes in their environment.^[9,10] Others have introduced the use of lipid-like peptides and other building blocks that self-assemble into bilayers as a model for dynamic membranes.^[11–14]

Another approach to the creation of dynamic assemblies which researchers have explored is the use of dissipative self-assembly. In this form of non-equilibrium self-assembly, the dynamics of the assembly process are regulated by fuel-driven chemical reaction cycles.^[15–18] The reaction cycle comprises a minimum of two reactions, *i.e.*, an activation reaction and a deactivation reaction (Scheme 1a). In the activation, fuel is irreversibly consumed to convert a precursor into a product. In the deactivation, the activated product is spontaneously reverted to the precursor, typically by solvolysis or reaction with a ubiquitous species in the solvent. In its finite lifetime, the metastable product is capable of self-assembly, resulting in dynamic assemblies that exchange building blocks rapidly and remodeling dynamics regulated by the kinetics of the reaction cycle. For example, in the dissipative self-assembly of fibers,^[19] behavior reminiscent of dynamic instabilities in microtubules^[20,21] and oscillatory behavior between morphologies^[22] has been observed. Other examples of recently described dissipative assemblies include active droplets,^[23] hydrophobic colloids,^[24] autocatalytic micelles,^[46] the formation of clusters of nanoparticles,^[25,26] DNA-based hydrogels^[27,28] and supramolecular polymers.^[29,30] Finally, transient vesicles may be formed by an ATP-hydrolyzing reaction cycle.^[31]


In this work, we describe the dissipative assembly of vesicles driven by a reaction cycle that hydrolyzes a carbodiimide. We find that the emerging vesicles are highly dynamic and remodel through several morphologies in their limited lifetime before eventually succumbing to the inevitable decay that comes with reinstating equilibrium. We quantitatively understand the kinetics of the reaction cycle and demonstrate mechanistic insights in how the kinetics affect the self-assembly.


The precursor in our reaction cycle has a C-terminal aspartic or glutamic acid, such that it carries two carboxylates: one on the C-terminus and one on its side group. These carboxylates

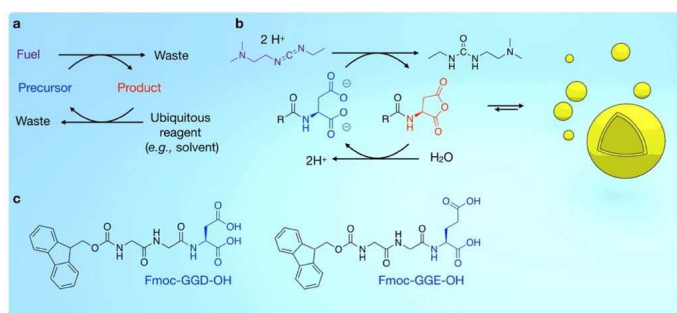
[a] C. Wanzke, A. Jussupow, Prof. Dr. V. R. I. Kaila, Prof. Dr. J. Boekhoven
Department of Chemistry
Technical University of Munich
Lichtenbergstrasse 4, 85748 Garching (Germany)
E-mail: job.boekhoven@tum.de

[b] F. Kohler, Prof. Dr. H. Dietz
Physik Department
Technical University of Munich
Am Coulombwall 4a, 85748 Garching (Germany)

[c] Prof. Dr. H. Dietz, Prof. Dr. J. Boekhoven
Institute for Advanced Study
Technical University of Munich
Lichtenbergstrasse 2a, 85748 Garching (Germany)

 Supporting information for this article is available on the WWW under <https://doi.org/10.1002/syst.201900044>

 An invited contribution to a Special Collection on Fuelled Self-Assembly
© 2019 The Authors. Published by Wiley-VCH Verlag GmbH & Co. KGaA. This is an open access article under the terms of the Creative Commons Attribution License, which permits use, distribution and reproduction in any medium, provided the original work is properly cited.



Scheme 1. Description of the chemical reaction cycle and reactants. a) The general design of a fuel-driven chemical reaction cycle. An activation reaction converts a precursor in a product driven by the irreversible consumption of fuel. A ubiquitous reactant, such as a molecule of solvent, spontaneously reacts with the product to yield the precursor; b) The reaction cycle we use to drive dissipative vesicles hydrolyzes a molecule of EDC (fuel) to EDU (waste) to form a transient anhydride; c) The chemical structures of the precursors used in this study.

can be condensed into their corresponding cyclic anhydride at the expense of a carbodiimide fuel (Scheme 1b).^[22,33] The conversion to the anhydride constitutes the activation reaction. As a fuel, we used EDC (1-ethyl-3-(3-dimethylaminopropyl) carbodiimide) which was irreversibly converted into its corresponding urea (waste). The cycle was carried out in water, and the anhydride thus hydrolyzed back to the precursor state. The latter reaction is the cycle's deactivation step. As precursors, we used the peptides Fmoc-GGD-OH and Fmoc-GGE-OH, in which Fmoc means fluorenyl-methyloxycarbonyl, G stands for glycine, D and E stand for aspartic and glutamic acid (Scheme 1c). These tripeptides were prepared on a 0.1 gram scale using solid phase peptide synthesis and preparative HPLC (high-performance liquid chromatography). The peptide purity was assessed by analytical HPLC, mass-spectroscopy and NMR (Table S1 and Figures S1, S2, S3). The precursor was dissolved at 10 mM in 200 mM MES buffer at pH 6.0. Both precursors were well-soluble at this concentration.

Upon addition of 100 mM of EDC to the solution of 10 mM Fmoc-GGD-OH, the initially transparent solution turned turbid within seconds. Importantly, the turbidity was a transient phenomenon: it rapidly increased and then decayed over 15 minutes until the original transparency was restored (Figure 1a). The turbidity was quantified by tracing the absorbance

at 500 nm wavelength, which confirmed the rapid increase and decay (Figure 1b). The turbidity was less pronounced and persisted for a shorter period when 50 mM EDC was added instead of 100 mM. The same experiments with Fmoc-GGE-OH as precursor resulted in a similar transient increase in turbidity (Figure 1c). Here, the turbidity reached lower levels but persisted for longer compared to Fmoc-GGD-OH. The emergence and decay of turbidity for both precursors upon application of EDC indicates a fuel-driven dissipative self-assembly process that leads to the formation of micrometer-scale light-scattering particles. This dissipative self-assembly process could be repeated up to three times with an addition of 50 mM EDC each before the turbidity started to fade because of the high waste concentration (Figure S4).

We used confocal laser scanning microscopy to study the nature of the transient assemblies. We added 2.5 μM of the hydrophobic dye Nile Red to a solution of 10 mM Fmoc-GGD-OH. Then, we added 100 mM EDC, to start the reaction cycle, and, every 30 seconds, we imaged the solution (Figure 2a). In the first minutes, microscopy revealed mostly spherical assemblies, with a radius in the range of 0.5 μm . Due to their small size, confocal microscopy could not resolve the exact nature of the assemblies, *i.e.*, whether they were small vesicles, colloids or droplets. After four minutes, we observed large vesicles as well as the small spherical assemblies. The large vesicles had a radius of several micrometers and we could resolve the membrane and inner compartment by confocal microscopy (Figure 2b). As time progressed, the number of these large vesicles started to increase. After 11 minutes, the number of large vesicles and smaller particles decreased until most of them had disappeared after 20 minutes. In this period, we also observed that the vesicles often had defects in the membrane (Figure 2b, white arrow).

The imaging experiments were performed in triplicate which yielded sufficient data to quantify the number of assemblies and their radii by image analysis software. The number of particles rapidly increased after the addition of the

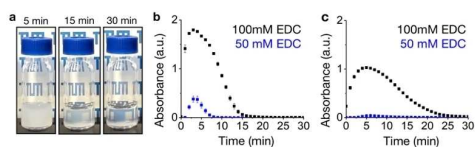


Figure 1. Macroscopic assessment of the dissipative assemblies. a) Photographs of the 10 mM Fmoc-GGD-OH fuelled with 100 mM EDC. The absorbance of 500 nm light as a function of time of b) 10 mM Fmoc-GGD-OH or c) 10 mM Fmoc-GGE-OH fuelled with 50 or 100 mM EDC. The error bar depicts the standard deviation from the average ($n=3$).

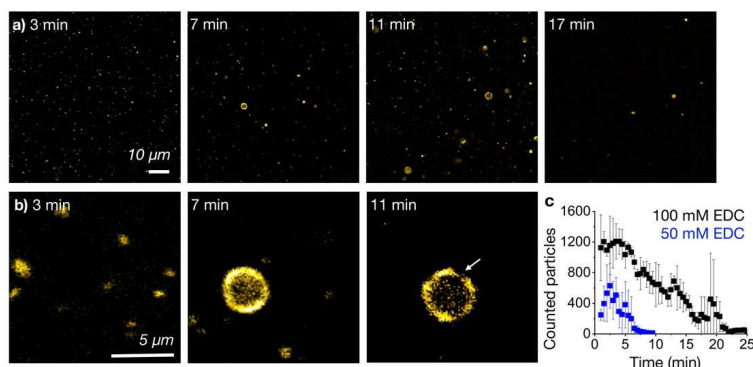


Figure 2. Microscopic assessment of the dissipative assemblies. a) Confocal micrographs of the assemblies formed by the addition of 100 mM EDC to 10 mM of Fmoc-GGD-OH. The time after the addition of EDC is indicated; b) Magnification of the micrographs as described in (a). The white arrow indicates defects in the membrane; c) The number of counted particles per micrograph (250 × 250 μm) as a function of time. The error bar depicts the standard deviation from the average ($n = 3$).

fuel. The maximum number of particles was reached after approximately 5 minutes, after which it decayed to close to zero in 20 minutes (Figure 2c). For Fmoc-GGD-OH fuelled with 50 mM EDC, we also found small spherical assemblies, but much fewer large vesicles (Figure S5). Finally, we performed a confocal microscopy study on 10 mM Fmoc-GGE-OH, fuelled with 100 mM EDC (Figure S6). We observed small spherical assemblies that could not be resolved as well as larger vesicles.

Cryogenic transmission electron microscopy (cryo-TEM) revealed that the small spherical assemblies we observed by confocal microscopy were vesicles (Figure 3). The vesicles had a radius in the range of several 100 nm, were multilamellar, and had a rugged membrane (Figure 3b). Smaller (*i.e.*, 50–100 nm) vesicles were often observed in the proximity of the large multilamellar ones (Figure 3a, black arrows). After 3 minutes of incubation with EDC, vesicles had a rugged membrane and where somewhat larger than the vesicles observed after 1 minute. After 5 minutes, the vesicles were again larger, but the ruggedness mostly smoothed out. Some vesicles had perforated membranes. After 7 minutes, the membranes looked smooth, and the holes in the membrane were less obvious. After 12 minutes, some of the vesicles had deflated, and what remained was the disrupted membranes (Figure S7). We cannot rule out that the deflation of the vesicles is a side effect from EM grid preparation. For Fmoc-GGE-OH fuelled with 100 mM EDC, we also performed a cryo-EM study and found similar results (Figure S8).

We studied the kinetics of the reaction cycle of 10 mM Fmoc-GGD-OH and 100 mM EDC by analytical HPLC and $^1\text{H-NMR}$. We followed the concentration of Fmoc-GGD-OH, its corresponding anhydride and the concentration of EDC over time by HPLC. The EDC concentration decayed throughout 40 minutes (Figure S9a). The intermediate O-acyl urea was not observed, which we previously explained by its rapid conversion to the anhydride.^[32] Indeed, the concentration of

anhydride rapidly increased in the first minutes after EDC addition (Figure S9b). After four minutes, the anhydride concentration started to decrease. The decrease in anhydride concentration meant that deactivation of anhydride was now faster than its activation. Finally, no significant amount of anhydride was detected after 40 min.

We could predict the evolution of the chemical reaction cycle quantitatively with a previously described kinetic model.^[23,32,34] The model calculates the concentration of each reactant every second in an experiment (Supporting notes 1). We used datasets from four HPLC experiments to fit the rate constants in the model. In all the experiments, the precursor concentration was kept at 10 mM, but between experiments, we varied the concentration of EDC from 25 to 100 mM (See Figure S9a–b and Table S4 for the k -values). For Fmoc-GGE-OH, we performed similar experiments (Figure S9c–d). The model describes the observed evolution of the concentration anhydride and EDC accurately (Figure 4a and S9a–d) and provides us with valuable insight into the dynamic evolution of the reaction cycle. For example, the model clarified that over the entire time when vesicles were found, the reaction cycle was dynamically operating, *i.e.*, activation and deactivation of building blocks was happening simultaneously which likely explains the dynamic evolution of the vesicles. Another insight was that we could fit the data with one set of rate constants, independent of whether assemblies were present or not (*e.g.*, 100 mM or 25 mM EDC). Through that observation, we conclude that the rate constants are not affected by the assembly process, which in turn means that hydrolysis is likely to happen both in solution or on the vesicles at equal rates.

We hypothesized that the anhydride product co-assembled with molecules of the anionic precursor. To test the hypothesis, we measured the chemical composition of the vesicle membranes by a $^1\text{H-NMR}$ spectroscopy study. We used the fact that molecules in a self-assembled state have a reduced transversal

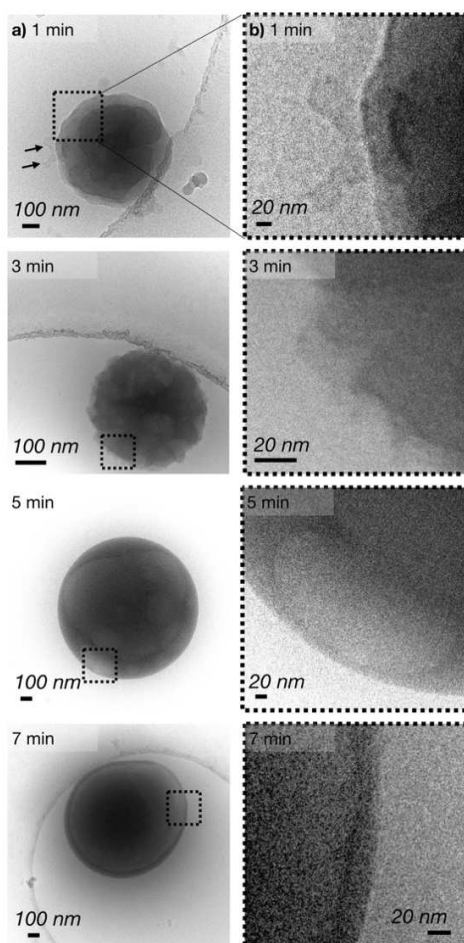


Figure 3. Microscopic assessment of the dissipative assemblies. a) Electron micrographs of the assemblies formed by the addition of 100 mM EDC to 10 mM of Fmoc-GGD-OH. The time after the addition of EDC is indicated. b) Magnification of the micrographs as described in (a).

relaxation time (T_2) which results in long correlation times followed by a broadening of the signal that gets hidden under the baseline. In other words, molecules that were part of the assembly became NMR-silent, while molecules that remained in solution were NMR-visible. That contrasts the HPLC data which measured the precursor and product concentration independent of their participation in the assembly.

Early in the cycle, the majority of the peptide was not visible by NMR spectroscopy and thus in the assemblies (Figure 4b). Even though the model predicted a maximum concentration of 2.7 mM of the anhydride product, as much as 6 mM of the

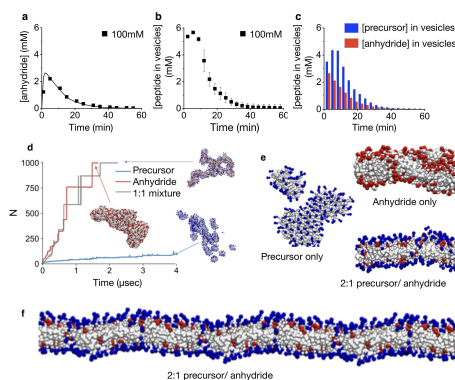


Figure 4. Kinetics and dynamics of the self-assembly process. a–c) Kinetic analysis of a sample of 10 mM Fmoc-GGD-OH fuelled with 100 mM EDC. a) The concentration anhydride against time as measured by HPLC (black markers) and calculated by the kinetic model (black line); b) The concentration peptide in an assembled state as measured by NMR; c) The concentration of precursor and product in the vesicles as a function of time; d–f) Molecular simulations of the Fmoc-GGD-OH. d) The weight-based average size of the assemblies over time. Structures of a finite (e) and infinite (f) preorganized bilayer after 5 μ s of MD simulations.

peptide was observed in the assemblies. From the NMR and kinetic model data, we can calculate the amount of precursor in the assembled state with the following Equation (1):

$$[\text{peptide}]_{\text{in vesicles}} - [\text{product}] = [\text{precursor}]_{\text{in vesicles}} \quad (1)$$

In the calculation, we assume that all the product (anhydride) is in the assemblies. The calculations show that over the entire cycle, the majority of the peptide in the vesicles is the dicarboxylate precursor (Figure 4c). The precursor in the assemblies may have either co-assembled with the product or remained in the assembly after hydrolysis of the product. The latter mechanism seems more likely given the fast hydrolysis rate of the anhydride (with a half-life of less than 1 minute, Table S4) and the fact that hydrolysis happens in solution and on the assemblies.

To further probe the molecular assembly mechanisms of the Fmoc-GGD-OH in the precursor and product forms, we performed coarse-grained molecular dynamics simulations (see Methods). We observed that both the precursor and product self-assembled and that the final structure strongly depended on the ratio of the anionic precursor and neutral product (Figure 4d–e). The precursor spontaneously assembled into small clusters of roughly 100 precursor molecules in the simulated setup (Figure 4d). The growth of larger assemblies was inhibited by the strong intermolecular electrostatic repulsion between the precursor molecules. In contrast, the anhydride product and mixtures of the product and precursor were able to spontaneously form larger assemblies. However, spontaneous formation of membranes was not observed, which is

probably due to the limited timescale of the simulation and the size of the simulated system.

Encouraged by the spontaneous self-assembly observed in the simulations, we studied the stability of pre-assembled finite bilayers with different chemical compositions as a prerequisite for the later vesicle formation process. Guided by the unbiased simulations described above, we organized the bilayer such that the hydrophobic Fmoc-groups of the precursor and product were pointing inwards, while the C-terminal residue was pointing towards the aqueous phase. We found that the bilayer was unstable and disassembled on hundreds of nanosecond timescales when it exclusively comprised the precursor (Figure 4e). In contrast, in simulations with one-third of the bilayer building blocks in the anhydride product state, the membrane remained stable on microsecond timescales. These results are also consistent with simulations on a pre-assembled membrane without border effects (Figure 4f). Finally, we found that membranes comprising exclusively product were unstable (Figure 4e and S10). The combined observations suggest there is a subtle balance between attractive and repulsive forces that need to be matched in order to form stable bilayers.

The combined data allowed us to create a tentative mechanism for the dynamic assembly of the vesicles driven by the hydrolysis of EDC (Scheme 2). Before the addition of EDC, no assemblies were present. Also, an hour after the addition of EDC, no assemblies were present. Both observations imply that the precursor, by itself, did not assemble. Within the minute after the addition of EDC, the concentration anhydride increased rapidly, while the concentration EDC decayed. Confocal microscopy, cryo-TEM, and turbidity measurements showed that the anhydride immediately started assembling into small vesicles. NMR experiments showed that the assemblies were a mixture of the precursor and product throughout the entire cycle which was supported by molecular simulations that revealed a subtle balance between the anhydride and precursor is required to form a stable membrane. Early in the cycle, the vesicles were multi-lamellar and ill-defined, which may be a result of the rapid increase of the anhydride concentration. After 5 minutes, the activation of the building block was slower than its deactivation, and the concentration building block was thus decreasing. The decrease in building blocks was also clear from the evolution of the turbidity and the evolution of the number of particles as counted by confocal microscopy, *i.e.*, all measurements showed the number of

vesicles decreased after roughly 5 minutes. In other words, new anhydride was formed, but, because its deactivation is faster than activation, the number of vesicles is decreasing. Microscopy analysis showed that, after 5 minutes, some of the vesicles had holes in their membrane, which we explain by the deactivation of the anhydride. The kinetic model has clarified that deactivation happens both in solution and on the vesicles which further backs our hypothesis. Finally, it is currently unclear how the vesicles disassemble. We hypothesize that the holes in the vesicles become larger and that the vesicle eventually dissipate entirely.

In this work, we showed the dissipative self-assembly of synthetic vesicles driven by the energy gained from the hydrolysis of a carbodiimide. These vesicles emerge in response to the addition of carbodiimide and decay when the carbodiimide runs low. As a result of the tightly coupled reaction cycle and the assembly and disassembly process, the vesicles dynamically evolve throughout the dissipative reaction cycle. That means that the vesicles are constantly remodeled by the reaction cycle. The dynamic formation of dissipative vesicles offers a new model platform to study membrane remodeling. In the future, the system could potentially help to create artificial membrane compartments.

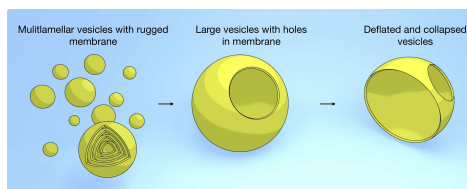
Experimental Section

Materials

1-Ethyl-3-(3-dimethylaminopropyl) carbodiimide (EDC), 2-(*N*-morpholino)ethanesulfonic acid (MES) buffer, trifluoroacetic acid (TFA) and Nile Red were purchased from Sigma-Aldrich and used without any further purification unless otherwise indicated. Tripeptides were synthesized as described as below and all the required reagents were purchased from Sigma-Aldrich. HPLC grade acetonitrile (ACN) was purchased from VWR.

Peptide Synthesis

Peptides were synthesized using standard fluoren-9-ylmethoxycarbonyl (Fmoc) solid-phase peptide synthesis on Wang resin (100–200 mesh, 1.1 mmol/g loading). Synthesis was performed on a CEM Liberty microwave-assisted peptide synthesizer. The first amino acid coupling to the resin was accomplished by using symmetrical anhydride methodology. Briefly, a 0.2 M solution of the Fmoc-amino acid symmetrical anhydride was prepared by allowing the corresponding Fmoc-protected amino acid (FmocD(OtBu)OH or FmocE(OtBu)OH, 12 mmol) and *N,N*-diisopropylcarbodiimide (DIC, 6 mmol) to react in 30 mL *N,N*-dimethylformamide (DMF) for 40 minutes. The solution was placed in the freezer for 15 minutes and the formed solid urea was filtered out before the next step. Loading of the resin was performed using the automated peptide synthesizer. The symmetrical anhydride solution (0.2 M, 12 mL) and 4-(dimethylamino)pyridine (DMAP) solution in DMF (20 mM, 2.5 mL) were added to the pre-swollen Wang resin (0.5 mmol, 1.1 mmol/g) and heated in the microwave (30 minutes, 75 °C). The coupling was repeated twice in order to increase the yield. The resin was then washed with DMF (2 × 10 mL). Before the following coupling the Fmoc protecting group was removed using a 20% solution of piperidine in DMF. The reaction mixture was heated in the microwave (1 × 1 minutes, 90 °C) and then washed with DMF (2 ×



Scheme 2. Tentative mechanism of dynamic formation and decay of dissipative vesicles.

10 mL). The cleavage was repeated twice. The coupling was achieved by using 4 equivalents (eq.) of Fmoc-glycine in DMF, 4 eq. of DIC and 4 eq. of ethyl (hydroxyimino)cyanoacetate (Oxyma). The resin solution was then heated in the microwave (1 × 2 minutes, 90 °C). This coupling was also repeated twice to increase the yield. Fmoc-cleavage and amino acid coupling were repeated as described. The tripeptide was then cleaved from the resin using a mixture (10 mL) of 50% DCM, 47.5% trifluoroacetic acid (TFA), 1.25% water, and 1.25% triisopropylsilane (TIPS) for 1.5 hours. The solvent was removed by co-distillation with ether by rotary evaporation and dried under reduced pressure. The product was purified using preparative reversed-phase high-performance liquid chromatography (HPLC, ThermoFisher Dionex Ultimate 3000, Hypersil Gold 250 × 4.8 mm) in a linear gradient of acetonitrile (ACN with 0.1% TFA, 40% to 98%) and water (with 0.1% TFA). Purified product was lyophilized and stored at −20 °C until further use. The purity of the peptide was analysed by liquid chromatography mass spectrometry (LC–MS) as well as analytical HPLC.

Sample Preparation

Stock solutions of the precursor were prepared by dissolving the precursor in 0.2 M MES buffer, after which the pH was adjusted to pH 6.0. Stock solutions of EDC were prepared by dissolving the EDC powder in MQ water. Typically, stock solutions of 2.0 M EDC were used freshly. Reaction networks were started by addition of the high concentration EDC to the peptide solution. All analysis was carried out at 25 °C.

Kinetic Model

A kinetic model was used to predict the evolution of the anhydride concentration over time. The model is described in detail in our previous work.³² The rate constants we used in this work are given in Table S4. The model is described in detail in supplementary notes 1. The Matlab-code we used is available here: <https://github.com/BoekhovenLab/Dynamic-vesicles/>

HPLC

The kinetics of the chemical reaction networks were monitored over time by means of analytical HPLC (ThermoFisher Dionex Ultimate 3000, Hypersil Gold 250 × 4.8 mm). A 750 μL sample was prepared as described above and placed into a screw cap HPLC vial. Samples of the solutions (1.0 μL) were directly injected without further dilution and tracked with a UV/Vis detector at 220 and 254 nm. All compounds involved were separated using a linear gradient of water with 0.1% TFA to ACN with 0.1% TFA from 40:60 to 2:98 in 8 minutes.

Calibration curves for the EDC (in MQ water, $\lambda_{\text{abs}} = 220$ nm) and precursors (in 0.2 M MES buffer, $\lambda_{\text{abs}} = 254$ nm) were performed in triplicate. Calibration was not possible for the anhydrides due to their intrinsic instability. Instead, the absorption coefficient of their corresponding precursor was used. Retention times and calibration values are given in Supporting Table S1, S2 and S3.

UV/Vis Spectroscopy

The UV/Vis measurements were carried out using a Multiskan FC (Thermo Fisher) microplate reader. Samples (200 μL) were directly prepared into a 96-well plate (tissue culture plate non-treated) as described above. The data was recorded at 500 nm at 25 (± 0.5) °C. We performed all measurements in triplicate.

Confocal Fluorescence Microscopy

Confocal fluorescence microscopy was performed on a Leica SP5 confocal microscope using a 63x oil immersion objective. Samples were prepared as described above, but with 2.5 μM Nile Red as dye. 20 μL of the sample was deposited on the PEG-coated glass slide and covered with a 12 mm diameter coverslip. Samples were excited with a 543 nm laser and imaged at 580–700 nm. Every 30 seconds, we acquired a 4096 × 4096 image of an area that covered 246 × 246 μm. We performed each experiment in triplicate.

Image Analysis

ImageJ's preinstalled "analyse particles" package was used to analyse the number of vesicles and their circumference under the assumption that the particles were perfectly spherical. Each data point corresponds to one image and was performed in triplicate.

Cryo-TEM

Samples for TEM were prepared as described above. The grids (C-Flat R2/2 or R4/2, 400 mesh, Cu) were freshly glow-discharged (50 mA) for 90 seconds prior to use. Preparation of the grids was performed in a FEI/Thermo Fisher Vitrobot at 25 °C with the relative humidity set to 100%. Sample (4 μL) was incubated for 30 seconds, blotted for 2.5 seconds (blotting force set to −1) and then also directly plunged into liquid ethane. The cryo-TEM grids were transferred and stored in liquid nitrogen, and when needed, placed into a Gatan cryo-transfer-specimen holder to insert into the microscope. The specimen temperature was maintained at −170 °C during the data collection. Cryo-TEM imaging was performed on a Tecnai Spirit microscope (FEI/Thermo Fisher) operating at 120 kV. The images were recorded in a low-dose mode on a CMOS camera.

LC-MS

LC–MS measurements were performed using an Agilent Technologies 1260 Infinity LC–MS system with a 6310 quadrupole spectrometer. The solvent system consisted of 0.1% formic acid in water as buffer A and 0.1% formic acid in acetonitrile as buffer B. The samples were analyzed in positive mode and followed by UV absorbance at 193, 254 and/or 280 nm.

Molecular Simulations

Coarse-grained molecular dynamics (CGMD) simulations were used to derive a molecular understanding of the assembly process of Fmoc–GGD–OH precursor/anhydride mixtures. In total 8 simulations were performed with a total length of 30 μs using Gromacs 2016.3³⁵ and the MARTINI 2.2 force field,^{36,37} with in-house parameters developed for the precursor and anhydride. We performed quantum chemical density functional theory (DFT) calculations at the B3LYP–D3/def2-TZVP level,^{38–41} performed using TURBOMOLE v. 7.2⁴² to validate the relative well-depth and anisotropic interactions between Fmoc molecules in the CG-models. Three CGMD self-assembly simulations were initiated based on random initial distributions of the simulation system. Additionally, we performed three simulations with a finite membrane bilayer, and two simulations with an infinite bilayer, where the edges of the bilayers were connected through periodic boundary conditions. Detailed information of the simulations setups is given in Table S5. All simulations were performed with periodic boundary condition. The systems were solvated and neutralized, and simulated at 310 K and 1 bar pressure, using an isothermal-isobaric (NpT) ensemble, and a timestep of 10 fs. A thermostat with a

coupling constant of $\tau_1 = 1.0 \text{ ps}^{[43]}$ was used together with the Parrinello-Rahman barostat^[44] with coupling constant of $\tau_p = 20.0 \text{ ps}$, and a compressibility of $\chi = 3.0 \times 10^{-4} \text{ bar}^{-1}$. In simulation with infinite bilayer, we employed a semi-isotropic barostat. A cut-off of 1.4 nm was used for the calculation of electrostatic and van der Waals interactions. VMD was used for analysis and visualization.^[45]

Acknowledgements

This project was supported by the German Research Foundation (DFG) through CRC/SFB 235 Project 16. J.B. is grateful for funding by the Technical University of Munich-Institute for Advanced Study, funded by the German Excellence Initiative and the European Union Seventh Framework Programme under grant agreement n° 291763 and the German Research Foundation (DFG) through CRC/SFB 863 Project B11. H.D. and F.K. acknowledge funding from the German Research Foundation via the Gottfried-Wilhelm-Leibniz Program.

Conflict of Interest

The authors declare no conflict of interest.

Keywords: dynamic self-assembly · dissipative self-assembly · remodeling · self-assembly · vesicles

- [1] G. van Meer, D. R. Voelker, G. W. Feigenson, *Nat. Rev. Mol. Cell Biol.* **2008**, *9*, 112–124.
- [2] T. Harayama, H. Riezman, *Nat. Rev. Mol. Cell Biol.* **2018**, *19*, 281–296.
- [3] Ü. Coskun, K. Simons, *Structure* **2011**, *19*, 1543–1548.
- [4] B. Wang, P. Tontonoz, *Annu. Rev. Physiol.* **2018**, *81*, 1–24.
- [5] C. B. Minkenberg, B. Homan, J. Boekhoven, B. Norder, G. J. M. Koper, R. Eelkema, J. H. van Esch, *Langmuir* **2012**, *28*, 13570–13576.
- [6] C. B. Minkenberg, W. E. Hendriksen, F. Li, E. Mendes, R. Eelkema, J. H. van Esch, *Chem. Commun.* **2012**, *48*, 9837.
- [7] C. B. Minkenberg, F. Li, P. van Rijn, L. Florusse, J. Boekhoven, M. C. A. Stuart, G. J. M. Koper, R. Eelkema, J. H. van Esch, *Angew. Chem. Int. Ed.* **2011**, *50*, 3421–3424; *Angew. Chem.* **2011**, *123*, 3483–3486.
- [8] C. B. Minkenberg, L. Florusse, R. Eelkema, G. J. M. Koper, J. H. van Esch, *J. Am. Chem. Soc.* **2009**, *131*, 11274–11275.
- [9] A. Seoane, R. J. Brea, A. Fuertes, K. A. Podolsky, N. K. Devaraj, *J. Am. Chem. Soc.* **2018**, *140*, 8388–8391.
- [10] K. Takakura, T. Yamamoto, K. Kurihara, T. Toyota, K. Ohnuma, T. Sugawara, *Chem. Commun.* **2014**, *50*, 2190–2192.
- [11] S. Zhang, *Nat. Biotechnol.* **2003**, *21*, 1171–1178.
- [12] D. G. Fatouros, D. A. Lamprou, A. J. Urquhart, S. N. Yannopoulos, I. S. Viziariakis, S. Zhang, S. Koutsopoulos, *ACS Appl. Mater. Interfaces* **2014**, *6*, 8184–8189.
- [13] A. Nagai, Y. Nagai, H. Qu, S. Zhang, *J. Nanosci. Nanotechnol.* **2007**, *7*, 2246–2252.
- [14] A. R. Sapala, S. Dhawan, V. Haridas, *RSC Adv.* **2017**, *7*, 26608–26624.
- [15] S. A. P. van Rossum, M. Tena-Solsona, J. H. van Esch, R. Eelkema, J. Boekhoven, *Chem. Soc. Rev.* **2017**, *46*, 5519–5535.
- [16] R. Merindol, A. Walther, *Chem. Soc. Rev.* **2017**, *46*, 5588–5619.
- [17] A. Sorrenti, J. Leira-Iglesias, A. J. Markvoort, T. F. A. de Greef, T. M. Hermans, *Chem. Soc. Rev.* **2017**, *46*, 5476–5490.
- [18] R. K. Grötsch, J. Boekhoven, *Self-Assem. Biomater.*, Elsevier, **2018**, pp. 235–250.
- [19] J. Boekhoven, A. M. Brizard, K. N. K. Kowgi, G. J. M. Koper, R. Eelkema, J. H. van Esch, *Angew. Chem. Int. Ed.* **2010**, *49*, 4825–4828; *Angew. Chem.* **2010**, *122*, 4935–4938.
- [20] J. Boekhoven, W. E. Hendriksen, G. J. M. Koper, R. Eelkema, J. H. van Esch, *Science* **2015**, *349*, 1075–1079.
- [21] S. Debnath, S. Roy, R. V. Uljin, *J. Am. Chem. Soc.* **2013**, *135*, 16789–16792.
- [22] J. Leira-Iglesias, A. Tassoni, T. Adachi, M. Stich, T. M. Hermans, *Nat. Nanotechnol.* **2018**, *13*, 1021–1027.
- [23] M. Tena-Solsona, C. Wanzke, B. Riess, A. R. Bausch, J. Boekhoven, *Nat. Commun.* **2018**, *9*, 2044.
- [24] B. Riefl, C. Wanzke, M. Tena-Solsona, R. K. Grötsch, C. Maity, J. Boekhoven, *Soft Matter* **2018**, *14*, 4852–4859.
- [25] R. K. Grötsch, A. Angi, Y. G. Mideksa, C. Wanzke, M. Tena-Solsona, M. J. Feige, B. Rieger, J. Boekhoven, *Angew. Chem. Int. Ed.* **2018**, *57*, 14608–14612.
- [26] R. K. Grötsch, C. Wanzke, M. Speckbacher, A. Angi, B. Rieger, J. Boekhoven, *J. Am. Chem. Soc.* **2019**, *141*, 25, 9872–9878.
- [27] L. Heinen, T. Heuser, A. Steinschulte, A. Walther, *Nano Lett.* **2017**, *17*, 4989–4995.
- [28] L. Heinen, A. Walther, *Sci. Adv.* **2019**, *9*.
- [29] A. Sorrenti, J. Leira-Iglesias, A. Sato, T. M. Hermans, *Nat. Commun.* **2017**, *8*, 15899.
- [30] J. Leira-Iglesias, A. Sorrenti, A. Sato, P. A. Dunne, T. M. Hermans, *Chem. Commun.* **2016**, *52*, 9009–9012.
- [31] S. Maiti, I. Fortunati, C. Ferrante, P. Scrimin, L. J. Prins, *Nat. Chem.* **2016**, *8*, 725–731.
- [32] M. Tena-Solsona, B. Riefl, R. K. Grötsch, F. C. Löhner, C. Wanzke, B. Käsdorf, A. R. Bausch, P. Müller-Buschbaum, O. Lieleg, J. Boekhoven, *Nat. Commun.* **2017**, *8*, 15895.
- [33] L. S. Kariyawasam, C. S. Hartley, *J. Am. Chem. Soc.* **2017**, *139*, 11949–11955.
- [34] B. Riefl, C. Wanzke, M. Tena-Solsona, R. K. Grötsch, C. Maity, J. Boekhoven, *Soft Matter* **2018**, *14*, 4852–4859.
- [35] M. J. Abraham, T. Murtola, R. Schulz, S. Páll, J. C. Smith, B. Hess, E. Lindahl, *SoftwareX* **2015**, *1–2*, 19–25.
- [36] S. J. Marrink, H. J. Risselada, S. Yefimov, D. P. Tieleman, A. H. de Vries, *J. Phys. Chem. B* **2007**, *111*, 7812–7824.
- [37] D. H. de Jong, G. Singh, W. F. D. Bennett, C. Arnarez, T. A. Wassenaar, L. V. Schäfer, X. Periole, D. P. Tieleman, S. J. Marrink, *J. Chem. Theory Comput.* **2013**, *9*, 687–697.
- [38] A. D. Becke, *J. Chem. Phys.* **1993**, *98*, 5648–5652.
- [39] C. Lee, W. Yang, R. G. Parr, *Phys. Rev. B* **1988**, *37*, 785–789.
- [40] S. Grimme, J. Antony, S. Ehrlich, H. Krieg, *J. Chem. Phys.* **2010**, *132*, 154104.
- [41] F. Weigend, R. Ahlrichs, *Phys. Chem. Chem. Phys.* **2005**, *7*, 3297.
- [42] R. Ahlrichs, M. Bär, M. Häser, H. Horn, C. Kölmel, *Chem. Phys. Lett.* **1989**, *162*, 165–169.
- [43] G. Bussi, D. Donadio, M. Parrinello, *J. Chem. Phys.* **2007**, *126*, 014101.
- [44] M. Parrinello, A. Rahman, *J. Appl. Phys.* **1981**, *52*, 7182–7190.
- [45] W. Humphrey, A. Dalke, K. Schulten, *J. Mol. Graph.* **1996**, *14*, 33–38.
- [46] S. M. Morrow, I. Colomer, S. P. Fletcher, *Nat. Commun.* **2019**, *10*, 1011.

Manuscript received: September 10, 2019
Accepted manuscript online: September 13, 2019
Version of record online: November 7, 2019

CHEMSYSTEMSCHEM

Supporting Information

© Copyright Wiley-VCH Verlag GmbH & Co. KGaA, 69451 Weinheim, 2020

Dynamic Vesicles Formed By Dissipative Self-Assembly

Caren Wanzke, Alexander Jussupow, Fabian Kohler, Hendrik Dietz, Ville R. I. Kaila, and Job Boekhoven* © 2019 The Authors. Published by Wiley-VCH Verlag GmbH & Co. KGaA. This is an open access article under the terms of the Creative Commons Attribution License, which permits use, distribution and reproduction in any medium, provided the original work is properly cited. An invited contribution to a Special Collection on Fuelled Self-Assembly

1. Supporting Tables

| name | purity [%] | structure | mass calculated [g/mol] | mass observed [g/mol] | retention time [min] (calibration value) |
|----------|----------------------------------|-----------|--|------------------------------|--|
| Fmoc-GGD | Synthesized (see methods) 97% | | Mw = 469.45 C ₂₃ H ₂₃ N ₃ O ₈ | 470.1 [Mw+H] ⁺ | 5.21 (13.03) |
| Fmoc-GGE | Synthesized (see methods) 97% | | Mw = 483.48 C ₂₄ H ₂₅ N ₃ O ₈ | 484.2 [Mw+H] ⁺ | 5.25 (11.28) |

Table S1. Characterization of precursors.

| name | structure | mass calculated [g/mol] | mass observed [g/mol] | retention time [min] (calibration value) |
|--------------------|-----------|--|------------------------------|--|
| Fmoc-GGD anhydride | | Mw = 451.44 C ₂₃ H ₂₁ N ₃ O ₇ | 452.1 [Mw+H] ⁺ | 6.39 (13.03) |
| Fmoc-GGE anhydride | | Mw = 465.46 C ₂₄ H ₂₃ N ₃ O ₇ | 466.1 [Mw+H] ⁺ | 6.19 (11.28) |

Table S2. Characterization of main products of the chemical reaction network.

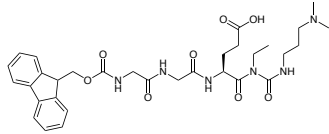
| name | structure | mass calculated [g/mol] | mass observed [g/mol] | retention time [min] |
|---------------------|---|--|------------------------------|----------------------|
| Fmoc-GGE N-acylurea |  | Mw = 638.72 C ₃₂ H ₄₂ N ₆ O ₈ | 639.3 [Mw+H] ⁺ | 6.03 |

Table S3. Characterization of the side products of the chemical reaction network.

| name | k_0 (M ⁻¹ ·s ⁻¹) | k_1 (M ⁻¹ ·s ⁻¹) | k_2 (s ⁻¹) | k_3 (s ⁻¹) | k_4 (s ⁻¹) | $t_{1/2}$ (min) |
|----------|---|---|--------------------------|--------------------------|--------------------------|-----------------|
| Fmoc-GGD | 1.35·10 ⁻⁵ | 0.09 | 0.20 | 0.10 | 0.035 | 0.33 |
| Fmoc-GGE | | 0.32 | 0.64 | 2.40 | 0.025 | 0.46 |

Table S4. Rate constant used in the kinetic model.

| Simulation type | Precursor molecules (number) | Product molecules (number) | Box size (nm x nm x nm) | Beads in simulation (number) | Simulation length (μs) |
|----------------------------------|------------------------------|----------------------------|-------------------------|------------------------------|------------------------|
| Self-assembly | 1000 | 0 | 30 x 30 x 30 | 129,919 | 4 |
| Self-assembly | 500 | 500 | 30 x 30 x 30 | 129,919 | 2 |
| Self-assembly | 0 | 1000 | 30 x 30 x 30 | 129,919 | 2 |
| Preorganized in a finite bilayer | 200 | 0 | 17 x 17 x 17 | 40,765 | 5 |
| Preorganized in a finite bilayer | 130 | 70 | 17 x 17 x 17 | 40,765 | 5 |
| Preorganized in a finite bilayer | 0 | 200 | 17 x 17 x 17 | 40,765 | 5 |

| Simulation type | Precursor molecules (number) | Product molecules (number) | Box size (nm x nm x nm) | Beads in simulation (number) | Simulation length (μ s) |
|-------------------------------------|------------------------------|----------------------------|-------------------------|------------------------------|------------------------------|
| Preorganized in an infinite bilayer | 800 | 0 | 25 x 10 x 35 | 77,473 | 1 |
| Preorganized in an infinite bilayer | 130 | 70 | 12 x 5 x 30 | 16,425 | 5 |

Table S5. Simulation type, number of precursor and product molecules, simulation box size, total number of beads, and simulation length. 130,000 beads correspond to *ca.* 2,000,000 in a full atomistic representation.

2. Supporting notes

Supporting notes 1: Description of model

A kinetic model was written in Matlab that described each reaction involved in the chemical reaction network except for the formation of the minor side reaction that formed the N-acylurea. The concentrations of each reactant were calculated for every second in the cycle. The model was used to fit the obtained HPLC data that described the evolution of the concentration of anhydride, EDC and acid over time. In all experiments, the concentration of the precursor was 10 mM.

The code for the model can be downloaded here:

<https://github.com/BoekhovenLab/Dynamic-vesicles/>

The model described five chemical reactions:

- 0) Direct hydrolysis of carbodiimide with a first order rate constant of $1.3 \times 10^{-5} \text{ sec}^{-1}$ as determined in previous work. Error! Bookmark not defined.
- 1) The formation of O-acylisourea by reaction with EDC (k_1). This second order rate constant was dependent on the nature of the precursor. The rate constant was determined for each precursor by HPLC, by monitoring the EDC consumption.
- 2) The formation of the anhydride with a first order rate constant. This rate constant could not be determined because the O-acylisourea was never observed. It was therefore set to be twice the rate of k_1 . As a result, the O-acylisourea did never reach concentrations over $1 \mu\text{M}$ in the model.
- 3) Direct hydrolysis of O-acylisourea (k_3). This reaction rate could not be obtained because the O-acylisourea was not observed. The ratio of k_2 and k_3 (anhydride formation and competing direct hydrolysis of O-acylisourea) was varied to fit the HPLC data for several concentrations of $[\text{fuel}]_0$ and $[\text{di-acid}]_0$.
- 4) Hydrolysis of anhydride proceeded with a first order rate (k_4). The rate constant was determined by HPLC for kinetic experiments where no assemblies were reached.

The rate of the hydrolysis reaction was calculated by multiplying the first order rate constant k_4 with the concentration of anhydride.

3. Supporting Figures

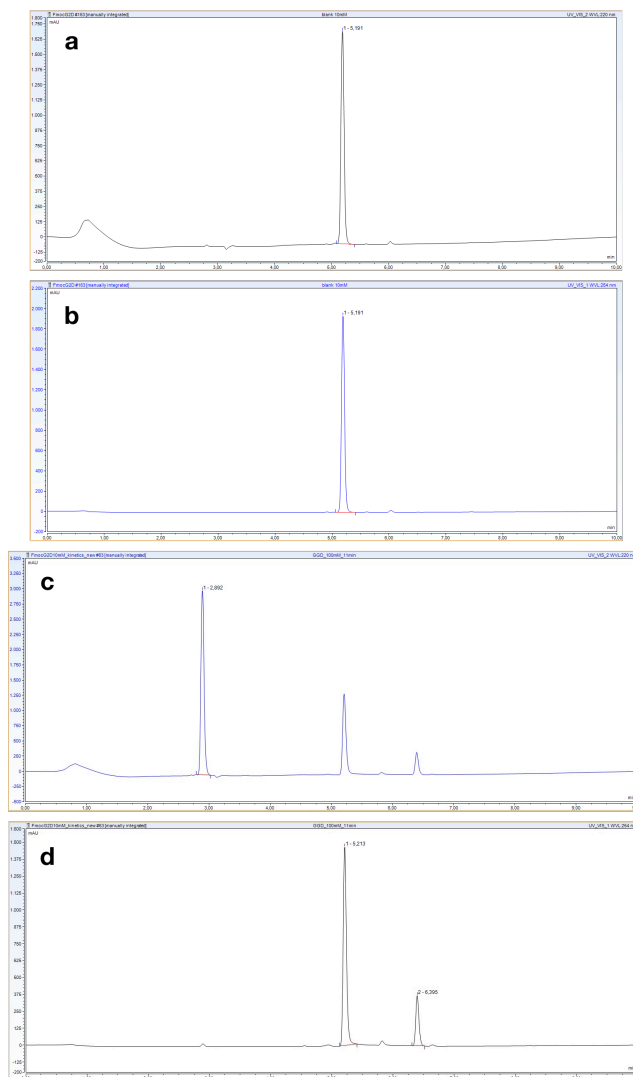


Figure S1. Example of a HPLC chromatogram of a 10 mM Fmoc-GGD-OH solution measured at a) 220 nm and b) 254 nm; as well as of the full reaction network 11 min after EDC addition measured at c) 220 nm and d) 254 nm.

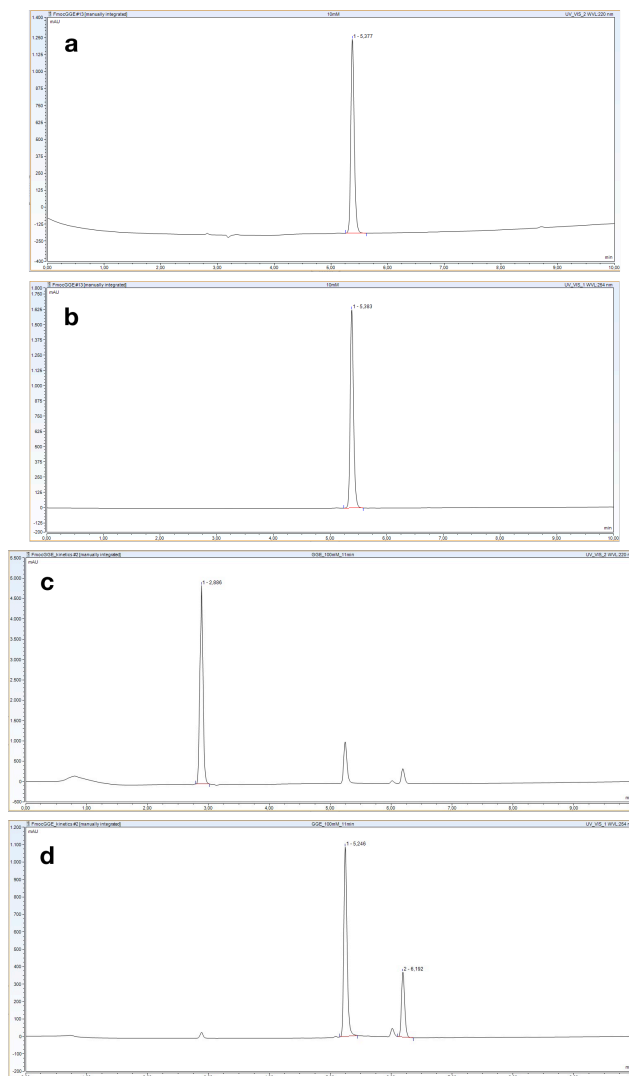


Figure S2. Example of a HPLC chromatogram of a 10 mM Fmoc-GGE-OH solution measured at a) 220 nm and b) 254 nm; as well as of the full reaction network 11 min after EDC addition measured at c) 220 nm and d) 254 nm.

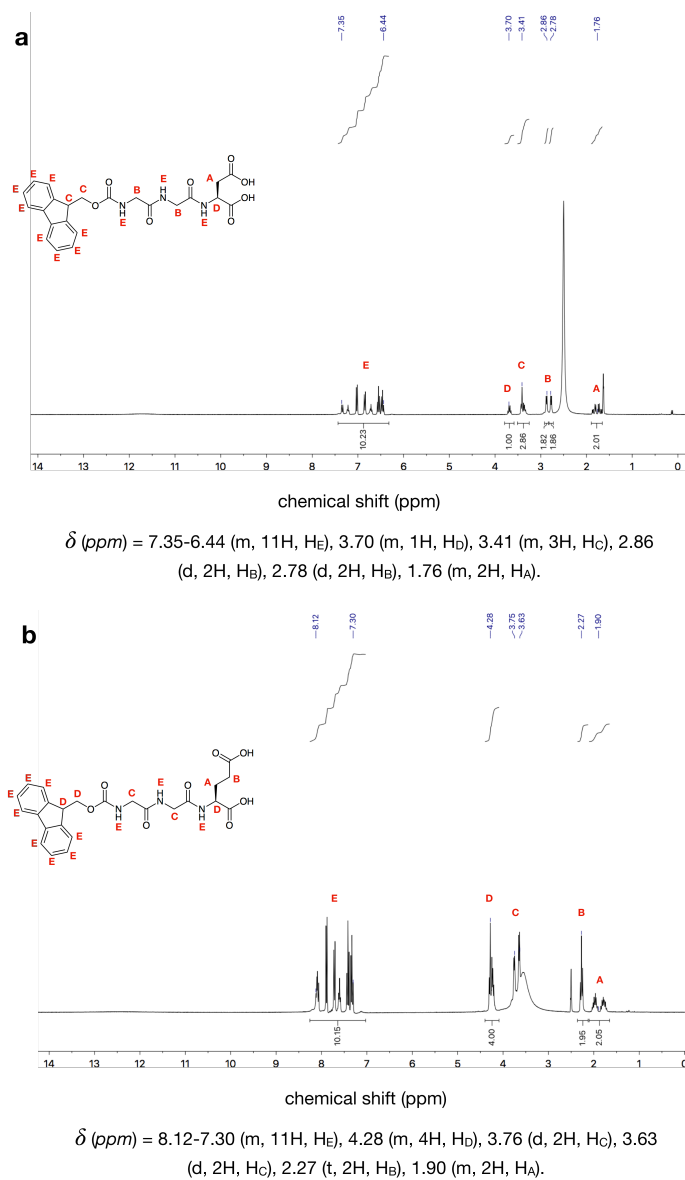


Figure S3. NMR spectrum of the precursors **a**) Fmoc-GGD-OH and **b**) Fmoc-GGE-OH in DMSO-d₆.

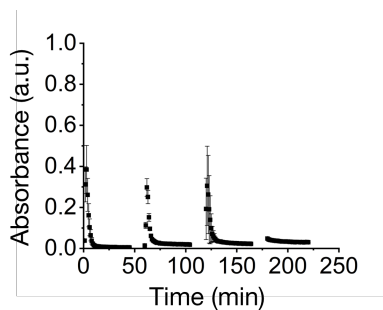


Figure S4. The absorbance of 500 nm light as a function of time of 10 mM Fmoc-GGD-OH fueled 4 times with 50 mM EDC. The error bar depicts the standard deviation from the average ($n = 3$).

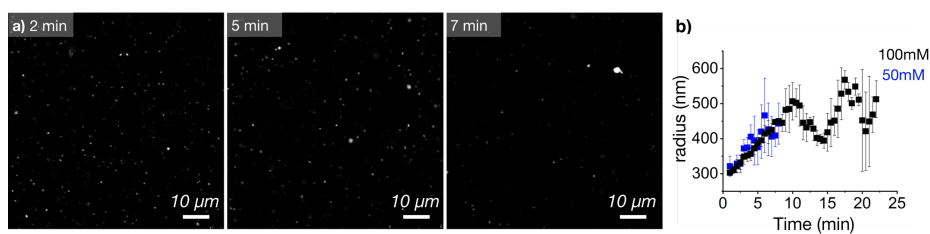


Figure S5. a) Confocal micrographs of the assemblies formed by the addition of 50 mM EDC to 10 mM of Fmoc-GGD-OH; b) Average radius of the counted particles in the confocal microscopy analysis against time for different concentrations EDC.

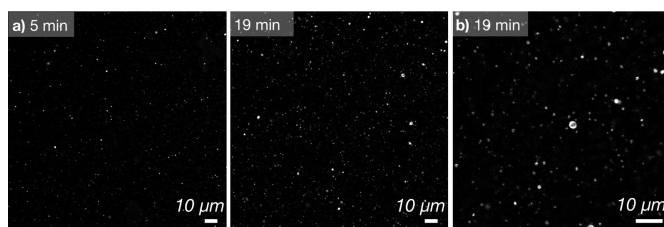


Figure S6. Confocal micrographs of the assemblies formed by the addition of 100 mM EDC to 10 mM of Fmoc-GGE-OH for a) 5 and 19 min after EDC addition and b) magnification of the micrograph.

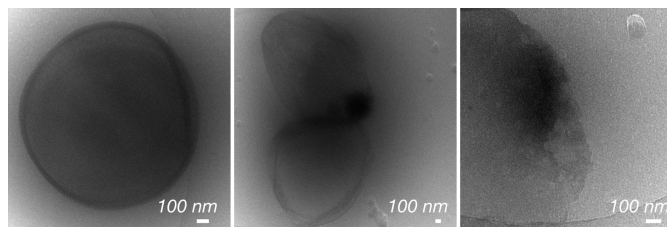


Figure S7. Cryo-TEM study of Fmoc-GGD-OH fueled with 100 mM EDC at 12 min after fuel addition.

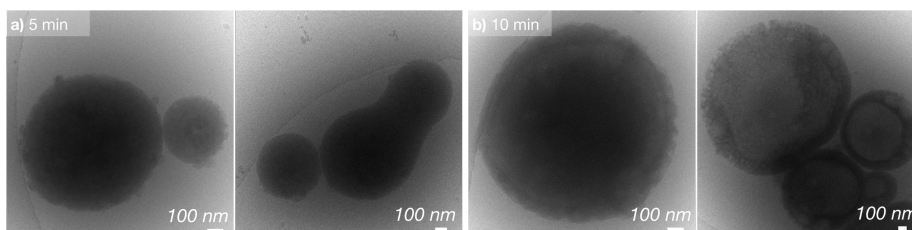


Figure S8. Cryo-TEM study of Fmoc-GGE-OH fueled with 100 mM EDC at a) 5 min and b) 10 min after fuel addition.

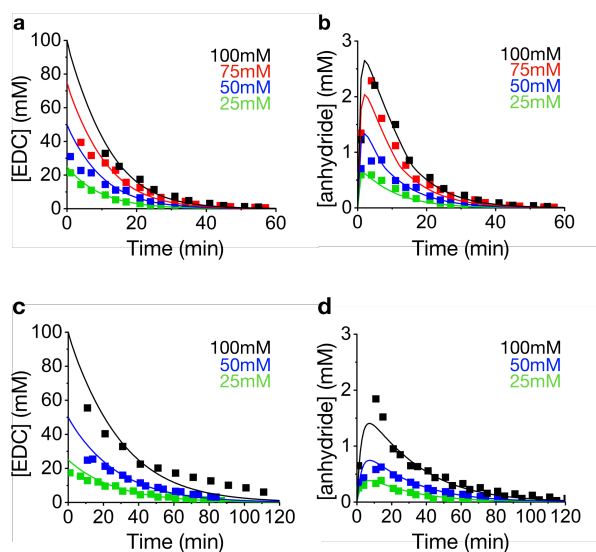


Figure S9. HPLC traces of the kinetic measurements following EDC concentration over time for a) Fmoc-GGD-OH and c) Fmoc-GGE-OH; Anhydride concentration over time for b) Fmoc-GGD-OH and d) Fmoc-GGE-OH, experimental data (squares) and fitted model traces (solid lines).

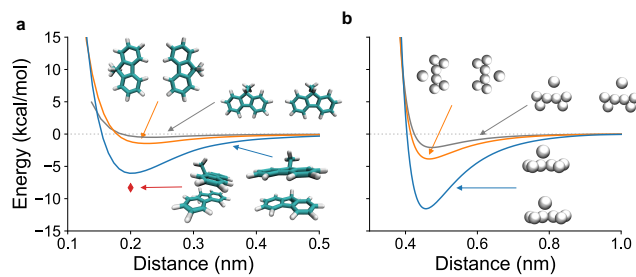


Figure S10. Anisotropic interactions between the aromatic groups of Fmoc molecules **a)** based on DFT calculation, with the geometry optimized minimum shown as a red diamond, and **b)** as modeled in the CGMD simulations.

5. Dissipative Assemblies that Inhibit Their Deactivation

Abstract.

In nature, self-assembled systems are connected with complex behavior and unique properties. Synthetic dissipative self-assembled structures are not yet endowed with such complexity. One reason is that there is no feedback between the synthetic reaction cycle and its assemblies. While working with various, short peptide sequences to design different self-assembled materials, we find that shortening the sequence of the vesicle-former Fmoc-GGD-OH that I discussed in the previous chapter to Fmoc-GD-OH creates a colloid-former with negative feedback on its own degradation. The already published example Fmoc-E-OH shows similar behavior. Thus, we focus in this publication on understanding and generalizing the mechanism of colloid formation as well as tuning the feedback. A crucial difference between other published structures and the observed colloids was the accessibility of water to the anhydride. The large, three dimensional colloids serve as hydrophobic pockets that exclude water and protect the anhydride from degradation. This limits the hydrolysis to the anhydride that is free in solution leading to a change of kinetic order and a significantly slower, constant zero-order rate. In other words, the kinetics of the hydrolysis are now depending on the solubility of the anhydride in water. We are not only able to incorporate negative feedback in our reaction cycle, but we can tune the level of it. One possibility shows that the system is switched off completely by the addition of a surfactant. Whereas, various concentrations of added salt show a tunability of the level of feedback. Interestingly, increasing feedback also provides a higher robustness to starvation periods. All in all, we demonstrated a new approach to implement feedback in dissipative reaction cycles that could lead to true complex behavior in future works.

This work has been published:

Title: Dissipative Assemblies that Inhibit Their Deactivation
Authors: Benedikt Rieß,* Caren Wanzke,* Dr. Marta Tena-Solsona, Dr. Raphael K. Grötsch, Dr. Chandan Maity, Prof. Dr. Job Boekhoven
First published: 23. May 2018
Journal: Soft Matter **2018**, *14*, 4852.
Publisher: The Royal Society of Chemistry
DOI: 10.1039/C8SM00822A

Reprinted with permission of The Royal Society of Chemistry.

This section states the individual work of each author in the publication above. C. Wanzke and B. Rieß designed and conducted all experiments. C. Wanzke synthesized and analyzed Fmoc-GD as well as Cbz-D. Furthermore, C. Wanzke imaged Fmoc-E and Fmoc-GD with a cryogenic transmission electron microscope. B. Rieß analyzed Fmoc-E and Cbz-E, studied the robustness of Fmoc-E and provided images from the fluorescence microscope. R. K. Grötsch studied Fmoc-E with DLS. M. Tena-Solsona and C. Maity helped with scientific problems. C. Wanzke, B. Rieß und J. Boekhoven wrote the manuscript. The work was performed under the supervision and guidance of J. Boekhoven.



Cite this: *Soft Matter*, 2018, 14, 4852

Received 20th April 2018,
Accepted 22nd May 2018
DOI: 10.1039/c8sm00822a

rsc.li/soft-matter-journal

Dissipative assemblies that inhibit their deactivation†

Benedikt Rieß,^{‡a} Caren Wanzke,^{‡a} Marta Tena-Solsona,^{ab} Raphael K. Grötsch,^a Chandan Maity^a and Job Boekhoven^{†*}

Dissipative self-assembly is a process in which energy-consuming chemical reaction networks drive the assembly of molecules. Prominent examples from biology include the GTP-fueled microtubule and ATP-driven actin assembly. Pattern formation and oscillatory behavior are some of the unique properties of the emerging assemblies. While artificial counterparts exist, researchers have not observed such complex responses. One reason for the missing complexity is the lack of feedback mechanisms of the assemblies on their chemical reaction network. In this work, we describe the dissipative self-assembly of colloids that protect the hydrolysis of their building blocks. The mechanism of inhibition is generalized and explored for other building blocks. We show that we can tune the level of inhibition by the assemblies. Finally, we show that the robustness of the assemblies towards starvation is affected by the degree of inhibition.

Introduction

Molecular self-assembly into various structures has received widespread attention over the past decades^{1–5} and has resulted in biomaterials,^{6,7} catalysts,⁸ molecular electronics,⁹ and many other supramolecular materials.¹⁰ Inspired by biological assemblies such as the GTP-driven assembly of microtubules,¹¹ or the ATP-fueled crosslinking of actin filaments,¹² the dissipative self-assembly of non-biological molecules has been pioneered.¹³ In dissipative assembly, the assembly process is induced by a chemical reaction network that consists of at least two chemical reactions.^{14–18} First, a precursor is activated for self-assembly by the irreversible consumption of a high-energy molecule (fuel) or photon (light). We refer to this reaction as the activation reaction. A second reaction reverts the activated product spontaneously to its initial precursor state. We refer to this reaction as the deactivation. The activated product, in its limited lifetime, can self-assemble. Researchers have described both light-driven¹⁹ and fuel-driven^{13,20} dissipative assembly.

The kinetics of the activation and deactivation control the material properties of dissipative assemblies, which makes them intrinsically different than their in-equilibrium counterparts. For example, these materials can be controlled over space

and time which opens the door to temporary materials with a predefined lifetime. To that end, researchers have developed self-erasing inks,^{21,22} hydrogels that disappear after a predefined lifetime^{22–25} colloids that can release hydrophobic molecules after a tunable time,²² and others.^{26–29} Other unique material properties of dissipative assemblies, include adaptivity and autonomous self-healing.²³

Until now, the complex behavior we find in dissipative biological assemblies, like oscillations or pattern formation,³⁰ have not been observed in artificial analogs. A reason for the discrepancy in complex behavior in dissipative assemblies is the lack of feedback mechanisms of dissipative assemblies on their chemical reaction network. For example, the assembly of tubulin into microtubules catalyzes its own deactivation.³¹ One of the goals for the field of dissipative self-assembly is thus to implement mechanisms by which the assemblies exert feedback on their activation and deactivation reaction.

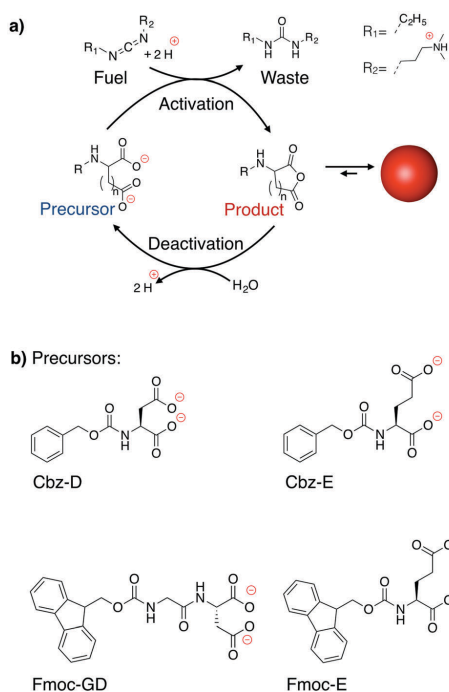
We recently introduced a new chemical reaction network that takes place in buffered water at pH 6.²² The chemical reaction network converts a dicarboxylate precursor into a transient anhydride at the expense of a carbodiimide (Scheme 1a). In the activation reaction, derivatives of aspartic (D) or glutamic (E) acid reacted with a carbodiimide to form their corresponding *O*-acylisourea. This *O*-acylisourea further reacted to form its corresponding anhydride. The reaction released one molecule of urea. We called the urea waste, as it had no further function in the cycle. Our previous study has shown that the waste does not affect the assemblies or kinetics significantly.²² In the deactivation reaction, the anhydride hydrolyzed back to the original dicarboxylate precursor. Upon addition of a finite amount of

^a Department of Chemistry, Technical University of Munich, Lichtenbergstrasse 4, 85748 Garching, Germany. E-mail: job.boekhoven@tum.de

^b Institute for Advanced Study, Technical University of Munich, Lichtenbergstrasse 2a, 85748 Garching, Germany

† Electronic supplementary information (ESI) available. See DOI: 10.1039/c8sm00822a

‡ These authors contributed equally to this work.



Scheme 1 (a) The chemical reaction network employed to drive self-assembly of anhydrides. The dicarboxylate precursor is converted into the metastable product (anhydride) by a high energy condensing agent (EDC). For Fmoc-E or Fmoc-GD as a precursor, this product is able to self-assemble into colloids. In the aqueous environment, the product is hydrolyzed back to the precursor. (b) The molecular structure of precursors used in this study.

carbodiimide fuel, the anhydride was temporarily present at the expense of the carbodiimide. Work by others demonstrated the generality of the carbodiimide induced transient anhydride formation.³²

While the dicarboxylate precursor carried two anions, the anhydride was charge-neutral. This hydrophobization converted soluble precursors into assembling anhydride products. We found that one specific precursor, *N*-fluorenylmethoxycarbonyl glutamic acid (Fmoc-E), formed colloids. These colloids significantly decreased the rate of hydrolysis of its anhydride building blocks.

In the current work, we study the underlying mechanism of the inhibition of the hydrolysis reaction in the presence of colloids. We show that the mechanism is a result of the assemblies protecting its anhydride product from deactivation and that the mechanism can be generalized for other colloid-forming anhydrides. We demonstrate that we can tune the level of the inhibition of the hydrolysis. With that control, we can manipulate the survival time of the colloids and their robustness towards periods of starvation from their energy source.

Results and discussion

Chemical reaction network

We studied the kinetics of the chemical reaction network using four different dicarboxylate precursors (Scheme 1b). Two precursors were derivatives of aspartic acid (D), while the other two were derivatives of glutamic acid (E). Of the aspartic acid derivatives, we used the *N*-carboxybenzyl protected amino acid (Cbz-D), and an *N*-fluorenylmethoxycarbonyl protected-glycine derivative (Fmoc-GD). Of the glutamic acid derivatives, we investigated Cbz-E and Fmoc-E. The anhydrides of the Cbz-amino acids were well soluble under all experimental conditions, whereas the anhydrides of Fmoc-E and Fmoc-GD assembled into colloids (*vide infra*). In all experiments, we used 10 mM solutions of the precursor in water buffered at pH 6 with MES. We added finite amounts of carbodiimide as fuel (1-ethyl-3-(3-dimethylaminopropyl)carbodiimide, EDC) to these solutions and measured the response of the chemical reaction network by high-pressure liquid chromatography and electrospray ionization mass spectroscopy (HPLC, ESI-MS, Fig. 1 and Tables S1–S3, ESI[†]). It should be noted that the reactions between fuel and Fmoc-E or Cbz-E resulted in a small amount of the *N*-acylurea (Table S3, ESI[†]) which did not interfere with the other reactions or the assemblies. Finally, we should note that our HPLC method was optimized and verified to ensure that all anhydride, be it in an assembly or not, was injected. In other words, the assembling species was not filtered out by the analysis method neither did it sediment during the experiment.

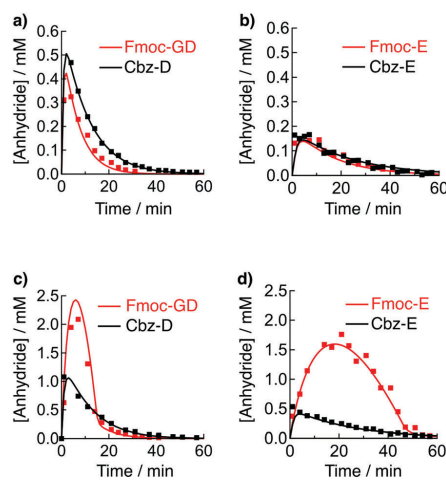


Fig. 1 Concentration anhydride against time in response to addition of EDC as determined by HPLC (markers) or the kinetic model (solid line) for (a) 10 mM Fmoc-GD (red) or Cbz-D (black) with 10 mM EDC, (b) 10 mM Fmoc-E (red) or Cbz-E (black) with 3 mM EDC, (c) 10 mM Fmoc-GD (red) or Cbz-D (black) with 25 mM EDC, (d) 10 mM Fmoc-E (red) and Cbz-E (black) with 10 mM EDC.

We recorded the concentration of the fuel, the precursor, and the product over time (Fig. 1a and b). These concentrations were used to fit a previously described kinetic model.²² The model could be used to predict the concentrations accurately when the chemical reaction network did not produce any assemblies (Fig. 1a and b, the rate constants can be found in Table S4, see Supplementary Notes 1 for a description of the kinetic model, ESI[†]). We found similar yields, reaction times and k -values for precursors based on the same terminal amino acid demonstrating that the reactivity was not drastically affected by the protecting group. For example, adding 3 mM of EDC to Cbz-E or Fmoc-E resulted in a maximum concentration of anhydride of 0.15 mM after 5 minutes.

When we added relatively large batches of fuel, differences between the evolution of the concentration product of Cbz-D and Fmoc-GD, as well as Cbz-E and Fmoc-E were evident (Fig. 1c and d). For instance, when we added 10 mM of EDC to 10 mM of Cbz-E, a maximum concentration of anhydride was found after 5 minutes at 0.42 mM whereas, for the same experiment with Fmoc-E, the maximum anhydride was a four-fold higher at 1.6 mM after 18 minutes. Similar higher anhydride concentrations and delays of the maxima were found for Fmoc-GD when compared to Cbz-D. The apparent change in the kinetics was not a result of a change in the activation kinetics as the EDC consumption showed a similar profile for Cbz-E compared to Fmoc-E as well as Cbz-D compared to Fmoc-GD (Fig. S1a and b, ESI[†]).

Morphological assessment of the assemblies

We used dynamic light scattering (DLS) to assess the nature of the assemblies of the anhydrides of Fmoc-E and Fmoc-GD. We initiated the cycle by addition of 10 mM EDC to 10 mM Fmoc-E, or 25 mM EDC to 10 mM Fmoc-GD which rapidly turned the transparent precursor solutions turbid. We measured an increase in the DLS scattering rate of at least an order of magnitude compared to before addition of fuel for both Fmoc-GD and Fmoc-E (Fig. 2a and b). The radii calculated by the fitted DLS data peaked after roughly 7 minutes at 390 nm, and after 20 minutes at 550 nm for Fmoc-GD and Fmoc-E, respectively (Fig. 2c and d). It is worth to note that these times correspond to the time of maximum anhydride concentration. The increased turbidity was temporary, and the scattering rates decreased to their original values after roughly 15 and 50 minutes, respectively. We found no evidence for assemblies when adding 10 mM or 3 mM of EDC to Fmoc-GD or Fmoc-E, respectively (Fig. 2a and b).

We utilized fluorescence microscopy with Nile Red as a hydrophobic dye to further assess the assemblies. Microscopy showed no assemblies before addition of the fuel. In contrast, minutes after addition of fuel, colloids were found for both Fmoc-GD and Fmoc-E (Fig. 3a–d). Using image analysis software on micrographs taken around 7 minutes for Fmoc-GD and 20 minutes for Fmoc-E, the radii of at least 2500 colloids were measured. The radii of the colloids were found to be in line with those found by DLS: 0.35 μm for Fmoc-GD and 0.4 μm for Fmoc-E (Fig. 3e and f). Finally, cryo-TEM microscopy further confirmed

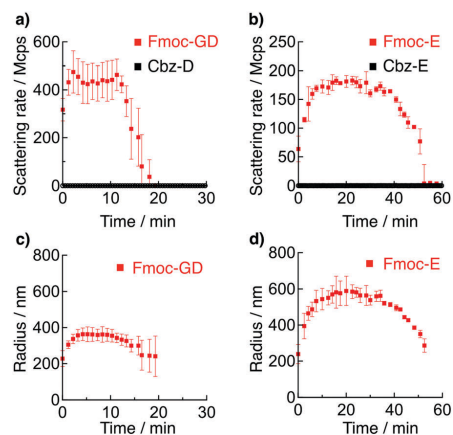


Fig. 2 Scattering rates against time as measured by DLS (a) Fmoc-GD (red) or Cbz-D (black) and 25 mM EDC, and (b) Fmoc-E (red) or Cbz-E (black) with 10 mM EDC. Note that the Cbz-based experiments did not increase the turbidity and their scattering rate thus remains around 0. (c and d) Hydrodynamic radii against time for the experiments described in a and b, respectively. We obtained no reliable data for the Cbz-based precursors because of the limited scattering. All error bars represent the standard deviation of the mean for a sample size $n = 3$.

that the colloids were already present within the first minutes of the chemical reaction network with a radius in the range of 300 to 400 nm (Fig. 3g and h). From all of the above observations, we concluded that the increased anhydride concentrations were a result of the presence of the colloids.

Mechanism of inhibition of the deactivation

In the following, we explain the mechanism of inhibition. In the presence of colloids, the activation of the anhydride remained unchanged (Fig. S1a and b, ESI[†]). The difference in the kinetics in the presence of colloids must thus be a result of the deactivation reaction. To that end, we hypothesized that the assemblies protect the anhydride from hydrolysis, *via* a simple mechanism. The colloids are relatively large and hydrophobic, which means that any anhydride in these colloids is effectively separated from the aqueous environment. In other words, the colloids protect their anhydrides from hydrolysis, but only the fraction that is found in the colloids. The anhydride that remained in solution thus remained susceptible to hydrolysis. The protection from hydrolysis explained the relatively high concentration of anhydride when colloids were formed.

To confirm our hypothesis, we adjusted the kinetic model to exclude from hydrolysis the fraction of the anhydride above the critical aggregation concentration (CAC). In other words, hydrolysis of the anhydride only occurred on the fraction that remained in solution, and hydrolysis was thus limited to a rate of $v_4 = k_4 \times \text{CAC}$. In that equation, k_4 is the first order rate constant for hydrolysis in solution. Empirically determining the CAC was challenging, given the metastability of the anhydride.

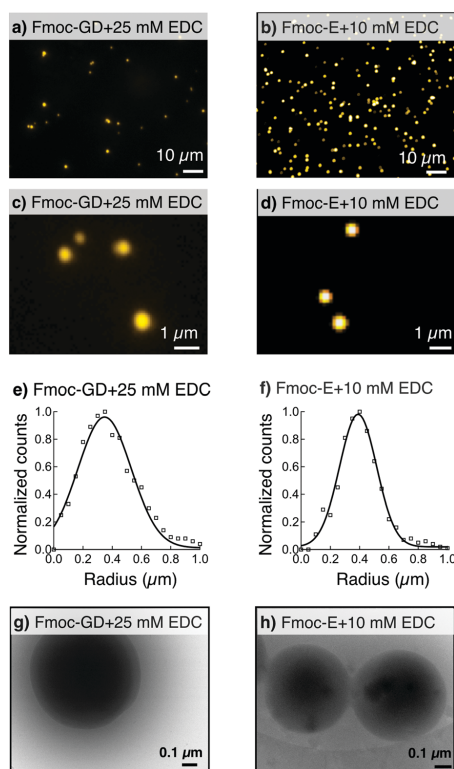


Fig. 3 Fluorescence microscopy micrographs of (a) Fmoc-GD with 25 mM EDC after roughly 7 minutes and (b) Fmoc-E with 10 mM EDC after roughly 20 minutes. Fluorescence microscopy micrographs of (c) Fmoc-GD with 25 mM EDC after roughly 7 minutes and (d) Fmoc-E with 10 mM EDC after roughly 20 minutes, with high magnification. (e and f) Histograms of the normalized colloid's radii distribution ($n > 2500$) of the micrographs of (c) and (d), respectively. Cryo-TEM of colloids under the same conditions in the first minute for (g) Fmoc-E and (h) Fmoc-GD.

Instead, we used the updated kinetic model and adjusted the CAC to fit the HPLC data (Table S4, ESI[†]). Since both k_4 and the CAC are both constants, the resulting rate is also a constant, *i.e.*, the hydrolysis followed 0th order kinetics. This rather simple addition to the kinetic model allowed us to fit all HPLC data for cycles that did or did not form assemblies (Fig. 1a–d).

Fig. 4 depicts a tentative mechanism of the evolution of the dissipative cycle. At the beginning of the cycle, the rate of building block activation was high, because the amount of fuel was at its highest. Within the first minute, the solution reached supersaturation and excess anhydride self-assembled into colloids. When these first colloids were present, we hypothesized that any activated anhydride was deposited on the existing colloids. This deposition was confirmed by the increase in radius as observed by DLS (Fig. 2). After 7 minutes

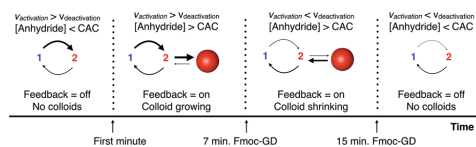


Fig. 4 Mechanism of kinetically controlled assembly into colloids during a dissipative cycle. The assemblies inhibit deactivation of anhydride (2) to carboxylate (1).

for Fmoc-GD and 20 minutes for Fmoc-E, the fuel level had decreased such that the activation rate is lower than hydrolysis rate. The net anhydride formation was thus negative, and the concentration of anhydride in the system decreased. As the hydrolysis happened in solution, the solution became undersaturated. The undersaturated solution could now accept anhydride from the colloids, resulting in a decrease of the colloids radii. Here, we assumed that anhydride disassembly from the colloids is faster than hydrolysis.³³ The colloids kept on supplying the undersaturated solution with anhydride until they had disappeared. At this point, the inhibition is switched off, and hydrolysis proceeded with first order kinetics.

While we understood the above mechanism qualitatively for Fmoc-E, we confirmed the mechanism for other colloid-forming assemblies and could quantitatively express the level of inhibition with our kinetic model. The quantitative understanding allows us to set some preliminary design rules for this type of inhibition in dissipative assemblies. First, the deactivation reaction of the assembling species needs to be driven either by reaction with the solvent or a reagent in the solvent. The assembly needs to be sufficiently large compared to its building blocks in all three dimensions, and it needs to exclude the building blocks from the solvent. We mention large in three dimensions, as we have not seen this effect in large one-dimensional fibers.²² Under these conditions, the assemblies protected their anhydride building blocks from hydrolysis. Finally, the disassembly rate is required to be faster than the hydrolysis rate, such that the rate determining step is the hydrolysis and not the exchange of building blocks between assemblies and solution.

Tuning the deactivation inhibition

We wondered if we could control the level of inhibition of the assemblies on the anhydride hydrolysis rate. We first performed experiments under conditions that prevent the self-assembly of the anhydride of Fmoc-E into the observed colloids. To do so, we added 1.0 mM of cetyltrimethylammonium bromide³⁴ (CTAB). CTAB is a common cationic surfactant with a critical micelle concentration of 0.1 mM under the employed conditions (Fig. S2, ESI[†]). We reasoned that CTAB micelles would solubilize the anhydride of Fmoc-E, thus inhibiting its self-assembly into colloids. Indeed, with CTAB, no increased turbidity was found after addition of 10 mM EDC to 10 mM Fmoc-E. HPLC analysis showed that the EDC consumption rate was similar compared to without CTAB (Fig. S1c, ESI[†]). However, the

Soft Matter

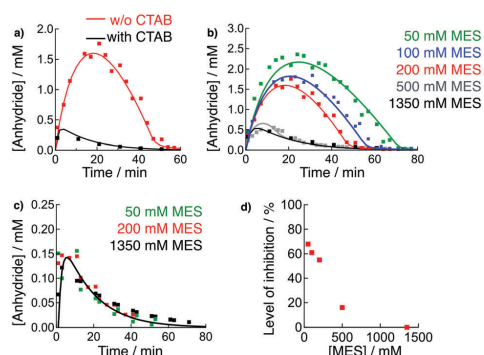


Fig. 5 (a) The concentration of Fmoc-E anhydride in response to 10 mM EDC with (black) or without (red) 1 mM of CTAB. (b) The concentration of Fmoc-E anhydride in response to 10 mM EDC with varying MES concentration. (c) The same experiment at b, but with only 3 mM of EDC. (d) Level of inhibition against the concentration of MES buffer. The inhibition level scaled between 0 and 100% where 0% is no inhibition, and 100% is complete inhibition of the hydrolysis.

anhydride concentration remained much lower compared to without CTAB (Fig. 5a). The HPLC data was fitted using the kinetic model, and we obtained a good fit by removing the inhibition mechanism (Table S4, ESI[†]). In summary, the addition of the surfactant increased the anhydride solubility and prevented the formation of colloids required for the inhibition of the deactivation.

In the next experiments, we aimed at tuning the level of inhibition by the colloids. To do so, the CAC is to be altered by minimal amounts. We found that the concentration MES buffer could tune the solubility of the precursor, *i.e.*, the more MES we added, the higher the solubility (Fig. S3, ESI[†]). Such an effect is referred to as “salting in.”³⁵ We assumed a similar trend for the anhydride of Fmoc-E. We also verified that at the relatively low buffer concentration of 50 mM MES, the buffer still had sufficient capacity to diminish fluctuations in pH (Fig. S4, ESI[†]). Addition of 10 mM EDC to 10 mM Fmoc-E in 50 mM MES buffer at pH 6 resulted in a maximum anhydride concentration around 2.5 mM (Fig. 5b). In contrast, when we performed the same experiment in 1350 mM MES, the maximum anhydride concentration was only 0.5 mM, and the evolution of the anhydride concentration resembled the one without the inhibition mechanism. To our surprise, the drastically different evolution of the chemical reaction network could be fitted by only adjusting the CAC in the kinetic model (Fig. 5b). The CAC in 200 mM MES was previously fitted to be 0.24 mM. For 50 mM MES, a good fit was obtained by decreasing the CAC to 0.17 mM. In contrast, for 1350 mM, we removed the inhibition mechanism to obtain a good fit (Fig. 5b).

As a control, we carried out a similar experiment but added only 3 mM of EDC to ensure the absence of assemblies under any of the conditions. Under these control conditions, the evolution of the anhydride concentration was similar for each

buffer concentration (Fig. 5c). We quantified the level of inhibition by calculating the 0th order hydrolysis rate as a fraction of the maximum hydrolysis rate without inhibition (Fig. 5d and Supplementary Notes 2, ESI[†] for calculations). In this calculation, 0% equals no inhibition, and 100% implies a complete inhibition of the hydrolysis.

Inhibition of deactivation makes the assemblies more robust

Finally, we set out to test the robustness of our assemblies towards periods of starvation. We fueled our assemblies with a batch of 10 mM EDC. After the fueling, we starved them from fuel for 50 minutes after which we gave them another batch of 10 mM EDC. We performed this fueling-starvation sequence for three rounds. We tested the response of two levels of inhibition: a system with an intermediate amount of inhibition ($\pm 50\%$ at 200 mM MES) and a system with a high amount of inhibition ($\pm 70\%$ at 50 mM MES). The model showed that for a low amount of inhibition, the concentration anhydride would fall below the CAC in the starvation period (Fig. 6a). In contrast, in the high inhibition experiment, the concentration would remain above the CAC throughout the experiment. In other words, in the high inhibition experiments, colloids can “survive” the entire experiment, whereas a colloid in the intermediate inhibition experiment will likely disassemble.

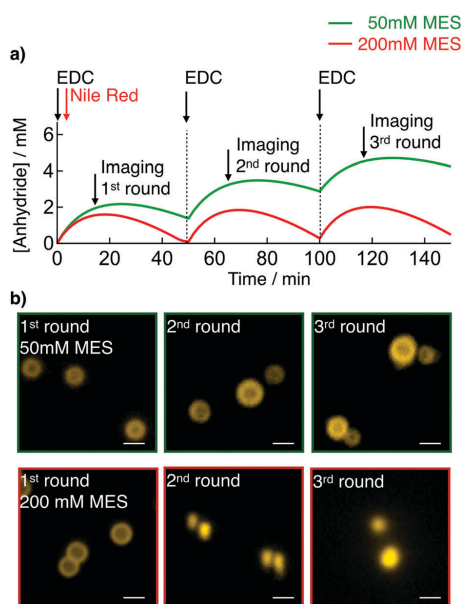


Fig. 6 (a) The concentration of anhydride against time as calculated by the kinetic model. Every 50 minutes a new batch of 10 mM EDC is added. 15 minutes after addition of EDC the solutions were imaged. (b) Micrographs of the samples as described in Fig. 4d. Scale bar corresponds to 1 μm . The left micrographs correspond to 50 mM MES and the right ones to 200 mM MES.

To confirm the survival or disassembly of the colloids, we had to mark them with a dye that could distinguish colloids that had disassembled from colloids that had remained assembled. To do so, 5 minutes after initiating the first cycle, 2.5 μM Nile Red was added. In the first 5 minutes, the colloids had grown to roughly 400 nm in radius. That means that the hydrophobic dye could only incorporate into a layer around the core of the particles, which looked like a ring under the microscope (Fig. 6b). If the colloids disassembled and reassembled later, they lost that unique dye distribution, which allowed us to distinguish them from colloids that had survived the experiment (*vide infra*). The samples were imaged 20 minutes after each fuel addition. In the first fueling round, microscopy revealed colloids of roughly 1 μm with the characteristic ring (Fig. 6b). After the 50 minute-starvation period, the second batch of fuel was added. In the second fueling round, both solutions showed particles of roughly 1 μm . In the high inhibition-experiment, microscopy showed particles, that maintained the characteristic ring, serving as a strong indication that they had survived the starvation period. In contrast, the colloids with intermediate inhibition showed a homogeneous distribution of the dye through the core of the particle (Fig. 6b). After the second starvation period, the system was refueled for the third time. The final imaging round showed similar particles as the second round.

The layered dye distribution throughout the colloids rendered them unique, and only a colloid that “survived” the entire experiment could carry the unique color code. In contrast, a particle that had disassembled would have released its dye into the solution and subsequently reincorporated it into the core of new colloids upon addition of new fuel. The coding allowed us to discriminate particles that had “survived” the starvation from particles that had “died.” These last experiments show that our colloids with a high level of inhibition all “survived” the starvation periods of 50 minutes. In contrast, the particles with low inhibition did not show the color coding and had thus fully disassembled during the starvation period.

Conclusions

Our work shows a method of incorporating a feedback mechanism into dissipative non-equilibrium assemblies. The understanding of the molecular mechanisms at play allows us to switch on or off the inhibition or to tune it. We show that increasing inhibition gives the inherently unstable assemblies increased robustness towards starvation periods.

Experimental

Materials

Fmoc-E, Cbz-E, Cbz-D, EDC, urea, MES were purchased from Sigma-Aldrich and Alfa-Aesar and used without any further purification unless otherwise indicated. Fmoc-GD was synthesized using standard fluoren-9-ylmethoxycarbonyl (Fmoc) solid-phase

peptide synthesis on Wang resin (100–200 mesh, 1.1 mmol g^{-1} loading). Peptides were synthesized on a CEM Liberty microwave-assisted peptide synthesizer. The ESI† gives a detailed description of the synthesis.

Kinetic model. We used a kinetic model to predict the evolution of the anhydride concentration over time. In brief, the kinetic model uses rate constant for six reactions in the chemical reaction network. Each second, the kinetic model calculates the concentrations of the reactants and product. The kinetic model and MatLab code are described in detail Supplementary Notes 1 (ESI†). Table S4 (ESI†) gives the rate constants.

Dynamic light scattering. We carried out DLS measurements on all solutions with a DynaPro NanoStar from Wyatt with a laser wavelength of 658 nm in disposable cuvette for DLS from Wyatt. The measurements for Fmoc-E with 10 mM EDC and Fmoc-GD with 25 mM EDC consisted of 5 acquisitions with an acquisition time of 10 seconds. The remaining experiments consisted of 1 acquisition with an acquisition time of 5 seconds. For measurements and analysis, we used the software Dynamics V7.

HPLC. We monitored the kinetics of the chemical reaction networks over time by using analytical HPLC (HPLC, Thermo-fisher Dionex Ultimate 3000, Hypersil Gold 250 \times 4.8 mm). A 750 μL sample was prepared as described above and placed into a screw cap HPLC vial. We injected samples of the solutions directly, without further dilution. The HPLC separated all compounds involved using a linear gradient of water with 0.1% TFA:ACN with 0.1% TFA from 40:60 to 2:98.

We performed calibration curves for the EDC ($\lambda_{\text{abs}} = 220 \text{ nm}$) and precursors ($\lambda_{\text{abs}} = 254 \text{ nm}$) in triplicate. Calibration was not possible for the anhydrides due to their intrinsic instability. Instead, we used the absorption coefficient of their corresponding precursor.

Fluorescence microscopy. Fluorescence microscopy was performed on a Leica DMI8 microscope using a 63 \times oil immersion objective. We prepared samples as described above but with 25 μM Nile Red as a dye. We deposited 20 μL of the sample on the glass slide and covered with a 12 mm diameter coverslip. Samples were excited with 543 nm laser and imaged at 580–700 nm. Particle diameters were counted using ImageJ cell counting package.

ESI-MS. ESI-MS measurements were performed using a Varian 500 MS LC ion trap spectrometer. The samples were diluted in acetonitrile and injected into an acetonitrile carrier flow (20 $\mu\text{L min}^{-1}$).

Cryogenic-transmission electron microscopy (cryo-TEM). Samples for TEM were prepared as described above. The grids (Quantifoil R2/2 on Cu-grid 400 mesh) were freshly glow-discharged for 30 (Fmoc-GD) or 90 seconds (Fmoc-E) before use. Preparation of the grids was performed in an FEI/Thermo Fisher Vitrobot at 25 $^{\circ}\text{C}$ with the relative humidity set to 100%. Fmoc-GD (5 μL) was incubated for 30 seconds, blotted twice for 3.5 seconds (blotting force set to -5) and then directly plunged into liquid ethane that was pre-cooled by liquid nitrogen. Fmoc-E (5 μL) was incubated for 15 seconds, blotted for 2 seconds (blotting force set to -1) and then also directly plunged into liquid ethane.

The cryo-EM grids were transferred and stored in liquid nitrogen, and when needed, placed into a Gatan cryo-transfer-specimen holder to insert into the microscope. The specimen temperature was maintained at $-170\text{ }^{\circ}\text{C}$ during the data collection. Cryo-TEM imaging of Fmoc-GD was performed on a Jeol JEM-1400 plus operating at 120 kV, and Cryo-TEM imaging of Fmoc-E was performed on a Tecnai Spirit microscope (FEI/Thermo Fisher) operating at 120 kV. The images were recorded in a low-dose mode on a CCD camera.

Solubility determination of precursors. The samples of Fmoc-E (10 mM) were prepared as described above in different buffer concentrations (50, 100, 200, 500 and 1350 mM MES). After the pH was adjusted to 1, the precipitate was filtered off with a 200 nm syringe filter. HPLC analysis was carried out like described above to determine the remaining Fmoc-E in solution.

Sample preparation. Stock solutions of the precursor were prepared by dissolving the precursor in MES buffer, after which the pH was adjusted to pH 6.0. Stock solutions of EDC were prepared by dissolving the EDC powder in MQ water. Typically, stock solutions of 1.0 M EDC were used freshly. Reaction networks were started by addition of the high concentration EDC to the peptide solution. All analysis was carried out at $25\text{ }^{\circ}\text{C}$.

Conflicts of interest

There are no conflicts to declare.

Acknowledgements

J. B. is grateful for funding by the Technical University of Munich – Institute for Advanced Study, funded by the German Excellence Initiative and the European Union Seventh Framework Programme under grant agreement no. 291763. B. R. acknowledges the Deutsche Forschungsgemeinschaft within the SFB No. 863. R. G. is grateful for funding by the International Research Training Group ATUMS (IRTG 2022). M. T. S. acknowledges the European Union's Horizon 2020 Research and Innovation program for the Marie Skłodowska Curie Fellowship under grant agreement no. 747007.

References

- J. D. Hartgerink, E. Beniash and S. I. Stupp, *Science*, 2001, **294**, 1684–1688.
- J. P. Hill, W. Jin, A. Kosaka, T. Fukushima, H. Ichihara, T. Shimomura, K. Ito, T. Hashizume, N. Ishii and T. Aida, *Science*, 2004, **304**, 1481–1483.
- P. A. Korevaar, S. J. George, A. J. Markvoort, M. M. Smulders, P. A. Hilbers, A. P. Schenning, T. F. De Greef and E. W. Meijer, *Nature*, 2012, **481**, 492–496.
- A. Lampel, S. A. McPhee, H. A. Park, G. G. Scott, S. Humagain, D. R. Hekstra, B. Yoo, P. W. J. M. Frederix, T. D. Li, R. R. Abzalimov, S. G. Greenbaum, T. Tuttle, C. Hu, C. J. Bettinger and R. V. Ulijn, *Science*, 2017, **356**, 1064–1068.
- P. W. Rothmund, *Nature*, 2006, **440**, 297–302.
- G. A. Silva, C. Czeisler, K. L. Niece, E. Beniash, D. A. Harrington, J. A. Kessler and S. I. Stupp, *Science*, 2004, **303**, 1352–1355.
- F. Tantakitti, J. Boekhoven, X. Wang, R. V. Kazantsev, T. Yu, J. Li, E. Zhuang, R. Zandi, J. H. Ortony, C. J. Newcomb, L. C. Palmer, G. S. Shekhawat, M. O. de la Cruz, G. C. Schatz and S. I. Stupp, *Nat. Mater.*, 2016, **15**, 469.
- M. D. Pluth, R. G. Bergman and K. N. Raymond, *Science*, 2007, **316**, 85–88.
- Y. Yamamoto, T. Fukushima, Y. Suna, N. Ishii, A. Saeki, S. Seki, S. Tagawa, M. Taniguchi, T. Kawai and T. Aida, *Science*, 2006, **314**, 1761–1764.
- J. Boekhoven and S. I. Stupp, *Adv. Mater.*, 2014, **26**, 1642–1659; D. B. Amabilino, D. K. Smith and J. W. Steed, *Chem. Soc. Rev.*, 2017, **46**, 2404–2420.
- A. Desai and T. J. Mitchison, *Annu. Rev. Cell Dev. Biol.*, 1997, **13**, 83–117.
- S. Köhler, V. Schaller and A. R. Bausch, *Nat. Mater.*, 2011, **10**, 462–468.
- J. Boekhoven, A. M. Brizard, K. N. Kowli, G. J. Koper, R. Eelkema and J. H. van Esch, *Angew. Chem., Int. Ed.*, 2010, **49**, 4825.
- S. A. P. van Rossum, M. Tena-Solsona, J. H. van Esch, R. Eelkema and J. Boekhoven, *Chem. Soc. Rev.*, 2017, **46**, 5519–5535.
- A. Sorrenti, J. Leira-Iglesias, A. J. Markvoort, T. F. de Greef and T. M. Hermans, *Chem. Soc. Rev.*, 2017, **46**, 5476–5490.
- L. Heinen and A. Walther, *Soft Matter*, 2015, **11**, 7857–7866.
- F. Della Sala, S. Neri, S. Maiti, J. L. Chen and L. J. Prins, *Curr. Opin. Biotechnol.*, 2017, **46**, 27–33.
- R. Merindol and A. Walther, *Chem. Soc. Rev.*, 2017, **46**, 5588–5619.
- J. J. de Jong, P. R. Hania, A. Pugzlys, L. N. Lucas, M. de Loos, R. M. Kellogg, B. L. Feringa, K. Duppen and J. H. van Esch, *Angew. Chem., Int. Ed.*, 2005, **44**, 2373–2376.
- C. G. Pappas, I. R. Sasselli and R. V. Ulijn, *Angew. Chem., Int. Ed.*, 2015, **54**, 8119–8123.
- R. Klajn, P. J. Wesson, K. J. Bishop and B. A. Grzybowski, *Angew. Chem., Int. Ed.*, 2009, **48**, 7035–7039.
- M. Tena-Solsona, B. Rief, R. K. Grötsch, F. C. Löhner, C. Wanzke, B. Käsdorf, A. R. Bausch, P. Müller-Buschbaum, O. Lieleg and J. Boekhoven, *Nat. Commun.*, 2017, **8**, 15895.
- T. Heuser, A.-K. Steppert, C. Molano Lopez, B. Zhu and A. Walther, *Nano Lett.*, 2014, **15**, 2213–2219.
- C. G. Pappas, I. R. Sasselli and R. V. Ulijn, *Angew. Chem., Int. Ed.*, 2015, **54**, 8119–8123.
- J. Boekhoven, W. E. Hendriksen, G. J. Koper, R. Eelkema and J. H. van Esch, *Science*, 2015, **349**, 1075–1079.
- S. Maiti, I. Fortunati, C. Ferrante, P. Scrimin and L. J. Prins, *Nat. Chem.*, 2016, **8**, 725–731.
- T. Heuser, A.-K. Steppert, C. Molano Lopez, B. Zhu and A. Walther, *Nano Lett.*, 2014, **15**, 2213–2219.

[View Article Online](#)

Paper

Soft Matter

- 28 J. Leira-Iglesias, A. Sorrenti, A. Sato, P. A. Dunne and T. M. Hermans, *Chem. Commun.*, 2016, **52**, 9009–9012.
- 29 A. Sorrenti, J. Leira-Iglesias, A. Sato and T. M. Hermans, *Nat. Commun.*, 2017, **8**, 15899.
- 30 F. J. Ndlec, T. Surrey, A. C. Maggs and S. Leibler, *Nature*, 1997, **389**, 305–308.
- 31 S. Roychowdhury and M. M. Rasenick, *Biochemistry*, 1994, **33**, 9800–9805.
- 32 L. S. Kariyawasam and C. S. Hartley, *J. Am. Chem. Soc.*, 2017, **139**, 11949–11955.
- 33 We can make this hypothesis because we find no delay between the kinetic of the chemical reaction network and the size or presence of the colloids. For example, the maximum size of the colloids is obtained at the same time as the maximum anhydride concentration, and the colloids disappear at exactly the moment the anhydride concentration falls below its solubility.
- 34 J. M. Neugebauer, *Methods Enzymol.*, 1990, **182**, 239–253.
- 35 P. Lo Nostro and B. W. Ninham, *Chem. Rev.*, 2012, **112**, 2286–2322.

Electronic Supplementary Material (ESI) for Soft Matter.
This journal is © The Royal Society of Chemistry 2018

Dissipative assemblies that inhibit their deactivation

Benedikt Rieß,^a Caren Wanzke,^a Marta Tena-Solsona,^{a,b} Raphael K. Grötsch,^a Chandan Maity,^a Job Boekhoven^{a,b}

Fmoc-GD synthesis. Fmoc-GD was synthesized using standard fluoren-9-ylmethoxycarbonyl (Fmoc) solid-phase peptide synthesis on Wang resin (100-200 mesh, 1.1 mmol/g loading). Synthesis was performed on a CEM Liberty microwave-assisted peptide synthesizer. The first amino acid coupling to the resin was accomplished by using symmetrical anhydride methodology. Briefly, a 0.2 M solution of the Fmoc-FmocD(OtBu)OH symmetrical anhydride was prepared by allowing the corresponding Fmoc-protected amino acid (FmocD(OtBu)OH, 12 mmol) and *N,N'*-diisopropylcarbodiimide (DIC, 6 mmol) to react in 30 mL *N,N*-dimethylformamide (DMF) for 40 minutes. The solution was placed in the freezer for 15 minutes and the solid urea formed was filtered out before next step. Loading of the resin was performed using the automated peptide synthesizer. The symmetrical anhydride solution (0.2 M, 12 mL) and 4-(dimethylamino)pyridine (DMAP) solution in DMF (20 mM, 2.5 mL) were added to the pre-swollen Wang resin (0.5 mmol, 1.1 mmol/g) and heated in the microwave (30 minutes, 75 °C). The coupling was repeated twice in order to increase the yield. The resin was then washed with DMF (2x10 mL). Before the following coupling the Fmoc protecting group was removed using a 20% solution of piperidine in DMF. The reaction mixture was heated in the microwave (1x1 minutes, 90 °C) and then washed with DMF (2x10 mL). The coupling was achieved by using 4 equivalents (eq.) of Fmoc-glycine in DMF, 4 eq. of DIC and 4 eq. of ethyl (hydroxyimino)cyanoacetate (Oxyma). The resin solution was then heated in the microwave (1x2 minutes, 90 °C). This coupling was also repeated twice to increase the yield. The peptide was then cleaved from the resin using a mixture (10 mL) of 50% DCM, 47.5% trifluoroacetic acid (TFA), 1.25% water, and 1.25% triisopropylsilane (TIPS). The solvent was removed by co-distillation with ether by rotary evaporation and dried under reduced pressure. The product was purified using reversed-phase high-performance liquid chromatography (HPLC, Thermofisher Dionex Ultimate 3000, Hypersil Gold 250x4.8 mm) in a linear gradient of acetonitrile (ACN with 0.1% TFA, 40% to 98%) and water with 0.1% TFA. Purified product was lyophilized and stored at -20 °C until further use. The purity of the peptide was analysed by electrospray ionization mass spectrometry in positive mode (ESI-MS) as well as analytical HPLC (Thermofisher *Dionex* Ultimate 3000, eluted with a gradient of 0.1% TFA in water: 0.1% TFA in ACN from 40:60 to 2:98 in 10 minutes, see below for results).

Supplementary Methods

Sample preparation. Stock solutions of the precursor were prepared by dissolving the precursor in MES buffer, after which the pH was adjusted to pH 6.0. Stock solutions of EDC were prepared by dissolving the EDC powder in MQ water. Typically, stock solutions of 1.0 M EDC were used freshly. Reaction networks were started by addition of the high concentration EDC to the peptide solution. All analysis was carried out at 25°C.

Supporting Figures

Supporting Table 1: Assessment of the used materials and their purity

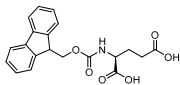
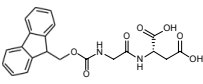
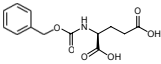
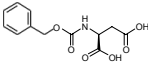
| name | purity [%] | structure | mass calculated [g/mol] | mass observed [g/mol] | retention time [min] |
|---------|-------------------------------|---|--|-------------------------------|----------------------|
| Fmoc-E | Commercial: 95% |  | Mw = 369.12 C ₂₀ H ₁₉ NO ₆ | 392.1 [Mw+Na] ⁺ | 6.14 |
| Fmoc-GD | Synthesized (see methods) 97% |  | Mw = 412.13 C ₂₁ H ₂₀ N ₂ O ₇ | 435.0 [Mw+Na] ⁺ | 5.61 |
| Cbz-E | Commercial: 97% |  | Mw = 281.09 C ₁₃ H ₁₅ NO ₆ | 304.1 [Mw+Na] ⁺ | 4.51 |
| Cbz-D | Commercial: 99% |  | Mw = 267.07 C ₁₂ H ₁₃ NO ₆ | 290.9 [Mw+Na] ⁺ | 4.47 |

Table S1. Characterization of precursors.

Supporting Table 2: Assessment of the products

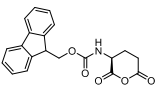
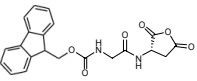
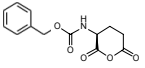
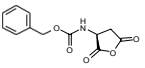
| name | structure | mass calculated [g/mol] | mass observed [g/mol] | retention time [min] |
|-------------------|---|--|--------------------------------|----------------------|
| Fmoc-E anhydride |  | Mw = 351.11 C ₂₀ H ₁₇ NO ₅ | 373.9 [Mw+Na] ⁺ | 7.68 |
| Fmoc-GD anhydride |  | Mw = 394.12 C ₂₁ H ₁₈ N ₂ O ₆ | 417.2 [Mw+Na] ⁺ | 7.02 |
| Cbz-E anhydride |  | Mw = 263.08 C ₁₃ H ₁₃ NO ₅ | 286.1 [Mw+Na] ⁺ | 6.14 |
| Cbz-D anhydride |  | Mw = 249.06 C ₁₂ H ₁₁ NO ₅ | 272.22 [Mw+Na] ⁺ | 6.36 |

Table S2. Characterization of main products of the chemical reaction network.

Supporting Table 3

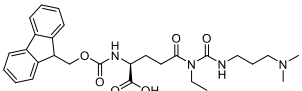
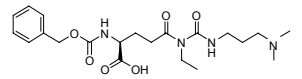
| name | structure | mass calculated [g/mol] | mass observed [g/mol] | retention time [min] |
|-------------------|---|--|-------------------------------|----------------------|
| Fmoc-E N-acylurea |  | Mw = 524.26 C ₂₈ H ₃₆ N ₄ O ₆ | 525.5 [Mw+H] | 6.97 |
| Cbz-E N-acylurea |  | Mw = 436.23 C ₂₁ H ₃₂ N ₄ O ₆ | 459.4 [Mw+Na] ⁺ | 4.82 |

Table S3. Characterization of the side products of the chemical reaction network.

Supporting Table 4

| Precursor | k ₁ (M ⁻¹ x sec ⁻¹) | k ₂ (sec ⁻¹) | k ₃ (sec ⁻¹) | k ₄ (sec ⁻¹) | CAC (mM) |
|-----------|---|-------------------------------------|-------------------------------------|-------------------------------------|-------------------------------|
| Cbz-D | 8.0*10 ⁻² | 2xk ₁ | 1.5xk ₁ | 1.5*10 ⁻² | N/A |
| Fmoc-GD | 11*10 ⁻² | 2xk ₁ | 1.5xk ₁ | 2.0*10 ⁻² | 0.60 (200 mM MES) |
| Cbz-E | 3.5*10 ⁻² | 2xk ₁ | 0.5xk ₁ | 1.0*10 ⁻² | N/A |
| Fmoc-E | 5.0*10 ⁻² | 2xk ₁ | 1.5xk ₁ | 0.75*10 ⁻² | N/A (1350 mM MES) |
| Fmoc-E | 5.0*10 ⁻² | 2xk ₁ | 1.5xk ₁ | 0.75*10 ⁻² | 0.45 (500 mM MES) |
| Fmoc-E | 5.0*10 ⁻² | 2xk ₁ | 1.5xk ₁ | 0.75*10 ⁻² | 0.24 (200 mM MES) |
| Fmoc-E | 5.0*10 ⁻² | 2xk ₁ | 1.5xk ₁ | 0.75*10 ⁻² | 0.21 (100 mM MES) |
| Fmoc-E | 5.0*10 ⁻² | 2xk ₁ | 1.5xk ₁ | 0.75*10 ⁻² | 0.17 (50 mM MES) |
| Fmoc-E | 5.0*10 ⁻² | 2xk ₁ | 1.5xk ₁ | 0.75*10 ⁻² | N/A (200 mM MES+1 mM CTAB) |

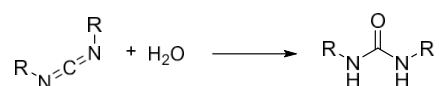
Table S4. Rate constant used in the kinetic model.

Supporting notes 1: Description of model

A kinetic model was written in MATLAB that described five reactions involved in the chemical reaction network except. It did not include minor side reaction that formed the N-acylurea. The concentrations of each reactant were calculated for every 1 second in the cycle. The model was used to fit the obtained HPLC data that described the evolution of the concentration of anhydride, EDC and acid over time. In all experiments, the concentration of the precursor was 10 mM. For all precursor/product combinations, at least three different batch sizes of fuel were used to obtain an accurate fit (e.g. 10 mM Cbz-D + 10, 25 and 50 mM of EDC).

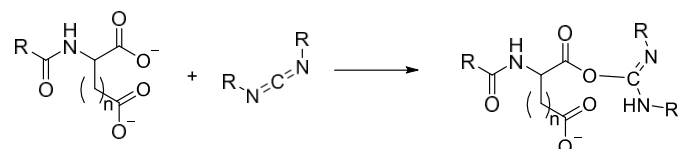
In the model, the following reactions were taken into account:

Reaction 0 (k_0)



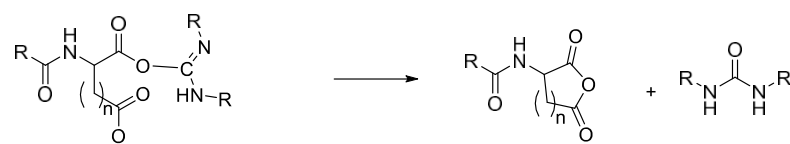
The direct hydrolysis of carbodiimide with a first order rate constant of $1.3 \times 10^{-5} \text{ sec}^{-1}$ as determined by HPLC in previous work.²² In the experiments, this reaction is irrelevant as it is so slow.

Reaction 1 (k_1)



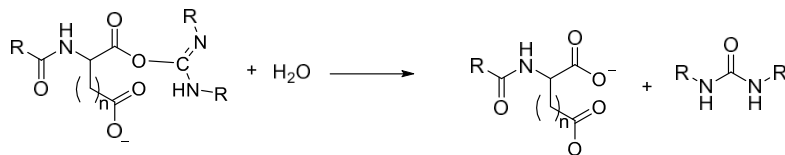
The formation of O-acylisourea by reaction with EDC with a second order rate constant that was dependent on the nature of the precursor (Table S4). The rate constant was determined for all precursors by HPLC, by monitoring the EDC consumption.

Reaction (k_2)



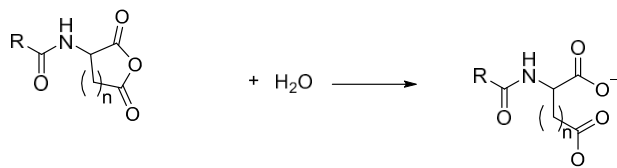
The formation of anhydride with a first order rate constant (Table S4). This rate constant could not be determined because the O-acylisourea was never observed. It was therefore set to be twice the rate of k_1 . As a result, the O-acylisourea did never reach concentrations over $1 \mu\text{M}$ in the model.

Reaction 3 (k_3)



The direct hydrolysis of O-acylisourea with a first order rate constant (Table S4). This reaction rate could not be obtained because the O-acylisourea was not observed. The ratio of k_2 and k_3 (anhydride formation and competing direct hydrolysis of O-acylisourea) was varied to fit the HPLC data for several concentrations of $[\text{fuel}]_0$ and $[\text{di-acid}]_0$.

Reaction 4 (k_4)



The hydrolysis of anhydride proceeded with a (pseudo)-first order rate as determined by HPLC (Table S4). This reaction describes the hydrolysis on the fraction of anhydride in solution. When the concentration was greater than the solubility of the anhydride, only the fraction that remained in solution was taken into account. In other words, above the solubility the rates was calculation by $k_4 \cdot \text{CAC}$.

The model that takes into account all these equations in MATLAB code:

```

%//// SETUP ////
clf, clear
hr = 3600; %amount of seconds per hour
t = 1*hr; %amount of hours to be calculated
plot_EDC = 0; %Plot the [EDC]? (0 or 1 for yes or no)
plot_ANH = 1; %Plot the [anhydride]? (0 or 1 for yes or no)

%///// SET THE INITIAL CONCENTRATIONS/////
COOH(1) = 0.02; %Concentration COOH groups in M (i.e. 0.020 mM for 10 mM fmoc-GD)
EDC(1) = 25/1000; %concentration EDC in M
COOEDC(1) = 0; %concentration O-acylurea in M
COOOC(1) = 0; %concentration O-acylurea in M

%/////SETTHERATECONSTANTS/////
CAC = 0.65/1000; %CAC in M
k0 = 1.35E-5;
k1 = 1.1e-1;
k2 = 2*k1;
k3 = 1.5*k1;
k4 = 2e-2;

%///// CALCULATIONS OF THE RATES/////
for i=1:t
    r0(i) = k0*EDC(i); %EDC => EDU (direct hydrolysis)
    r1(i) = k1*EDC(i)*COOH(i); %COO + EDC => COOEDC
    r2(i) = k2*COOEDC(i); %COO + COOEDC => COOOC + EDU
    r3(i) = k3*COOEDC(i); %COOEDC => COO + EDCU
    if COOOC(i) > CAC %test if concentration anhydride is greater than its solubility
        r4(i) = CAC*k4; %COOOC => 2COO
    else
        r4(i) = k4*COOOC(i); %COOOC => 2COO
    end

    EDC(i+1) = EDC(i)-r1(i)-r0(i); %Calculation of all the new concentrations.
    COOH(i+1) = COOH(i)-r1(i)-r2(i)+2*r4(i)+r3(i);
    COOEDC(i+1) = COOEDC(i)+r1(i)-r2(i)-r3(i);
    COOOC(i+1) = COOOC(i)+r2(i)-r4(i);
end

%///// PLOTTING ////
if plot_EDC == 1
    plot(1:t/60,EDC(1:t)*1000,'-m'); %plots [EDC] in mM and a data point per minute in magenta
    hold on
end

if plot_ANH == 1
    plot(1:t/60,COOOC(1:t)*1000,'-b'); %plots [Anhydride] in mM and a data point per minute in blue
    hold on
end
end
    
```

Supporting notes 2: Description of the quantification of feedback.

According to the above described model, when 10 mM of EDC was added to 10 mM of Fmoc-E and no feedback was in place, the maximum hydrolysis rate was found after 5.1 minutes at a rate of 4.02 $\mu\text{M}/\text{sec}$. When feedback was in place, the maximum hydrolysis rate was limited to $k_4 \cdot \text{CAC}$, where k_4 is the 1st order rate constant for hydrolysis and CAC is the critical aggregation concentration. This relation implied that the r_4 decreased with decreasing CAC. In order to quantify the feedback, the decreased r_4 as a result of the feedback was divided by the maximum rate (4.02 $\mu\text{M}/\text{sec}$). This fraction was normalized between 0 and 100%, where 100% implied full inhibition of the hydrolysis ($r_4=0 \mu\text{M}/\text{sec}$) and 0% meant no inhibition of the hydrolysis ($r_4=4.02 \mu\text{M}/\text{sec}$).

Supporting Figure 1

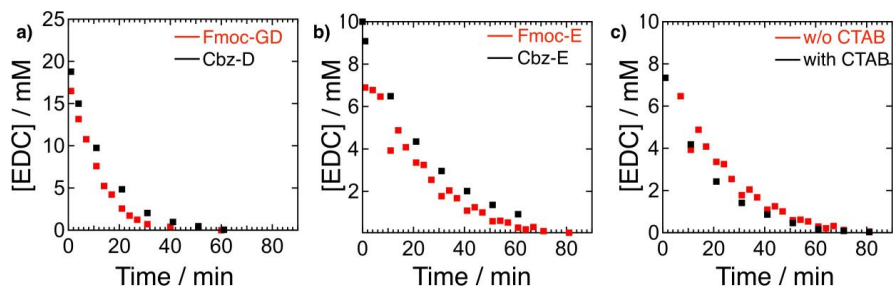


Fig. S1. Concentration EDC against time in response determined by HPLC (markers) for a) 10 mM Fmoc-GD (red) or Cbz-D (black) with 25 mM EDC, b) 10 mM Fmoc-E (red) or Cbz-E (black) with 10 mM EDC, c) 10 mM Fmoc-E with (red) or without (black) CTAB and 10 mM EDC.

Supporting Figure 2

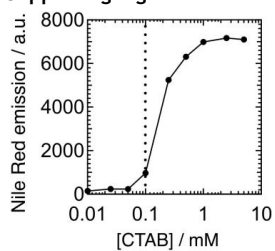


Fig. S2. Nile Red emission intensity at 635 nm again concentration of CTAB. A drastic increase intensity was observed around 0.1 mM, indicative of the critical micelle concentration of CTAB.

Supporting Figure 3

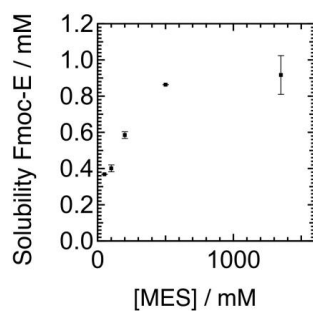


Fig. S3. Solubility of Fmoc-E at pH 1 at different MES concentrations. The error bars depict the standard deviation (n=3).

Supporting Figure 4

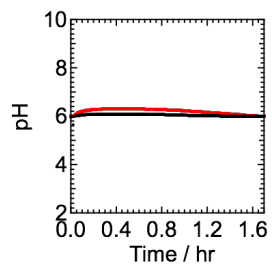


Fig. S4. pH against time for a solution of 10 mM Fmoc-E in response to 10 mM EDC for 200 mM MES buffer (black) and 50 mM MES (red).

6. Active Droplets in a Hydrogel Release Drugs with a Constant and Tunable Rate

Abstract.

After successfully implementing feedback in dissipative reaction cycles using hydrophobic domains, the goal in this publication is to adapt this concept to another self-assembled structure. Moreover, we want to investigate if the hydrophobic oil droplets formed by dissipative self-assembly can be used to carry a specific cargo and to release it at a constant rate. The strategy is to use the same reaction cycle, that is now well-understood, but change the Fmoc-protected peptide tail of the precursor to a simpler aliphatic one. The resulting precursors are butenyl-, hexenyl-, octenyl- and decenyl-succinic acids. These precursors form oil droplets upon fuel addition. As desired, the oil droplets have the same effect, since they serve as a hydrophobic domain where the anhydride is protected from hydrolysis. In other words, we detected the same negative feedback on the degradation of the anhydride and thereby also the change in kinetics from first- to zero-order. The zero-order kinetics depend on the solubility of the precursor that we can tune with the length of the carbon tail. Increasing the carbon tail results in decreased solubility as well as slower kinetics and longer lifetimes of the emulsions. Moreover, the oil droplets could be used to compartmentalize a hydrophobic drug. Emulsions are commonly used in drug delivery, but the release mechanisms follow diffusion-based first-order kinetics. We embedded the droplets in a hydrogel to create a stable material. Because of the decay, the release profile follows constant, zero-order release and this mechanism can be explained with the partition coefficient of the drug in the oily phase. The droplet volume decreases constantly but the partition coefficient stays the same and over time that forces the drug back in the solution. The release rates can be tuned by adding different amounts of fuel to generate different lifetimes or various amounts of drug. The system is simple, tunable, and versatile since it can be generalized for hydrophobic drugs.

This work has been published:

Title: Active Droplets in a Hydrogel Release Drugs with a Constant and Tunable Rate
Authors: Caren Wanzke, Dr. Marta Tena-Solsona, Benedikt Rieß, Laura Tebcharani, Prof. Dr. Job Boekhoven
First published: 12. February 2020
Journal: Materials Horizons
Publisher: The Royal Society of Chemistry
DOI: 10.1039/C9MH01822K.

Reprinted with permission of The Royal Society of Chemistry.

This section states the individual work of each author in the publication above. C. Wanzke designed and conducted all experiments. M. Tena-Solsona synthesized the precursor molecules and imaged the droplets with confocal microscopy. B. Rieß performed experiments at the spectrofluorometer and the fluorescence microscope. L. Tebcharani helped with HPLC measurements to get drug release profiles. The manuscript was written by C. Wanzke and J. Boekhoven. The work was performed under the supervision and guidance of J. Boekhoven.



Active droplets in a hydrogel release drugs with a constant and tunable rate†

Cite this: DOI: 10.1039/c9mh01822k

Received 12th November 2019,
Accepted 3rd February 2020

DOI: 10.1039/c9mh01822k

rsc.li/materials-horizons

Caren Wanzke,^a Marta Tena-Solsona,^{ab} Benedikt Rieß,^a Laura Tebcharani^a and
Job Boekhoven^{ib} *^{ab}

Materials that release drugs with a constant, zero-order rate are of great importance to improve therapeutic efficacy and reduce toxic side effects. The development of such materials is challenging, particularly the development of versatile platforms of which the release rate can be tuned. Here, we report a platform that comprises active oil-droplets with a tunable lifetime embedded in a hydrogel. The oil droplets are a type of dissipative (dynamic) assembly that is formed by a fuel-driven chemical reaction cycle. Once the fuel is depleted, the oil droplets decay following zero-order reaction kinetics due to a unique self-protection mechanism. We entrap hydrophobic drugs in the oil-phase, and we use the zero-order decay to dictate the release profiles of the entrapped drugs. The drug release has a constant rate over most of the release period, which is unique for drug delivery vehicles, particularly when considering the simplicity of the design. Moreover, we can tune the rate of the drug release and the length of the release period.

New concepts

In this manuscript, we introduce a concept that allows tuning of the linear release of hydrophobic drugs with extreme precision. Drug delivery platforms with this specific zero-order kinetics are rare and particularly interesting for the pharmaceutical industry because they deliver the constant amount of active ingredient per time unit, thus preventing over- or underdoses. The concept uses oil-droplets that are regulated by a chemically fueled reaction cycle. That means, the droplets emerge in response to fuel and are sustained by the fuel. However, once the fuel is depleted, the droplets will decay. Due to a unique decay mechanism, these emulsions fall apart with zero-order kinetics. That means, the emulsion decays linearly until all droplets are gone. Moreover, we can tune the lifetime of the emulsion from minutes to days. A variety of hydrophobic drugs is encapsulated within the droplets, and we demonstrate that the release of these drugs also follows zero-order kinetics. Moreover, we show that the release can be regulated with extreme precision. Since the release mechanism is well understood, we have full control over the delivery platform, and it can be customized easily.

Introduction

In aqueous emulsions, droplets of an insoluble oil are dispersed in a continuous water phase. These emulsions are of great importance for the food-, cosmetics- and healthcare industries.^{1–3} The healthcare industry commonly applies them as drug delivery vehicles^{3–5} because of their ability to increase the solubility and bioavailability of poorly water-soluble drugs. A recent development for controlled release is a hybrid of emulsions and hydrogels, the so-called emulgels.⁶ These possess the properties of both the gel and the emulsion and act as a dual control release system by entrapping the emulsion within a gel.

Besides solubilizing hydrophobic drugs, an ideal drug carrier should also control the release profile of the solubilized drug.

^a Chemistry Department, Technical University of Munich, Lichtenbergstr. 4, 85748, Garching, Germany. E-mail: job.boekhoven@tum.de

^b Institute for Advanced Study, Technical University of Munich, Lichtenbergstr. 2a, 85748, Garching, Germany

† Electronic supplementary information (ESI) available. See DOI: 10.1039/c9mh01822k

Most drug carriers, including emulsions, hydrogels, and emulgels, release their encapsulated active agent in a “fast-then-slow” manner. The consequence is an initial stage where the plasma drug level is high, followed by lower plasma drug concentration, which may be too low to achieve therapeutic effects.^{7,8} These are typically diffusion-controlled first-order processes following Higuchi’s kinetics.^{9,10} In contrast, zero-order drug release profiles release a drug at a constant rate, thus resulting in a desirable constant plasma drug level over the entire release period. Materials that fulfill the requirements for zero-order release remain challenging to develop and are relatively rare.^{9,11–20}

Dissipative supramolecular materials are materials that have a tunable lifetime, and could thus be promising for the field of drug delivery.^{21–25} They are formed by the self-assembly of molecules, in which the assembling molecule is a metastable product of a chemical reaction cycle (see Fig. 1a, for example). In the cycle, an activation reaction converts a precursor molecule into the metastable product at the expense of the irreversible consumption of a high-energy molecule (fuel). The activated product can then assemble into the supramolecular material.

Communication

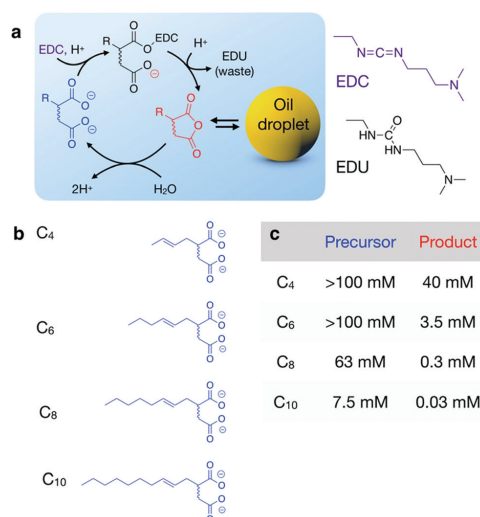


Fig. 1 Chemical structures of the chemical reaction cycle and precursors. (a) Chemical reaction cycle driven by the consumption of EDC. The anhydride product phase-separates into oil droplets. (b) Structures of the precursors used. (c) Table of the solubilities of the precursors and products in 0.2 M MES buffer at pH 6.0 and 25 °C.

A second chemical reaction, the deactivation, reverts the product to the precursor. The combined reactions imply that the material emerges after the application of fuel and that the assemblies require the continuous application of fuel to sustain.²⁶ When a finite amount of fuel is added, materials with a finite lifetime emerge.²² Such transient materials could be explored in the context of drug delivery.^{21–24} Examples of dissipative supramolecular materials include hydrogels driven by the consumption of methylating agents^{27,28} or fueled by biocatalytic reactions,^{26,29} as well as solutions of dynamic vesicles^{30,31} and others.^{23,32–36} Self-regulating peptide hydrogels as a supramolecular material have also been shown to function for a burst-release of dyes.²⁴

In this work, we demonstrate that a dissipative supramolecular material, *i.e.*, an emulsion of active oil droplets, is a great platform to deliver hydrophobic drugs. Due to the simplicity of the chemistry, we can accurately tune the lifetime of the emulsion from minutes to days. The building blocks in the emulsion are completely recyclable. Due to a unique feedback mechanism, we can deliver drugs from these emulsions with zero-order release profiles. Furthermore, we can tune the zero-order rate of the drug release and for how long the release lasts.

Results and discussion

We recently introduced a reaction cycle that leads to the formation of an emulsion of active oil droplets.^{37–39} The cycle comprises well-soluble succinic acid derivatives as the precursor (Fig. 1a).

These precursors react with 1-ethyl-3-(3-dimethylaminopropyl)carbodiimide (EDC) to form a reactive *O*-acylurea intermediate. The intermediate then reacts with a second intramolecular acid to form the corresponding anhydride. Depending on the hydrophobicity of the product, it phase-separates into oil droplets. However, in the aqueous environment, the anhydride product is metastable and hydrolyzes to the original precursor, thus closing the chemical reaction cycle. The result is a solution that temporarily contains oil droplets at the expense of carbodiimide as fuel. The temporary nature of the emulsion and the hydrophobicity of the oil droplets prompted us to study its potential as a drug delivery system in this study.

The precursor in the chemical reaction cycle we used (Fig. 1a) is based on derivatives of succinic acid, in which the succinic acid is functionalized with an unsaturated aliphatic tail (Fig. 1b). We used 2-buten-1-ylsuccinic acid (C₄), 2-hexen-1-ylsuccinic acid (C₆), 2-octen-1-ylsuccinic acid (C₈) and 2-decen-1-ylsuccinic acid (C₁₀, Fig. 1b), in which the carbon number denotes the number of carbons in the tail attached to the succinic acid. By a Nile Red assay,^{40,41} we found the solubilities of the precursors in 0.2 M MES buffer at pH 6.0 (Fig. 1c and Fig. S1, ESI[†]). In other words, under all of the further used condition, none of the precursors was able to aggregate or self-assemble.

We used high-pressure liquid chromatography (HPLC) to measure the evolution of the chemical reaction cycle. We added a batch of 10 mM EDC to a solution of precursor and followed the concentration of precursor, anhydride, and EDC with time (Fig. 2a and Fig. S2, ESI[†]). The intermediate *O*-acylurea was never observed, pointing to its rapid conversion into the anhydride. The C₄ anhydride concentration peaked at roughly 2.5 mM after around 5 minutes. Beyond this maximum, the anhydride concentration decayed exponentially, and after 40 minutes, we observed no more anhydride. When we added 10 mM EDC to 10 mM C₆, a very similar concentration evolution was observed.

In contrast, when we added 10 mM to 10 mM C₈, a different profile was observed for the anhydride concentration. It peaked at around 6 mM after roughly 30 minutes, after which it linearly decayed until we found no more anhydride after 2 hours. Finally, when we added 7.5 mM EDC to 7.5 mM C₁₀, we observed the transient anhydride that persisted for almost 20 hours. For each precursor, no evidence was found of the unwanted side product *N*-acylurea by HPLC (ESI[†], Tables S1, S2 and Fig. S3).

After the addition of 10 mM EDC, the solutions of C₄ and C₆ remained transparent during the entire experiment (Fig. 2b). In contrast, the solution with C₈ as precursor rapidly turned turbid and remained so for over two hours. UV/Vis measured the absorbance at 500 nm as quantification of turbidity for the samples. The experiment with C₄ and C₆ did not show an increase in turbidity (Fig. 2c). In contrast, the samples with C₈ with 10 mM EDC and C₁₀ with 7.5 mM EDC rapidly increased in turbidity. After roughly 20 minutes, the turbidity started to decrease. For C₈, the absorbance fell back to its original value after 156 minutes, while this value was reached after just under 20 hours for C₁₀. The sample with C₆ as precursor could also turn turbid, but only upon the addition

Materials Horizons

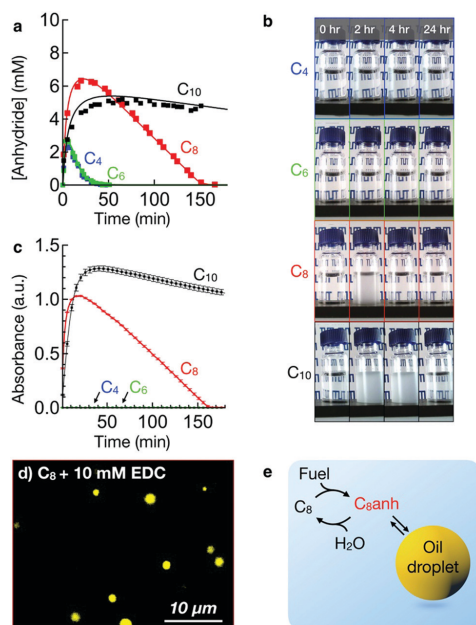


Fig. 2 Kinetics of the reaction cycle. (a) Concentration anhydride over time when 10 mM EDC was added to 10 mM C_4 , 10 mM C_6 , 10 mM C_8 or 7.5 mM EDC was added to 7.5 mM C_{10} . Markers represent HPLC data, while lines represent the kinetic model. (b) Photographs of samples described in (a), after addition of EDC. (c) Absorbance of 500 nm light as a measure for sample turbidity against time for the experiments described in (a). Scale bars represent standard deviation from the average of 3 experiments ($n = 3$). For clarity, only one in every five data points is shown by a marker and connected by a solid line. Note that the absorbance levels of experiments with C_4 , C_6 remain around 0. (d) Confocal micrograph of 10 mM C_8 combined with 10 mM EDC after 10 minutes. (e) Schematic representation of the self-protection mechanism. Hydrolysis can only take place on the fraction of anhydride that remains in solution.

of larger batches of fuel (*vide infra*). By confocal fluorescence microscopy with the dye Nile Red, we found that the turbidity was a result of micron-sized oil droplets that had phase-separated from the aqueous solution (Fig. 2d).

The linear decay of the concentration anhydride when droplets were present (Fig. 2a) and the linear decay of the turbidity (Fig. 2c) can be explained by a “self-protection” mechanism of the droplets.⁴² In the inhibition mechanism, the phase separation isolates the major anhydride fraction from the aqueous phase and thereby protects it from attack by water. Hydrolysis can thus only take place on the fraction of anhydride that remains in solution, which is equal to its solubility (Fig. 2e). As a result, the hydrolysis rate (v) in the presence of droplets can be calculated by multiplying the hydrolysis rate constant (k) with the solubility of the anhydride ($v = k \times \text{solubility}$). Since the anhydride solubility is constant, the hydrolysis rate follows zero-order kinetics. Moreover, the mechanism also explains why the higher carbon number

anhydrides with lower solubilities (Fig. 1c), hydrolyze slower. For example, C_{10} with a solubility of 0.03 mM hydrolyzes an order of magnitude slower compared to C_8 with a solubility of 0.3 mM. The decay is also correlated to the lifetime of the material, which is roughly ten times greater for C_{10} compared to C_8 . Indeed, a kinetic model can be used to fit the evolution of the concentrations of all reactive species in the chemical cycles (see Fig. 2a, ESI,[†] Table S3, and Notes 1).

Because we envisioned to use the temporary emulsions as drug a delivery device, we were interested in how the kinetics of the chemical reaction cycle affected the lifetime of the emulsion. Such understanding will help us to control the release rate of hydrophobic drugs and the period of release (*vide infra*). We used the turbidity of the samples as a proxy for the presence of the oil droplets in the active emulsion. In order to quantify the lifetime, the turbidity of the solutions was measured over time after the addition of fuel (Fig. 2c for representative traces). We set an arbitrary threshold value of 0.05 absorbance units (a.u.), *i.e.*, above this value, the samples were turbid, and active droplets were considered present. The time point at which the turbidity decreased below the threshold value was considered the lifetime of the temporary emulsion (Fig. 3a). As an example, when we added 10 mM EDC to 10 mM C_8 , the turbidity of the sample reproducibly fell below the threshold after 156 minutes.

The most straightforward manner of tuning the lifetime was by varying the batch of fuel added. For instance, when 25 mM of EDC was added to 10 mM C_8 , the sample remained turbid for 421 minutes (7.0 hours, Fig. 3b). In contrast, when 100 mM EDC was added, the lifetime lasted 1240 minutes (20.6 hours). The increase of the lifetime with increasing fuel followed a linear trend, such that, when the amount of fuel was doubled, the lifetime was roughly twice as high. We found that the precursor concentration had little influence on the lifetime of the emulsion (Fig. 3c). For instance, the lifetimes of the emulsions formed by 10 mM or 50 mM C_8 , each fueled with 10 mM EDC, were both 170 minutes. The parameter that had the most considerable influence on the lifetime of the active emulsion was the carbon number of the aliphatic tail. For 25 mM EDC with C_6 , a lifetime of only 24 minutes was found, which contrasts the lifetime of 421 minutes that was found for C_8 under the same conditions (Fig. 3b). Furthermore, for C_{10} , a maximum lifetime of 1700 minutes (28.4 hours) was found with an addition of 10 mM EDC. In other words, by varying the carbon number of the precursor, the lifetime could be tuned over two orders of magnitude. The trend of decreasing solubility of the anhydride with decreasing carbon tail-length explains the extended lifetimes of longer carbon tail anhydride emulsions.

We tested the influence of pH and temperature on the lifetime and found the longest lifetimes for pH 6.0, but the lifetime was not drastically shorter at pH 7.4 (Fig. 3d). Unsurprisingly, increasing the temperature decreased the lifetime. For example, increasing the temperature from 25 °C to body temperature decreased the lifetime by roughly a three-fold, which follows the rule of thumb that reaction rates approximately double with a 10 °C increase.^{43,44} Finally, we found that

Communication

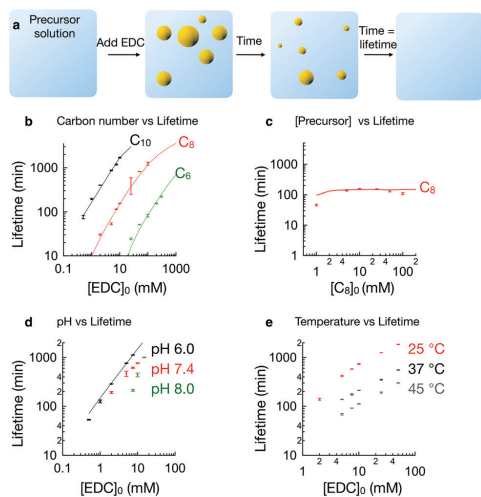


Fig. 3 Lifetimes of the active emulsion can be tuned. (a) Schematic representation of the transient active droplets. (b–e) The lifetime of the emulsion as measured by absorbance at 500 nm. Lifetimes of the active emulsions: (b) for 10 mM precursor C₆, C₈, and 7.5 mM precursor C₁₀, and different amounts of EDC added to initiate the cycle. The solution was buffered at pH 6.0 and kept at 25 °C. (c) For 10 mM EDC added to C₈ at various concentrations. The solution was buffered at pH 6.0 and kept at 25 °C. (d) For 7.5 mM C₁₀, buffered in 0.2 M MES at different pH values and in response to different amounts of EDC. The solutions were kept at 25 °C. (e) For 7.5 mM C₁₀ at different temperatures and in response to different amounts of EDC. The solutions were buffered in 0.2 M MES at pH 7.4.

also under physiological conditions, the lifetime of this emulsion could be tuned accurately by varying the amount of fuel (Fig. 3e).

The kinetic model was used to confirm the lifetime of the emulsions as determined by the UV/Vis experiments. For these calculations, the time at which the anhydride concentration decreased below its solubility was used as the lifetime of the active emulsion (Fig. 3b, solid lines). The lifetimes calculated by the model matched the lifetimes found by the turbidity measurements with high precision. The latter demonstrates our thorough understanding of the kinetics involved in the chemical reaction cycle. For the conditions at elevated pH and temperature, no HPLC data was available to adjust the model.

Finally, we tested the reusability of our active emulsions. To our surprise, the reaction cycle we introduce here was incredibly robust, and we could repeat more than 15 batch-induced cycles without any notable difference between the first and the last cycle. We explain the robustness of the cycle by the lack of side products and the solubility of the waste product EDU (Fig. 4).

Encouraged by the tunability and the robustness of the system, we were wondering if the active droplets could be applied as a drug release platform. The assumption we make is that we could trap the droplets in the hydrogel, and thus that negligible anhydride leaks out of the hydrogel. As the droplets hydrolyzed they would release their precursor and drug into the

View Article Online

Materials Horizons

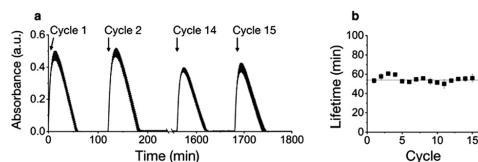


Fig. 4 The active droplets can be recycled without signs of fatigue. Addition of 5 mM EDC for each cycle to a 10 mM C₈ solution. (a) Absorbance spectrum over time and (b) lifetime of cycle vs. cycle number. The error bars depict the standard deviation ($n = 3$).

surrounding medium. The hypothesis was that if every time period a constant amount of the anhydride was hydrolyzed, the total droplet volume in the emulsion should decrease linearly too. When we encapsulate drugs within the oil droplets of the active emulsion, the linear decay of the droplet volume could result in a linear release of the drug. The zero-order deactivation of these active emulsions would be a great advantage over the typical first-order release profiles of drugs. Thus, the active droplets were immobilized in an agar hydrogel following the preparation depicted in Fig. 5. The droplets were first prepared as described above. After 30 minutes, a drug was added to the solution. The drug-loaded active droplets were trapped in an agar gel, which was subsequently covered with buffer. The drug release from the drug-loaded droplets to the aqueous phase was measured by HPLC. Confocal micrographs show that the addition of hot agar gel had no obvious influence on the size and shape of the oil droplets (Fig. S4a and b, ESI[†]). Furthermore, there was no obvious difference between drug-loaded or non-drug-loaded droplets found by microscopy (Fig. S4c and d, ESI[†]). It should be noted that the agar gel had cooled down significantly at the point of mixing it with the droplets (see ESI[†] Notes 2). As drugs, we used the hydrophobic anti-inflammatory drug nimesulide and the hydrophobic calcium channel blocker nitrendipine with a low water-solubility of 0.075 mM⁴⁵ and 0.25 mM,⁴⁶ respectively. We also used the more hydrophilic antiviral drug Acyclovir with a solubility of 7.19 mM⁴⁷ (Fig. 6a and ESI[†], Table S4).

We measured the release profiles of the three drugs with varying hydrophobicity from an agar gel without active droplets as a control. A mixture of 7.5 mM C₁₀ and 50 μM drug was prepared and trapped in a 1% agar gel, which was subsequently covered with buffer. As expected, HPLC showed the drug release from the hydrogel followed first-order kinetics. Moreover, 50% of the drug had released after roughly 20 minutes, independent of the hydrophobicity of the drug (Fig. 6b, black traces).

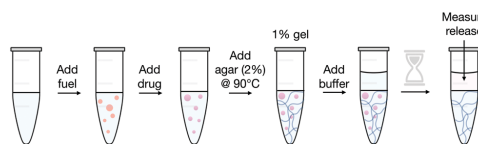


Fig. 5 Schematic representation of the preparation of active emulsions in gels.

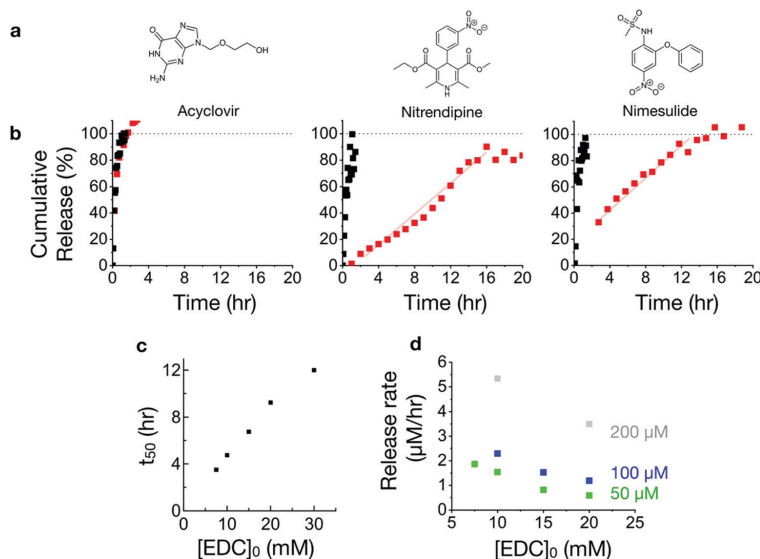


Fig. 6 (a) Chemical structures of the drugs. (b) Representative release profiles of the three drugs at 50 μM without EDC (black traces) and with 10 mM EDC (red traces). Note the linear release of the two hydrophobic drugs. From left to right: Acyclovir, nitrendipine, nimesulide. (c) Plot of the time after which 50% (25 μM) nimesulide was released against initial EDC concentration. (d) Release rate of nimesulide in the zero-order regime against initial concentration EDC. Different initial drug concentrations were used.

We could drastically delay the release of the two hydrophobic drugs with the active oil droplets. For example, when the release of nitrendipine was tested from a hydrogel with active droplets formed by the addition of 10 mM EDC, we found that 50% of the drug was released after almost 10 hours (Fig. 6b, red traces). Compared to the control experiment, that implies that the presence of the droplets delays the release by a 30-fold. Furthermore, the release-rate for the two hydrophobic drugs followed a clear zero-order release profile, which means that the release rate was almost constant for the entire 15-hour period. The time at which most drugs were released (16 hours) coincided with the lifetime of the active emulsion as measured by a UV/Vis experiment (Fig. S5a, ESI[†]). A similar zero-order release profile was observed for the other hydrophobic drug, nimesulide (Fig. 6b). Both drugs showed an initial burst release of 10% for nitrendipine and around 20% for nimesulide. Finally, we tested the release of the hydrophilic drug Acyclovir, which was similar to the control without the active emulsion, suggesting that it, likely due to its hydrophobicity, did not partition into the droplets (Fig. 6b). By HPLC, we could also measure the release profiles of the precursor from the hydrogels (Fig. S5b, ESI[†]). We found these release profiles were identical for each precursor and drug combination above mentioned and followed zero-order kinetics. These observations confirm that the hydrolysis of the anhydride in the hydrogel still takes place following zero-order. Moreover, we can also conclude that the hydrolysis kinetics are not significantly affected by the partitioning of the drug.

We used nimesulide to study further the release profiles and which parameters influenced its properties. In line with the lifetime experiments described above, we found that the amount of EDC determined the period the release lasted. To quantify the relation, we determined the time after which 50% of the drug was released for several initial EDC concentrations (Fig. 6c). Indeed, the time after which half of the drugs were released increased linearly with the initial fuel. In line with the way the amount of EDC determined the lifetime, the release period also doubled if the amount of EDC was doubled. An increase in the drug release period means that the drug release rate should decrease. Indeed, when we plot the zero-order drug release rate, it decreases with increasing initial EDC concentration (Fig. 6d and Fig. S6a–c, ESI[†]). We found the same trends for the release profiles of the droplet precursor C₁₀, *i.e.*, the release period is determined by the amount of EDC added (Fig. S5c, ESI[†]). Moreover, we found that the precursor release periods correspond to the measured lifetimes of the active emulsions by UV/Vis (Fig. S5a, ESI[†]).

Finally, we tested the influence of the total amount of drug in the system on the release rate. We found that the release rate increased as the total concentration drug increased (Fig. 6d).

The release profiles of nimesulide regulated by C₁₀ point to a high partitioning of the drug into the droplets. To verify that, we measured the concentration of drug that remained in solution, just after preparing the droplets. Thus, instead of adding agar gel to the active emulsion, we spun down the solution and separated oily and aqueous phase. Independent of

initial EDC and drug concentration, the aqueous phase contained around 20% of nimesulide (ESI,† Table S5), which matches the burst release seen in the drug release profiles.

The results above show that the zero-order release is directly controlled by the hydrolysis rate of the anhydride and the total amount of the drug in the carrier. We can explain these results by a simple drug partition mechanism. Due to their hydrophobicity, nimesulide and nitrendipine mainly partition into the hydrophobic anhydride droplets. The fraction that remains in the aqueous phase is susceptible to diffuse out of the gel-phase and distribute evenly between the gel and liquid phase. Because the anhydride is unstable and hydrolyzes, the total volume of the active droplet phase decreases over time. Moreover, because of the unique zero-order hydrolysis of the anhydride, the droplet phase decreases its volume linearly. As a consequence, the volume in which the drug can partition decreases over time, forcing the drug into the aqueous phase. Increasing the initial concentration EDC increases the total droplet volume but not the hydrolysis rate. The drug thus releases over a more extended period at a lower rate. Increasing the concentration drug increases the concentration in the droplet phase, but not the hydrolysis rate. The release rate thus increases.

Conclusions

In this work, we introduced a new type of dissipative supra-molecular material that constitutes phase-separated oil droplets. Due to the zero-order deactivation of the activated building block, the droplets decay linearly over time. We used that unique decay profile to release hydrophobic drugs at a constant rate. Because we understand the underlying mechanism and kinetics of the system, we could tune the zero-order release rate and the release period of the hydrophobic drugs. The underlying mechanism is general and should apply to other hydrolyzable oils. Moreover, in theory, any method of dispersing the drug-loaded oil droplets in an aqueous environment would be sufficient to start the reaction. In other words, the need for the harmful EDC as fuel is not a prerequisite for the zero-order release. In future work, we thus aim to develop a mechanistically similar hydrogel that can deliver a variety of drugs following zero-order kinetics, without the need for fuel.

Funding sources

Financial support comes from the Deutsche Forschungsgemeinschaft (DFG, German Research Foundation) – Project-ID 364653263 – TRR 235 project P16. JB is grateful for funding by the Technical University of Munich – Institute for Advanced Study, funded by the German Excellence Initiative and the European Union Seventh Framework Programme under grant agreement no. 291763. MTS acknowledges the European Union's Horizon 2020 Research and Innovation program for the Marie Skłodowska Curie Fellowship under grant agreement no. 747007.

Conflicts of interest

The authors declare no financial conflict of interest. CW and JB hold a pending patent application on the technology discussed in this manuscript (Hydrogel Compositions for the Controlled and Constant Release of Active Agents, EP 19 199 465.6).

Notes and references

- 1 J. M. Lakkis, *Encapsulation and controlled release technologies in food systems*, Wiley Blackwell, Chichester, West Sussex, UK, Hoboken, NJ, USA, 2nd edn, 2016.
- 2 M. Kakran and M. N. Antipina, *Curr. Opin. Pharmacol.*, 2014, **18**, 47–55.
- 3 L. C. Collins-Gold, R. T. Lyons and L. C. Bartholow, *Adv. Drug Delivery Rev.*, 1990, **5**, 189–208.
- 4 A. Narang, D. Delmarre and D. Gao, *Int. J. Pharm.*, 2007, **345**, 9–25.
- 5 S. S. Davis, C. Washington, P. West, L. Illum, G. Liversidge, L. Sternson and R. Kirsh, *Ann. N. Y. Acad. Sci.*, 1987, **507**, 75–88.
- 6 Ajazuddin, A. Alexander, A. Khichariya, S. Gupta, R. J. Patel, T. K. Giri and D. K. Tripathi, *J. Controlled Release*, 2013, **171**, 122–132.
- 7 J. Wang, B. M. Wang and S. P. Schwendeman, *J. Controlled Release*, 2002, **82**, 289–307.
- 8 K. E. Uhrich, S. M. Cannizzaro, R. S. Langer and K. M. Shakesheff, *Chem. Rev.*, 1999, **99**, 3181–3198.
- 9 Y.-N. Zhao, X. Xu, N. Wen, R. Song, Q. Meng, Y. Guan, S. Cheng, D. Cao, Y. Dong, J. Qie, K. Liu and Y. Zhang, *Sci. Rep.*, 2017, **7**, 5524.
- 10 F. van de Manacker, K. Braeckmans, N. el Morabit, S. C. De Smedt, C. F. van Nostrum and W. E. Hennink, *Adv. Funct. Mater.*, 2009, **19**, 2992–3001.
- 11 L. Lei, X. Liu, Y.-Y. Shen, J.-Y. Liu, M.-F. Tang, Z.-M. Wang, S.-R. Guo and L. Cheng, *Eur. J. Pharm. Biopharm.*, 2011, **78**, 49–57.
- 12 M. Ali, S. Horikawa, S. Venkatesh, J. Saha, J. W. Hong and M. E. Byrne, *J. Controlled Release*, 2007, **124**, 154–162.
- 13 L. Zhang, J. Alfano, D. Race and R. N. Davé, *Eur. J. Pharm. Sci.*, 2018, **117**, 245–254.
- 14 C. Celia, S. Ferrati, S. Bansal, A. L. van de Ven, B. Ruozi, E. Zabre, S. Hosali, D. Paolino, M. G. Sarpietro, D. Fine, M. Fresta, M. Ferrari and A. Grattoni, *Adv. Healthcare Mater.*, 2014, **3**, 230–238.
- 15 H. Zhang, R. Hao, X. Ren, L. Yu, H. Yang and H. Yu, *RSC Adv.*, 2013, **3**, 22927.
- 16 D. Fine, A. Grattoni, S. Hosali, A. Ziemys, E. De Rosa, J. Gill, R. Medema, L. Hudson, M. Kojic, M. Milosevic, L. Brousseau III, R. Goodall, M. Ferrari and X. Liu, *Lab Chip*, 2010, **10**, 3074.
- 17 C. S. Brazel and N. A. Peppas, *Eur. J. Pharm. Biopharm.*, 2000, **49**, 47–58.
- 18 P. I. Lee, *J. Pharm. Sci.*, 1984, **73**, 1344–1347.
- 19 Q. Wang, J. Wang, Q. Lu, M. S. Detamore and C. Berkland, *Biomaterials*, 2010, **31**, 4980–4986.
- 20 M. J. Webber, J. B. Matson, V. K. Tamboli and S. I. Stupp, *Biomaterials*, 2012, **33**, 6823–6832.

View Article Online

Materials Horizons

Communication

- 21 S. A. P. van Rossum, M. Tena-Solsona, J. H. van Esch, R. Eelkema and J. Boekhoven, *Chem. Soc. Rev.*, 2017, **46**, 5519–5535.
- 22 B. Rieß and J. Boekhoven, *ChemNanoMat*, 2018, **4**, 710–719.
- 23 R. K. Grötsch, A. Angi, Y. G. Mideksa, C. Wanzke, M. Tena-Solsona, M. J. Feige, B. Rieger and J. Boekhoven, *Angew. Chem., Int. Ed.*, 2018, **57**, 14608–14612.
- 24 T. Heuser, E. Weyandt and A. Walther, *Angew. Chem., Int. Ed.*, 2015, **54**, 13258–13262.
- 25 B. Rieß, R. K. Grötsch and J. Boekhoven, *Chem*, 2019, S2451929419305182.
- 26 A. Sorrenti, J. Leira-Iglesias, A. Sato and T. M. Hermans, *Nat. Commun.*, 2017, **8**, 15899.
- 27 J. Boekhoven, A. M. Brizard, K. N. K. Kowli, G. J. M. Koper, R. Eelkema and J. H. van Esch, *Angew. Chem., Int. Ed.*, 2010, **49**, 4825–4828.
- 28 J. Boekhoven, W. E. Hendriksen, G. J. M. Koper, R. Eelkema and J. H. van Esch, *Science*, 2015, **349**, 1075–1079.
- 29 S. Debnath, S. Roy and R. V. Ulijn, *J. Am. Chem. Soc.*, 2013, **135**, 16789–16792.
- 30 S. Maiti, I. Fortunati, C. Ferrante, P. Scrimin and L. J. Prins, *Nat. Chem.*, 2016, **8**, 725–731.
- 31 C. Wanzke, A. Jussupow, F. Kohler, H. Dietz, V. R. I. Kaila and J. Boekhoven, *ChemSystemsChem*, 2020, **2**, e1900044.
- 32 S. M. Morrow, I. Colomer and S. P. Fletcher, *Nat. Commun.*, 2019, **10**, 1011.
- 33 L. Heinen and A. Walther, *Sci. Adv.*, 2019, **5**, eaaw0590.
- 34 L. S. Kariyawasam and C. S. Hartley, *J. Am. Chem. Soc.*, 2017, **139**, 11949–11955.
- 35 J. Leira-Iglesias, A. Tassoni, T. Adachi, M. Stich and T. M. Hermans, *Nat. Nanotechnol.*, 2018, **13**, 1021–1027.
- 36 J. Leira-Iglesias, A. Sorrenti, A. Sato, P. A. Dunne and T. M. Hermans, *Chem. Commun.*, 2016, **52**, 9009–9012.
- 37 M. Tena-Solsona, C. Wanzke, B. Riess, A. R. Bausch and J. Boekhoven, *Nat. Commun.*, 2018, **9**, 2044.
- 38 C. Donau, F. Späth, M. Sosson, B. Kriebisch, F. Schnitter, M. Tena-Solsona, H.-S. Kang, E. Salibi, M. Sattler, H. Mutschler and J. Boekhoven, *ChemRxiv*, 2020, DOI: 10.26434/chemrxiv.11648598.v1.
- 39 M. Tena-Solsona, J. Janssen, C. Wanzke, F. Schnitter, H. Park, B. Rieß, J. M. Gibbs, C. A. Weber and J. Boekhoven, *ChemRxiv*, 2019, DOI: 10.26434/chemrxiv.9978539.v1.
- 40 M. C. A. Stuart, J. C. van de Pas and J. B. F. N. Engberts, *J. Phys. Org. Chem.*, 2005, **18**, 929–934.
- 41 J. Boekhoven, P. van Rijn, A. M. Brizard, M. C. A. Stuart and J. H. van Esch, *Chem. Commun.*, 2010, **46**, 3490.
- 42 B. Rieß, C. Wanzke, M. Tena-Solsona, R. K. Grötsch, C. Maity and J. Boekhoven, *Soft Matter*, 2018, **14**, 4852–4859.
- 43 K. J. Laidler, *J. Chem. Educ.*, 1984, **61**, 494.
- 44 I. A. Leenson, *J. Chem. Educ.*, 1999, **76**, 1459.
- 45 NIH, ChemIDplus ‘Nimesulide’, <https://chem.nlm.nih.gov/chemidplus/rn/startswith/51803-78-2>, accessed September 2018.
- 46 NIH, ChemIDplus ‘Nitrendipine’, <https://chem.nlm.nih.gov/chemidplus/rn/39562-70-4>, accessed September 2018.
- 47 NIH, ChemIDplus ‘Acyclovir’, <https://chem.nlm.nih.gov/chemidplus/rn/59277-89-3>, accessed September 2018.

Electronic Supplementary Material (ESI) for Materials Horizons.
This journal is © The Royal Society of Chemistry 2020

Supporting information for:

Active droplets in a hydrogel release drugs with a constant
and tunable rate.

Caren Wanzke,^a Marta Tena-Solsona,^a Benedikt Rieß,^a Laura Tebcharani,^a Job Boekhoven^{a,b}

^a Chemistry Department, Technical University of Munich, Lichtenbergstr. 4, 85748, Garching. Email: job.boekhoven@tum.de
^b Institute for Advanced Study, Technical University of Munich, Lichtenbergstr. 2a, 85748, Garching
† Electronic Supplementary Information (ESI) available: [details of any supplementary information available should be included here]. See DOI: 10.1039/x0xx00000x

Materials and methods

Materials. We purchased (*E/Z*)-2-Buten-1-ylsuccinic anhydride (C₄ anhydride), (*E/Z*)-2-hexen-1-ylsuccinic anhydride (C₆ anhydride), (*E/Z*)-2-decen-1-ylsuccinic anhydride (C₁₀ anhydride) from TCI Chemicals. (*E/Z*)-2-Octen-1-ylsuccinic anhydride (C₈ anhydride), 1-ethyl-3-(3-dimethylaminopropyl) carbodiimide (EDC), 2-(*N*-morpholino)ethanesulfonic acid (MES) buffer, trifluoroacetic acid (TFA) and Nile Red were purchased from Sigma-Aldrich and used without any further purification unless otherwise indicated. HPLC grade acetonitrile (ACN) was purchased from VWR. We purchased Agar-agar from Carl-Roth and synthesized the succinic acid derivatives (C₄-C₁₀) as described below.

Synthesis of the succinic acid derivatives. We synthesized the precursor acids by treating the corresponding anhydrides with two (mass)-equivalents of MQ water and stirred overnight at room temperature. We found no starting material by HPLC. We lyophilized the mixture, and it stored at -20 °C until further use.

Sample preparation. We prepared stock solutions of the precursors by dissolving the acid in 0.2 M MES buffer, after which we adjusted the pH to pH 6.0, 7.4 or 8.0. Stock solutions of EDC were prepared by dissolving the EDC powder in MQ water. We prepared the stock solutions of 1.0 M EDC freshly. Reaction cycles were started by addition of the high concentration EDC to the acid solution. We carried out all experiments at 25 (±0.5), 37 (±0.5) or 45 (±0.5) °C

Kinetic model. We used a kinetic model for predicting the evolution of the anhydride concentration over time. Supporting Notes 1 describes the model briefly. More details can be found in our previous work.¹ The rate constants we used in this work are given in Supporting Table S3.

HPLC. We monitored the kinetics of the chemical reaction cycles over time by analytical HPLC (HPLC, ThermoFisher Dionex Ultimate 3000, Hypersil Gold 250 x 4.8 mm). A 1.0 mL sample was prepared as described above and placed into a screw cap HPLC vial. Samples of the solutions were directly injected without further dilution (injection volume: 25 µL) and tracked with a UV/Vis detector at 220 and 240 nm. All compounds involved were separated using a linear gradient of H₂O: ACN each with 0.1% TFA.

Method 1: H₂O: ACN from 40:60 to 2:98 in 8 min for C₄ and C₆; Method 2: H₂O: ACN from 98:2 to 2:98 in 12 min for C₈ and C₁₀;

Both methods were followed by 2 min 98% ACN. Calibration curves for the EDC (in MQ water), acids (in MES buffer), anhydrides (in ACN) and drugs (in ACN or MQ-water) were performed with the corresponding method in triplicate. Retention times and calibration values are given in Supporting Table S1, S2 and S4.

UV/Vis Spectroscopy. The UV/Vis measurements were carried out using a Multiskan FC (ThermoFisher) microplate reader. Samples (200 µL) were directly prepared into a 96 well-plate (tissue culture plate non-treated). The Temperature (25 (±0.5), 37 (±0.5) or 45 (±0.5) °C) was set 30 min before starting the measurement. Each experiment was performed at 500 nm and in triplicate.

Confocal Fluorescence Microscopy. We used a Leica SP5 confocal microscope using a 63x oil immersion objective to image the droplets. We prepared samples as described above but with 25 µM Nile Red as dye. 20 µL of the sample was deposited on a PEG-coated glass slide and covered with a 12 mm diameter coverslip. Samples were excited with 543 nm laser and imaged at 580-700 nm.

Fluorescence Microscopy. We used a Leica DMI8 inverted wide-field microscope (63x Oil objective) with TXR filter (Exc. 540-580; Em. 592-668; DC 585). The samples were prepared as described above for the confocal fluorescence microscopy.

ESI. We used a Varian 500 MS LC ion trap to perform ESI-MS measurements. The samples were diluted in acetonitrile before injection into an acetonitrile carrier flow (20 µL min⁻¹).

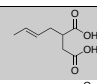
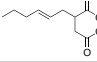
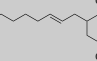
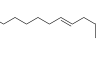
Nile Red Assay. The Nile Red assay was performed on a Jasco (FP-8300) spectrofluorometer with external temperature control (MCB-100). Samples were directly prepared in the 10 mm quartz cuvette (Precision Cells Inc.) by mixing different concentrations of precursor (from 0.01 to 100 mM in 0.2 M MES buffer) with Nile Red (5 μ M). The fluorescence intensities were measured at 635 nm with an excitation at 550 nm. The corresponding blue shift was calculated by subtracting the intensity of the blank (0.2 M MES buffer with 5 μ M Nile Red) from the corresponding sample.

Drug Release Experiments. A 2% agar-agar stock in 0.2 M MES buffer pH 6.0 was heated to 90 °C. For the first-order release experiments, X μ L of a 5 mM stock solution of the drug (in acetonitrile for Nimesulide/Nitrendipine, in dimethylsulfoxide for Acyclovir) was added to 500 μ L 7.5 mM C₁₀ precursor in 0.2 M MES buffer pH 6.0. 500 μ L of the hot agar was added, and 60 μ L of this mixture was immediately put on the bottom of a 96 well plate. After 1 min 120 μ L of 0.2 M MES buffer was added as a supernatant. The release of precursor and drug to the supernatant was measured via HPLC. For every HPLC injection, a separate well was prepared. For the zero-order release experiments, the precursor solution was activated as described above. The drug was added after 30 min and agar after 45 min. We carried out the rest of the experiment as described above.

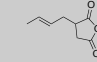
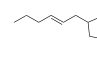
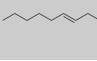
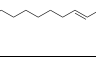
Spin Down Experiments. 500 μ L of the precursor solution was activated as described above. After 30 min, X μ L of a 5 mM stock solution of the drug (in acetonitrile for Nimesulide/Nitrendipine, in dimethylsulfoxide for Acyclovir) was added. One hour in the experiment, the solution was put in a centrifuge for 5 min (*rcf* = 5.5). The aqueous phase (200 μ L) was measured by HPLC to determine the amount of drug left.

Supporting Tables

Supporting Table S1. Characterization of precursors.

| name | structure | mass calculated [g/mol] | mass observed [g/mol] | retention time [min] @220nm | calibration value (mAU/mM) |
|----------------------|---|---|------------------------------|--------------------------------|-------------------------------|
| C ₄ acid |  | Mw = 172.1 C ₈ H ₁₂ NO ₄ | 171.1 [Mw-H] ⁻ | 4.16 (method 1) | 2.83 |
| C ₆ acid |  | Mw = 200.1 C ₁₀ H ₁₆ N ₂ O ₄ | 199.1 [Mw-H] ⁻ | 5.60 (method 1) | 2.78 |
| C ₈ acid |  | Mw = 228.1 C ₁₂ H ₂₄ NO ₄ | 227.1 [Mw-H] ⁻ | 10.96 (method 2) | 3.22 |
| C ₁₀ acid |  | Mw = 256.2 C ₁₄ H ₂₄ NO ₄ | 255.1 [Mw-H] ⁻ | 11.83 (method 2) | 3.25 |

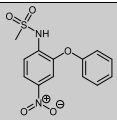
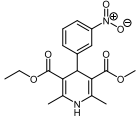
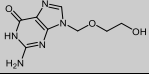
Supporting Table S2. Characterization of products.

| name | structure | mass calculated [g/mol] | mass observed [g/mol] | retention time [min] @220nm | calibration value (mAU/mM) |
|---------------------------|---|---|------------------------------|--------------------------------|-------------------------------|
| C ₄ anhydride |  | Mw = 154.1 C ₈ H ₁₀ NO ₃ | 155.2 [Mw+H] ⁺ | 6.68 (method 1) | 4.78 |
| C ₆ anhydride |  | Mw = 182.1 C ₁₀ H ₁₄ N ₂ O ₃ | 183.1 [Mw+H] ⁺ | 7.78 (method 1) | 5.19 |
| C ₈ anhydride |  | Mw = 210.1 C ₁₂ H ₁₈ NO ₃ | 211.2 [Mw+H] ⁺ | 12.84 (method 2) | 5.04 |
| C ₁₀ anhydride |  | Mw = 238.2 C ₁₂ H ₁₁ NO ₅ | 239.2 [Mw+H] ⁺ | 13.39 (method 2) | 5.48 |

Supporting Table S3: Rate constants used in the kinetic model.

| precursor | k ₁ [M ⁻¹ s ⁻¹] | k ₂ | k ₃ | k ₄ [s ⁻¹] | CAC [mM] |
|----------------------|--|------------------|---------------------|--------------------------------------|-------------|
| C ₄ acid | 0.2 | 1xk ₁ | 0.25xk ₁ | 3.5*10 ⁻³ | 40 |
| C ₆ acid | 0.2 | 1xk ₁ | 0.25xk ₁ | 3.5*10 ⁻³ | 3.5 |
| C ₈ acid | 0.2 | 1xk ₁ | 0.25xk ₁ | 3.5*10 ⁻³ | 0.3 |
| C ₁₀ acid | 0.2 | 1xk ₁ | 0.25xk ₁ | 3.5*10 ⁻³ | 0.03 |

Supporting Table S4: Characterization of drugs.

| name | structure | mass calculated [g/mol] | mass observed before the cycle [g/mol] | mass observed after the cycle [g/mol] | retention time [min] | calibration value (mAU/mM) |
|--------------|---|--|---|---|---------------------------------|----------------------------------|
| Nimesulide |  | Mw = 308.31 C ₁₃ H ₁₂ N ₂ O ₅ S | 307.0 [Mw-H] ⁻ | 307.0 [Mw-H] ⁻ | 11.10 (220 nm) (method 2) | 0.340 |
| Nitrendipine |  | Mw = 360.36 C ₁₈ H ₂₀ N ₂ O ₆ | 359.1 [Mw-H] ⁻ | 359.2 [Mw-H] ⁻ | 11.48 (240 nm) (method 2) | 0.530 |
| Acyclovir |  | Mw = 225.21 C ₈ H ₁₁ N ₅ O ₃ | 248.1 [Mw+Na] ⁺ | 248.1 [Mw+Na] ⁺ | 5.38 (240 nm) (method 2) | 0.192 |

Supporting Table S5: Percentage of Nimesulide measurable in the aqueous phase after 1h for 7.5 mM C₁₀ with different amounts of EDC and different initial concentrations of Nimesulide. The error depicts the standard deviation (n=3).

| EDC [mM] | c (Nimesulide) [μM] | | |
|-------------|---------------------|--------------|--------------|
| | 50 | 100 | 150 |
| 7.5 | 19.5 ± 1.2 % | 24.0 ± 3.2 % | 19.0 ± 8.8 % |
| 10 | 14.5 ± 0.7 % | 19.2 ± 1.1 % | 17.1 ± 0.3 % |
| 15 | | 17.7 ± 1.5 % | 15.2 ± 1.2 % |

Supporting Notes

Supporting Notes 1. Description of kinetic model

A kinetic model was written in Matlab that described each reaction involved in the chemical reaction network. The concentrations of each reactant were calculated for every 1 second in the cycle. The model was used to the obtained fit HPLC data that described the evolution of the concentration of anhydride, EDC and acid over time. The concentration of the C₄-, C₆-, C₈-precursor was 10 mM and of the C₁₀-precursor was 7.5 mM.

The model described five chemical reactions:

Direct hydrolysis of carbodiimide with a first order rate constant of $1.3 \times 10^{-5} \text{ sec}^{-1}$ as determined in previous work.¹

The formation of O-acylisourea by reaction with EDC (k_1). This second order rate constant was determined for each precursor by HPLC, by monitoring the EDC consumption.

The formation of the anhydride with a first order rate constant. This rate constant could not be determined because the O-acylisourea was never observed. It was therefore set to be twice the rate of k_1 . As a result, the O-acylisourea did never reach concentrations over 1 μM in the model.

Direct hydrolysis of O-acylisourea (k_3). This reaction rate could not be obtained because the O-acylisourea was not observed. The ratio of k_2 and k_3 (anhydride formation and competing direct hydrolysis of O-acylisourea) was varied to fit the HPLC data for several concentrations of [fuel]₀ and [di-acid]₀.

Hydrolysis of anhydride in solution proceeded with a first order rate (k_4) The rate constant was determined by HPLC for kinetic experiments where no assemblies were reached.

The rate of the hydrolysis reaction was calculated by multiplying the first order rate constant k_4 with the concentration of anhydride. When the concentration reached values above the CAC, the hydrolysis rate was calculated by multiplying the rate constant by the CAC.

Supporting Notes 2. Preparation of the activated gels.

The behavior of our droplets is sensitive to temperature (Fig. 3e). We thus explain here the preparation of the gels with active droplets for the drug release experiments in more detail.

We ensure that the solution of droplets was kept at room temperature until the agar gel was added. We add 500 μL of the liquified agar gel at 90°C to 500 μL of emulsion at 25°C in an Eppendorf tube. The total solution of 1000 μL can, theoretically, never exceed a temperature between 55 and 60°C when mixing is done rapidly. This estimation is a high estimate because it does not take into account the thermal capacity of the walls of the tube, or the pipet tips. Then, immediately after mixing, we pipette 60 μL of the solution on the bottom of a well in a 96 well-plate which is at room temperature. There it directly solidifies because of the further drop in temperature. Taken together, the upper temperature of the droplets is significantly below 60°C, and it experiences this temperature for less than a minute. In that minute, we assume that the droplet do not hydrolyze significantly faster than the rest of the experiment.

Supporting Figures

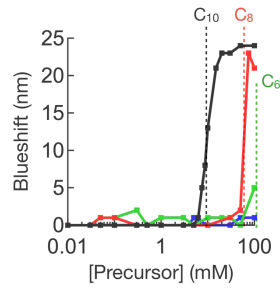


Fig. S1. Nile Red Assay at fluorescence spectroscopy for precursor C₆, C₈ and C₁₀.

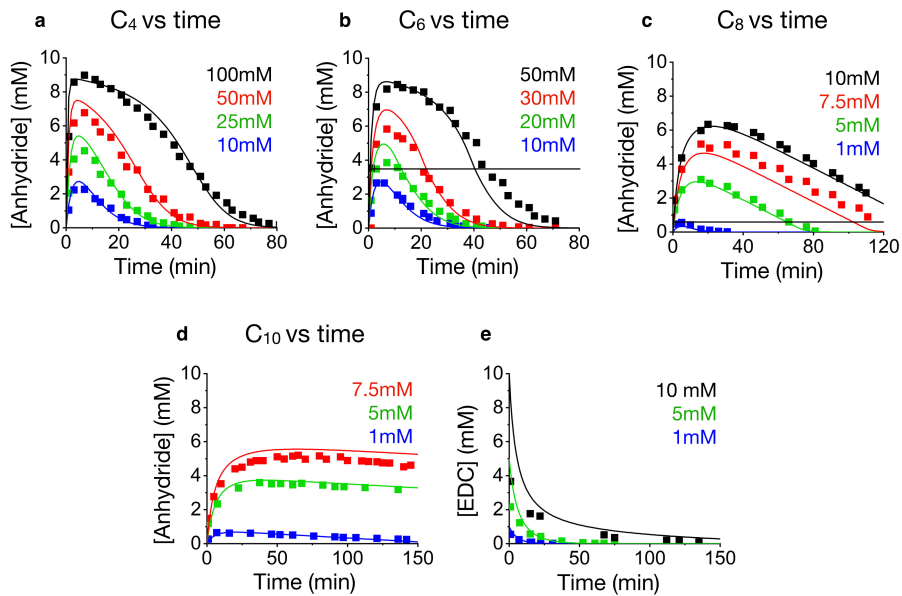


Fig. S2. HPLC kinetics for different precursor with different concentrations EDC, markers represent HPLC data, while lines represent the kinetic model a) 10 mM C₄ acid b) 10 mM C₆ acid c) 10 mM C₈ acid and d) 7.5 mM C₁₀ acid; EDC consumption of e) 7.5 mM C₁₀ acid with different concentrations of EDC.

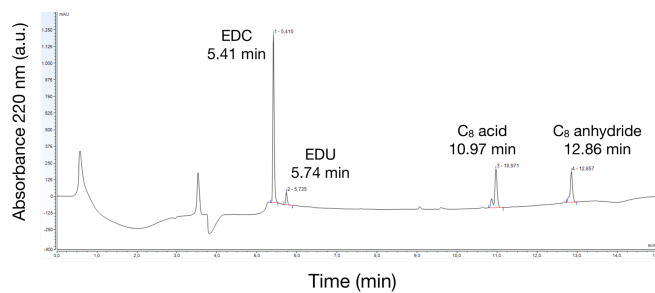


Fig. S3. Representative HPLC trace of 10 mM C_8 acid after 15 min of EDC addition (5 mM).

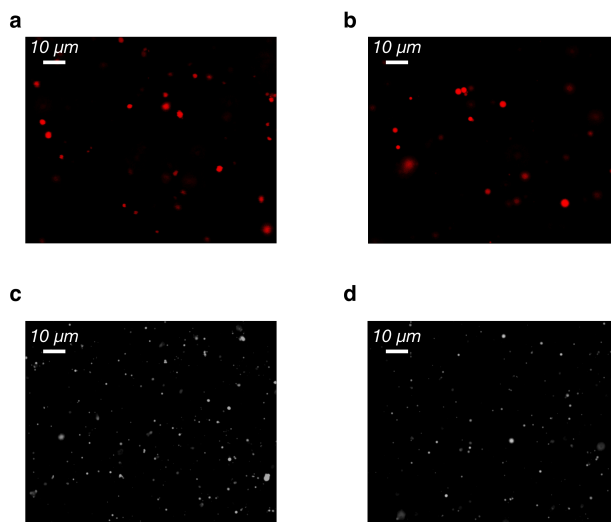


Fig. S4. Confocal micrographs of 7.5mM C_{10} acid with 10mM EDC **a)** directly before gel addition (44min) and **b)** directly after gel addition (46min). Fluorescence micrographs of 7.5mM C_{10} acid with 10mM EDC **c)** with 50 μ M Nimesulide and **d)** with 200 μ M Nimesulide both directly after gel addition.

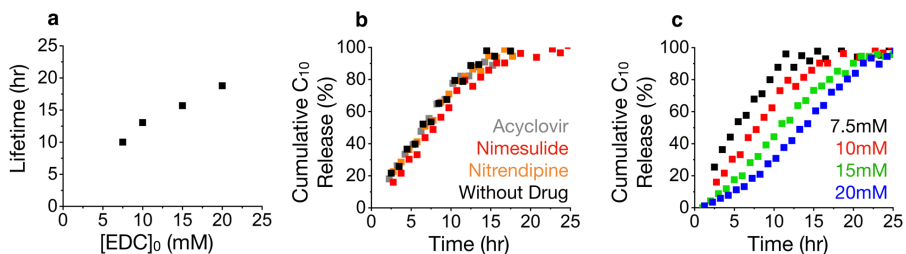


Fig. S5. **a)** Lifetimes of the active emulsion in gel vs. starting concentrations EDC determined by UV/Vis. Cumulative C_{10} release measured by HPLC from the active emulsion following zero-order release for **b)** 7.5mM C_{10} acid with 50 μ M of different drugs or without drug with 10mM starting concentration EDC **c)** 7.5 mM C_{10} acid with different starting concentrations EDC. All release profiles are measured in a 1% agar gel at pH 6.0 and 25 $^{\circ}$ C.

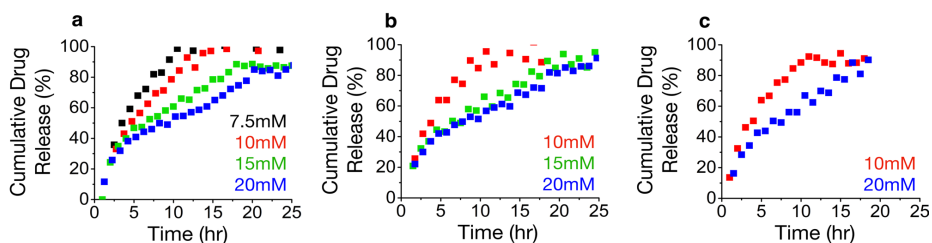


Fig. S6. Cumulative drug release measured by HPLC from the active emulsion following zero-order release for **a)** 50 μ M Nimesulide with different starting concentrations EDC, **b)** 100 μ M Nimesulide with different starting concentrations EDC, **c)** 200 μ M Nimesulide with different starting concentrations EDC. All release profiles are measured in a 1% agar gel at pH 6.0 and 25 $^{\circ}$ C.

References

- ¹ Tena-Solsona, M.; Rieß, B.; Grötsch, R. K.; Löhrer, F. C.; Wanzke, C.; Käs Dorf, B.; Bausch, A. R.; Müller-Buschbaum, P.; Lieleg, O.; Boekhoven, J., Non-equilibrium dissipative supramolecular materials with a tunable lifetime. *Nature Communications* **2017**, *8*, 15895.

7. Conclusion and Outlook

The concept of dissipative supramolecular materials has great potential for designing new materials with unique functions. Inspired by nature, scientists made first attempts to couple chemical reaction networks to material properties. As described in chapter 1, several reactions, from biocatalytic to completely synthetic, were utilized to create transient self-assembled structures.

This thesis aims to go beyond the proof-of-concept phase and find relevant applications for these dissipative supramolecular materials. A few examples of new materials with more applied functionalities have already been shown, that I discuss in chapter 2. The areas vary from self-erasing inks and hydrogels to nano-reactors and transient materials that control the release of molecules. Especially the controlled release of molecules is an interesting feature since the pharmaceutical industry can benefit from new release mechanisms and strategies. Hereby, the type of release and the control over the release profile is important for a medical application. Zero-order release is particularly advantageous because of its high efficiency and minimizing toxic effects. Developing a new drug delivery vehicle that is simple and versatile as well as shows a controlled zero-order release profile is an ideal goal.

A first step to achieve this goal is described in chapter 4. Vesicles or colloids can be interesting structures for the base of a drug delivery vehicle since they are able to encapsulate active reagents. I designed a peptide-based precursor that forms transient vesicles and used an acid-anhydride based chemical reaction cycle to kinetically control the self-assembly process. A similar peptide, that I discuss in chapter 5, self-assembled into transient colloids upon fuel addition. Interestingly, the colloids showed negative feedback on its degradation because the anhydride product was protected from water. This feedback mechanism resulted in a change of kinetics from first-order to zero-order hydrolysis. Since zero-order release is ideal for controlled drug delivery I tried to implement this feedback in emulsion-based structures that are already commonly used in healthcare.

The transient active emulsions I discuss in chapter 6 were not only based on commercially available and simple precursors, but the oil-droplets showed the same negative feedback. The hydrophobic domains protected the anhydride product from deactivation changing the hydrolysis kinetics to zero-order. This generated a system that had no side-products, excellent reusability, controlled and predictable lifetime, as well as high robustness towards different temperatures and pH. Encouraged by the simplicity, tunability, and zero-order kinetics of the system, I tried to apply it as a drug delivery vehicle. The activated oil droplets were loaded with hydrophobic drugs and embedded in a hydrogel to create a stable matrix. The measured release profiles of the drugs followed zero-order kinetics over a defined period of time that can be tuned from 10 to 20 hours.

In conclusion, this work describes the development of new synthetic and transient materials based on simple precursors. Starting with vesicles that offer a new model platform to study membrane remodeling, followed by colloids that implemented a negative feedback mechanism in our reaction cycle, to oil-droplets that can be used as a zero-order drug delivery platform. The concept of dissipative self-assembly created transient materials that were expanded towards relevant applications. The designed platform is controllable, predictable, simple, versatile, cheap, applicable for different hydrophobic drugs, and enabled a novel way to deliver drugs with a zero-order release profile.

A drawback of the designed system that can restrict the application in the pharmaceutical industry is that EDC as the fuel, as well as its corresponding urea, are rather toxic for organisms. However, we discovered that the pure anhydride in water forms an emulsion that shows zero-order kinetics as well. The simplified system contains even less components since the EDC for activation is no longer a requirement. We tested the system and the zero-order release of hydrophobic drugs was maintained. The control over the release rates is now the starting concentration of anhydride as well as the drug. The simpler and more applicable system led to a pending patent. Future work involves the engineering of a storable and user-friendly platform that can be tested *in vivo*.

8. Materials and Methods

Materials. Fmoc-E, Cbz-E, Cbz-D, (*E/Z*)-2-Octen-1-ylsuccinic anhydride (C₈ anhydride), 1-Ethyl-3-(3-dimethylaminopropyl) carbodiimide (EDC), 2-(*N*-morpholino)ethanesulfonic acid (MES) buffer, trifluoroacetic acid (TFA), urea, and Nile Red were purchased from Sigma-Aldrich. (*E/Z*)-2-Buten-1-ylsuccinic anhydride (C₄ anhydride), (*E/Z*)-2-hexen-1-ylsuccinic anhydride (C₆ anhydride), and (*E/Z*)-2-decen-1-ylsuccinic anhydride (C₁₀ anhydride) were purchased from TCI Chemicals. Agar-agar was purchased from Carl-Roth. All were used without any further purification unless otherwise indicated. Di- and Tripeptides were synthesized using standard fluoren-9-ylmethoxycarbonyl (Fmoc) solid-phase peptide synthesis on Wang resin (100-200 mesh, 1.1 mmol/g loading). Peptides were synthesized on a CEM Liberty microwave-assisted peptide synthesizer as described below. All the required reagents were purchased from Sigma-Aldrich. HPLC grade acetonitrile (ACN) was purchased from VWR.

Peptide synthesis.

Fmoc-GGD and Fmoc-GGE synthesis. Peptides were synthesized using standard fluoren-9-ylmethoxycarbonyl (Fmoc) solid-phase peptide synthesis on Wang resin (100-200 mesh, 1.1 mmol/g loading). Synthesis was performed on a CEM Liberty microwave-assisted peptide synthesizer. The first amino acid coupling to the resin was accomplished by using symmetrical anhydride methodology. Briefly, a 0.2 M solution of the Fmoc-amino acid symmetrical anhydride was prepared by allowing the corresponding Fmoc-protected amino acid (FmocD(OtBu)OH or FmocE(OtBu)OH, 12 mmol) and *N,N'*-diisopropylcarbodiimide (DIC, 6 mmol) to react in 30 mL *N,N*-dimethylformamide (DMF) for 40 minutes. The solution was placed in the freezer for 15 minutes and the formed solid urea was filtered out before the next step. Loading of the resin was performed using the automated peptide synthesizer. The symmetrical anhydride solution (0.2 M, 12 mL) and 4-(dimethylamino)pyridine (DMAP) solution in DMF (20 mM, 2.5 mL) were added to the pre-swollen Wang resin (0.5 mmol, 1.1 mmol/g) and heated in the microwave (30 minutes, 75 °C). The coupling was repeated twice in order to increase the yield. The resin was then washed with DMF (2x10 mL). Before the following coupling the Fmoc protecting group was removed

using a 20% solution of piperidine in DMF. The reaction mixture was heated in the microwave (1x1 minutes, 90 °C) and then washed with DMF (2x10 mL). The cleavage was repeated twice. The coupling was achieved by using 4 equivalents (eq.) of Fmoc-glycine in DMF, 4 eq. of DIC and 4 eq. of ethyl (hydroxyimino)cyanoacetate (Oxyma). The resin solution was then heated in the microwave (1x2 minutes, 90 °C). This coupling was also repeated twice to increase the yield. Fmoc-cleavage and amino acid coupling were repeated as described. The tripeptide was then cleaved from the resin using a mixture (10 mL) of 50% DCM, 47.5% trifluoroacetic acid (TFA), 1.25% water, and 1.25% triisopropylsilane (TIPS) for 1.5 hours. The solvent was removed by co-distillation with ether by rotary evaporation and dried under reduced pressure. The product was purified using preparative reversed-phase high-performance liquid chromatography (HPLC, Thermofisher Dionex Ultimate 3000, Hypersil Gold 250x4.8 mm) in a linear gradient of acetonitrile (ACN with 0.1% TFA, 40% to 98%) and water (with 0.1% TFA). Purified product was lyophilized and stored at -20 °C until further use. The purity of the peptide was analysed by liquid chromatography mass spectrometry (LC-MS) as well as analytical HPLC.

Stock solutions of these precursor were prepared by dissolving the precursor in 0.2 M MES buffer, after which the pH was adjusted to pH 6.0. Stock solutions of EDC were prepared by dissolving the EDC powder in MQ water. Typically, stock solutions of 2.0 M EDC were used freshly. Reaction networks were started by addition of the high concentration EDC to the peptide solution. All analysis was carried out at 25 °C.

Fmoc-GD synthesis. Fmoc-GD was synthesized using standard fluoren-9-ylmethoxycarbonyl (Fmoc) solid-phase peptide synthesis on Wang resin (100-200 mesh, 1.1 mmol/g loading). Synthesis was performed on a CEM Liberty microwave-assisted peptide synthesizer. The first amino acid coupling to the resin was accomplished by using symmetrical anhydride methodology. Briefly, a 0.2 M solution of the Fmoc-FmocD(OtBu)OH symmetrical anhydride was prepared by allowing the corresponding Fmoc-protected amino acid (FmocD(OtBu)OH, 12 mmol) and N,N'-diisopropylcarbodiimide (DIC, 6 mmol) to react in 30 mL N,N-dimethylformamide (DMF) for 40 minutes. The solution was placed in the freezer for 15 minutes and the solid urea formed was filtered out before next step. Loading of the resin was performed using the automated peptide synthesizer. The symmetrical anhydride solution (0.2 M, 12 mL) and 4-(dimethylamino)pyridine (DMAP) solution in DMF (20 mM, 2.5 mL) were

added to the pre-swollen Wang resin (0.5 mmol, 1.1 mmol/g) and heated in the microwave (30 minutes, 75 °C). The coupling was repeated twice in order to increase the yield. The resin was then washed with DMF (2x10 mL). Before the following coupling the Fmoc protecting group was removed using a 20% solution of piperidine in DMF. The reaction mixture was heated in the microwave (1x1 minutes, 90 °C) and then washed with DMF (2x10 mL). The coupling was achieved by using 4 equivalents (eq.) of Fmoc-glycine in DMF, 4 eq. of DIC and 4 eq. of ethyl (hydroxyimino)cyanoacetate (Oxyma). The resin solution was then heated in the microwave (1x2 minutes, 90 °C). This coupling was also repeated twice to increase the yield. The peptide was then cleaved from the resin using a mixture (10 mL) of 50% DCM, 47.5% trifluoroacetic acid (TFA), 1.25% water, and 1.25% triisopropylsilane (TIPS). The solvent was removed by co-distillation with ether by rotary evaporation and dried under reduced pressure. The product was purified using reversed-phase high-performance liquid chromatography (HPLC, Thermofisher Dionex Ultimate 3000, Hypersil Gold 250x4.8 mm) in a linear gradient of acetonitrile (ACN with 0.1% TFA, 40% to 98%) and water with 0.1% TFA. Purified product was lyophilized and stored at -20 °C until further use. The purity of the peptide was analysed by electrospray ionization mass spectrometry in positive mode (ESI-MS) as well as analytical HPLC (Thermofisher *Dionex* Ultimate 3000, eluted with a gradient of 0.1% TFA in water: 0.1% TFA in ACN from 40:60 to 2:98 in 10 minutes, see below for results).

Stock solutions of the precursor were prepared by dissolving the precursor in MES buffer, after which the pH was adjusted to pH 6.0. Stock solutions of EDC were prepared by dissolving the EDC powder in MQ water. Typically, stock solutions of 1.0 M EDC were used freshly. Reaction networks were started by addition of the high concentration EDC to the peptide solution. All analysis was carried out at 25°C.

Synthesis of the succinic acid derivatives.

Precursor acids were synthesized by treating the corresponding anhydrides with two (mass)-equivalents of MQ water and stirred overnight at room temperature. No starting material was found by HPLC. We lyophilized the mixture and stored it at -20 °C until further use.

We prepared stock solutions of the precursors by dissolving the acid in 0.2 M MES buffer, after which we adjusted the pH to pH 6.0, 7.4 or 8.0. Stock solutions of EDC

were prepared by dissolving the EDC powder in MQ water. We prepared the stock solutions of 1.0 M EDC freshly. Reaction cycles were started by addition of the high concentration EDC to the acid solution. We carried out all experiments at 25 (± 0.5), 37 (± 0.5) or 45 (± 0.5) °C

High Performance Liquid Chromatography (HPLC). The kinetics of the chemical reaction networks were monitored over time by means of analytical HPLC (ThermoFisher Dionex Ultimate 3000, Hypersil Gold 250 x 4.8 mm). A 750 μ L sample was prepared as described above and placed into a screw cap HPLC vial. Samples of the solutions (1.0 μ L or 25 μ L) were directly injected without further dilution and tracked with a UV/Vis detector at 220, 240, and 254 nm. All compounds involved were separated using a linear gradient of H₂O: ACN each with 0.1% TFA.

Method 1: H₂O: ACN from 40:60 to 2:98 in 8 min;

Method 2: H₂O: ACN from 98:2 to 2:98 in 12 min;

Both methods were followed by 2 min 98% ACN. Calibration curves for the EDC (in MQ water), acids (in MES buffer), anhydrides (in ACN) and drugs (in ACN or MQ-water) were performed with the corresponding method in triplicate.

UV/Vis Spectroscopy. The UV/Vis measurements were carried out using a Multiskan FC (ThermoFisher) microplate reader. Samples (200 μ L) were directly prepared into a 96 well-plate (tissue culture plate non-treated). The Temperature (25 (± 0.5), 37 (± 0.5) or 45 (± 0.5) °C) was set 30 min before starting the measurement. Each experiment was performed at 500 nm and in triplicate.

Dynamic light scattering (DLS). We carried out DLS measurements on all solutions with a DynaPro NanoStar from Wyatt with a laser wavelength of 658 nm in disposable cuvette for DLS from Wyatt. The measurements consisted of 5 acquisitions with an acquisition time of 10 seconds for turbid samples. The remaining experiments consisted of 1 acquisition with an acquisition time of 5 seconds. For measurements and analysis, we used the software Dynamics V7.

Liquid Chromatography - Mass Spectrometry (LC-MS). LC-MS measurements were performed using an Agilent Technologies 1260 Infinity LC-MS system with a 6310 quadrupole spectrometer. The solvent system consisted of 0.1% formic acid in

water as buffer A and 0.1% formic acid in acetonitrile as buffer B. The samples were analyzed in positive mode and followed by UV absorbance at 193, 254 and/or 280 nm.

Electrospray Ionization (ESI). We used a Varian 500 MS LC ion trap to perform ESI-MS measurements. The samples were diluted in acetonitrile before injection into an acetonitrile carrier flow (20 $\mu\text{L min}^{-1}$).

Nile Red Assay. The Nile Red assay was performed on a Jasco (FP-8300) spectrofluorometer with external temperature control (MCB-100). Samples were directly prepared in the 10 mm quartz cuvette (Precision Cells Inc.) by mixing different concentrations of precursor (from 0.01 to 100 mM in 0.2 M MES buffer) with Nile Red (5 μM). The fluorescence intensities were measured at 635 nm with an excitation at 550 nm. The corresponding blue shift was calculated by subtracting the intensity of the blank (0.2 M MES buffer with 5 μM Nile Red) from the corresponding sample.

Solubility determination of Fmoc-E. The samples of Fmoc-E (10 mM) were prepared as described above in different buffer concentrations (50, 100, 200, 500 and 1350 mM MES). After the pH was adjusted to 1, the precipitate was filtered off with a 200 nm syringe filter. HPLC analysis was carried out like described above to determine the remaining Fmoc-E in solution.

Fluorescence Microscopy. Fluorescence microscopy was performed on a Leica DMI8 microscope using a 63x oil immersion objective with TXR filter (Exc. 540-580; Em. 592-668; DC 585). We prepared samples as described above but with 2.5 μM Nile Red as a dye. We deposited 20 μL of the sample on the glass slide and covered with a 12 mm diameter coverslip. Samples were excited with 543 nm laser and imaged at 580-700 nm. Particle diameters were counted using ImageJ cell counting package.

Confocal Fluorescence Microscopy. Confocal fluorescence microscopy was performed on a Leica SP5 confocal microscope using a 63x oil immersion objective. Samples were prepared as described above, but with 2.5 μM Nile Red as dye. 20 μL of the sample was deposited on the PEG-coated glass slide and covered with a 12 mm diameter coverslip. Samples were excited with a 543 nm laser and imaged at 580-

700 nm. Every 30 seconds, we acquired a 4096 x 4096 image of an area that covered 246 x 246 μm . We performed each experiment in triplicate.

Image analysis. ImageJ's preinstalled "analyse particles" package was used to analyse the number of vesicles and their circumference under the assumption that the particles were perfectly spherical. Each data point corresponds to one image and was performed in triplicate.

Cryogenic-Transmission Electron Microscopy (cryo-TEM). Samples for TEM were prepared as described above. The grids (Quantifoil R2/2, 400 mesh, Cu or C-Flat R2/2 or R4/2, 400 mesh, Cu) were freshly glow-discharged (50 mA) for 90 seconds prior to use. Preparation of the grids was performed in a FEI/Thermo Fisher Vitrobot at 25 °C with the relative humidity set to 100%. Sample (4 μL) was incubated for 30 seconds, blotted for 2.0 to 3.0 seconds (blotting force set to -1) and then also directly plunged into liquid ethane. The cryo-TEM grids were transferred and stored in liquid nitrogen, and when needed, placed into a Gatan cryo-transfer-specimen holder to insert into the microscope. The specimen temperature was maintained at -170 °C during the data collection. Cryo-TEM imaging was performed on a Jeol JEM-1400 or a Tecnai Spirit microscope (FEI/Thermo Fisher) operating at 120 kV. The images were recorded in a low-dose mode on a CCD camera.

Drug Release Experiments. A 2% agar-agar stock in 0.2 M MES buffer pH 6.0 was heated to 90 °C. For the first-order release experiments, X μL of a 5 mM stock solution of the drug (in acetonitrile for Nimesulide/Nitrendipine, in dimethylsulfoxide for Acyclovir) was added to 500 μL 7.5 mM C₁₀ precursor in 0.2 M MES buffer pH 6.0. 500 μL of the hot agar was added, and 60 μL of this mixture was immediately put on the bottom of a 96 well plate. After 1 min 120 μL of 0.2 M MES buffer was added as a supernatant. The release of precursor and drug to the supernatant was measured via HPLC. For every HPLC injection, a separate well was prepared. For the zero-order release experiments, the precursor solution was activated as described above. The drug was added after 30 min and agar after 45 min. We carried out the rest of the experiment as described above.

Spin Down Experiments. 500 μL of the precursor solution was activated as described above. After 30 min, X μL of a 5 mM stock solution of the drug (in acetonitrile for Nimesulide/Nitrendipine, in dimethylsulfoxide for Acyclovir) was added. One hour in the experiment, the solution was put in a centrifuge for 5 min ($\text{rcf} = 5.5$). The aqueous phase (200 μL) was measured by HPLC to determine the amount of drug left.

9. Further Publications

Besides the three publications reprinted above, I contributed to five more publications of the group from Prof. Job Boekhoven. Additionally, Prof. Job Boekhoven and I have a pending patent that resulted from the discoveries I described in chapter 6. The following section is a full list of the achievements during my PhD.

Publications:

- 1 K. Dai, J. Rodon Fores, C. Wanzke, B. Winkeljann, A. Bergmann, O. Lieleg, J. Boekhoven, "Regulating chemically fueled peptide assemblies by molecular design" *J. Am. Chem. Soc.* **2020**, *142* (33), 14142.
- 2 C. Wanzke, M. Tena-Solsona, B. Rieß, L. Tebcharani, J. Boekhoven, 'Active droplets in a hydrogel release drugs with a constant and tunable rate' *Mater. Horiz.* **2020**, *7*, 1397.
- 3 C. Wanzke, A. Jussupow, F. Kohler, H. Dietz, V.R.I. Kaila, J. Boekhoven, 'Dynamic vesicles formed by dissipative self-assembly' *ChemSystemsChem* **2020**, *2*, e1900044.
- 4 M. Tena-Solsona, J. Janssen, C. Wanzke, F. Schnitter, H. Park, B. Rieß, J.M. Gibbs, C.A. Weber, J. Boekhoven, 'Kinetic Control over Droplet Ripening in Fuel-Driven Active Emulsions' *ChemRxiv*, **2019**, preprint, DOI: 10.26434/chemrxiv.9978539.v1.
- 5 R.K. Grötsch, C. Wanzke, M. Speckbacher, A. Angi, B. Rieger, J. Boekhoven, 'Pathway dependence in the fuel-driven dissipative self-assembly of nanoparticles' *J. Am. Chem. Soc.* **2019**, *141* (25), 9872.
- 6 R.K. Grötsch,* A. Angi,* Y.G. Mideksa, C. Wanzke, M. Tena-Solsona, M. Feige, B. Rieger, J. Boekhoven, 'Dissipative self-assembly of photoluminescent silicon nanocrystals' *Angew. Chem.* **2018**, *57*, 14608.

- 7 B. Rieß,* C. Wanzke,* M. Tena-Solsona, R.K. Grötsch, C. Maity, J. Boekhoven, 'Dissipative assemblies that inhibit their deactivation' *Soft Matter* **2018**, *14*, 4852.
- 8 M. Tena-Solsona, C. Wanzke, B. Rieß, A. Bausch, J. Boekhoven, 'Self-selection of dissipative assemblies from primitive chemical reaction networks' *Nat. Commun.* **2018**, *9*, 2044.
- 9 M. Tena-Solsona,* B. Rieß,* R.K. Grötsch, F. Löhrer, C. Wanzke, B. Käsdorf, A. Bausch, P. Mueller-Buschbaum, O. Lieleg, J. Boekhoven, 'Non-equilibrium dissipative supramolecular materials with a tunable lifetime' *Nat. Commun.* **2017**, *8*, 15895.

* These Authors contributed equally to this work.

Patents:

- 1 J. Boekhoven, C. Wanzke 'Hydrogel Compositions for the Controlled and Constant Release of Active Agents', EP 19 199 465.6.

10. Acknowledgments

Being a PhD student, I guess everyone who made this experience agrees, is a special situation in life. I was surrounded by people my age, we were interested in and working in the same field, not as competitors but as a team, as colleagues and in the end as friends. We brainstormed, listened, discussed, learned, taught, helped, wrote and shared, not only knowledge, instruments, problems but also a coffee-machine, endless hours in the lab and a beer (or a wine) from time to time.

To begin with, I want to thank *Prof. Job Boekhoven* for giving me this great opportunity to work in this interesting area and creating a research environment that was harmonic and thriving as well as scientifically challenging. Thank you for all the discussions, trust in me and my ideas and support in every direction.

I would like to thank my committee, *Prof. Matthias Feige*, *Prof. Oliver Lieleg* and *Prof. Max von Delius*, for accepting to review my work.

Of course, I want to thank the whole Boekhoven Lab. First of all, *Dr. Marta Tena-Solsona*, *Dr. Raphael Grötsch* and *Benedikt Rieß*, thank you so much for the warm welcome in the group, answering all my questions and explaining me everything in the beginning as well as including me in the group within a second. No matter what I had to deal with, you guys were there and made it fun. I really appreciated every day working with you in the lab and I could not imagine a better OG team of this group. (Special mention of Benno and Rapha for always handling my 'Dienstreiseantrag'! Thanks, without you I would be poor ;)

Especially, I want to say thank you to *Maximilian Schneider*, *Laura Tebcharani* and *Christine Kriebisch* for working with me on the drug delivery project. Your motivation and ideas were great and without you the project would not be where it is right now.

Dear rest of the group: *Fabian Schnitter*, *Patrick Schwarz*, *Carsten Donau*, *Kun Dai*, *Michi Würbser*, *Alexander Bergmann*, *Xiaoyao Chen*, *Michele Stasi*, *Dr. Jennifer Rodon-Fores*, *Fabian Späth* and *Brigitte Kriebisch*, thank you for all the help and support! I enjoyed every discussion, every lunch, every laughter, every BBQ and, of course, every game of Schafkopf!

Furthermore, I want to thank all of my collaboration partners for their work. *Theresa Lutz* and *Prof. Oliver Lieleg* for the toxicity experiments in the drug delivery project, *Alexander Jussupow* and *Prof. Ville Kaila* for the molecular simulations in the vesicle project and, *Fabian Kohler* and *Prof. Hendrik Dietz* for letting me use the TEM as well as their support. For financial support I want to acknowledge the TUM as well as the DFG CRC/SFB 235 'Emergence of Life'.

Arzu, even though you are part of the group you do not really fit in the list above. Thank you for our secret friendship, for your honest and diverse opinion and that you are always right.

Liebste Bremen Crew! *David, Ahmad, Tunay*, ihr seid von Anfang an dabei gewesen. Wir haben die ersten drei Jahre des Studiums zusammen verbracht, zusammen gefeiert und auch zusammen gelitten. Obwohl wir danach alle unsere eigenen Wege gegangen sind, wart ihr doch immer an meiner Seite. Danke!

Lara, eigentlich kann ich nur sagen: Danke für alles! Ohne dich wäre ich jetzt wahrscheinlich nicht wo ich bin. Danke für endlose Gespräche, fürs ins Gewissen reden, fürs Vertrauen, fürs 'an mich glauben', fürs positiv bleiben und sogar quasi fürs Promotionsstelle finden :)

Tanja, danke, dass du immer an meiner Seite bist, dass du mich auffängst und mir zuhörst. Danke fürs ehrlich sein, fürs auslachen und miteinander lachen, fürs ablenken und fürs 5-Tage-in-einer-Woche-feiern-gehen aber vor allem fürs da sein. Seit Schulzeiten aber besonders in den letzten Jahren.

Danke an alle meine Freunde, neue und alte, *Dani, Coco, Corinna, Max, Kerstin, Lohse, Anna-Lisa, Franzi, Chris, Maxi* und an dich, *Ferdinand*, fürs Kraft und Halt geben in den letzten Monaten.

Zuletzt natürlich tausend Dank an euch, liebe *Mama*, lieber *Papa*, für all die Möglichkeiten, die ihr mir eröffnet, das Vertrauen, das ihr mir geschenkt, und die Kraft, die ihr mir gegeben habt.

11. References

- (1) G. M. Whitesides, B. Grzybowski, *Science* **2002**, *295*, 2418.
- (2) M. Fialkowski, K. J. M. Bishop, R. Klajn, S. K. Smoukov, C. J. Campbell, B. A. Grzybowski, *The Journal of Physical Chemistry B* **2006**, *110*, 2482-2496.
- (3) G. Whitesides, J. Mathias, C. Seto, *Science* **1991**, *254*, 1312-1319.
- (4) G. M. Whitesides, M. Boncheva, *Proceedings of the National Academy of Sciences* **2002**, *99*, 4769-4774.
- (5) L. Isaacs, D. N. Chin, N. B. Bowden, Y. Xia, G. M. Whitesides, in *Supramolecular Materials and Technologies, Vol. 4* (Ed.: D. N. Reinhoudt), John Wiley and Sons Ltd., New York, **1999**, pp. 1-46.
- (6) J.-M. Lehn, in *Chemical Synthesis: Gnosis to Prognosis* (Eds.: C. Chatgililoglu, V. Snieckus), Springer Netherlands, Dordrecht, **1996**, pp. 511-524.
- (7) B. Olenyuk, J. A. Whiteford, A. Fechtenkötter, P. J. Stang, *Nature* **1999**, *398*, 796-799.
- (8) F. J. Martin, R. C. MacDonald, *Biochemistry* **1976**, *15*, 321-327.
- (9) V. Grantcharova, E. J. Alm, D. Baker, A. L. Horwich, *Current Opinion in Structural Biology* **2001**, *11*, 70-82.
- (10) N. G. A. Abrescia, L. Malinina, L. G. Fernandez, J. A. Subirana, T. Huynh-Dinh, S. Neidle, *Nucleic Acids Research* **1999**, *27*, 1593-1599.
- (11) B. Alberts, A. Johnson, J. Lewis, *Molecular Biology of the Cell, Vol. 4*, Garland Science, New York, **2002**.
- (12) D. Philp, J. F. Stoddart, *Angewandte Chemie International Edition in English* **1996**, *35*, 1154-1196.
- (13) B. A. Grzybowski, C. E. Wilmer, J. Kim, K. P. Browne, K. J. M. Bishop, *Soft Matter* **2009**, *5*, 1110-1128.
- (14) S. A. P. van Rossum, M. Tena-Solsona, J. H. van Esch, R. Eelkema, J. Boekhoven, *Chemical Society Reviews* **2017**, *46*, 5519-5535.
- (15) F. Tantakitti, J. Boekhoven, X. Wang, R. V. Kazantsev, T. Yu, J. Li, E. Zhuang, R. Zandi, J. H. Ortony, C. J. Newcomb, L. C. Palmer, G. S. Shekhawat, M. O. de la Cruz, G. C. Schatz, S. I. Stupp, *Nature Materials* **2016**, *15*, 469-476.
- (16) A. Sorrenti, J. Leira-Iglesias, A. J. Markvoort, T. F. A. de Greef, T. M. Hermans, *Chemical Society Reviews* **2017**, *46*, 5476-5490.
- (17) R. K. Grötsch, J. Boekhoven, in *Self-assembling Biomaterials* (Eds.: H. S. Azevedo, R. M. P. da Silva), Woodhead Publishing, **2018**, pp. 235-250.
- (18) A. Patist, S. G. Oh, R. Leung, D. O. Shah, *Colloids and Surfaces A: Physicochemical and Engineering Aspects* **2001**, *176*, 3-16.
- (19) D. A. Fletcher, R. D. Mullins, *Nature* **2010**, *463*, 485-492.
- (20) T. Aida, E. W. Meijer, S. I. Stupp, *Science* **2012**, *335*, 813-817.
- (21) M. J. Webber, E. A. Appel, E. W. Meijer, R. Langer, *Nature Materials* **2016**, *15*, 13-26.
- (22) M. R. Chierotti, R. Gobetto, *Supramolecular Chemistry: From Molecules to Nanomaterials*, **2012**.
- (23) D. B. Amabilino, D. K. Smith, J. W. Steed, *Chemical Society Reviews* **2017**, *46*, 2404-2420.
- (24) A. R. Hirst, B. Escuder, J. F. Miravet, D. K. Smith, *Angewandte Chemie International Edition* **2008**, *47*, 8002-8018.
- (25) P. Jonkheijm, P. van der Schoot, A. P. H. J. Schenning, E. W. Meijer, *Science* **2006**, *313*, 80-83.

-
- (26) G. Lebon, D. Jou, J. Casas-Vázquez, *Understanding Non-equilibrium Thermodynamics*, Springer-Verlag, Berlin Heidelberg, **2008**.
- (27) J. A. Shapiro, *Annual Review of Microbiology* **1998**, *52*, 81-104.
- (28) I. M. Cheeseman, A. Desai, *Nature Reviews Molecular Cell Biology* **2008**, *9*, 33-46.
- (29) A. Desai, T. J. Mitchison, *Annual Review of Cell and Developmental Biology* **1997**, *13*, 83-117.
- (30) T. Mitchison, M. Kirschner, *Nature* **1984**, *312*, 237-242.
- (31) B. Rieß, R. K. Grötsch, J. Boekhoven, *Chem* **2019**, DOI: 10.1016/j.chmpr.2019.22.008.
- (32) J. Boekhoven, A. M. Brizard, K. N. K. Kowłgi, G. J. M. Koper, R. Eelkema, J. H. van Esch, *Angewandte Chemie International Edition* **2010**, *49*, 4825-4828.
- (33) J. Boekhoven, W. E. Hendriksen, G. J. M. Koper, R. Eelkema, J. H. van Esch, *Science* **2015**, *349*, 1075.
- (34) J. J. D. de Jong, P. R. Hania, A. Pugžlys, L. N. Lucas, M. de Loos, R. M. Kellogg, B. L. Feringa, K. Duppen, J. H. van Esch, *Angewandte Chemie International Edition* **2005**, *44*, 2373-2376.
- (35) R. Klajn, P. J. Wesson, K. J. M. Bishop, B. A. Grzybowski, *Angewandte Chemie International Edition* **2009**, *48*, 7035-7039.
- (36) D. Samanta, R. Klajn, *Advanced Optical Materials* **2016**, *4*, 1373-1377.
- (37) S. Debnath, S. Roy, R. V. Ulijn, *Journal of the American Chemical Society* **2013**, *135*, 16789-16792.
- (38) S. Maiti, I. Fortunati, C. Ferrante, P. Scrimin, L. J. Prins, *Nature Chemistry* **2016**, *8*, 725.
- (39) C. G. L. Wolf, E. K. Rideal, *Biochemical Journal* **1922**, *16*, 548-555.
- (40) F. M. Menger, K. L. Caran, *Journal of the American Chemical Society* **2000**, *122*, 11679-11691.
- (41) A. Sorrenti, J. Leira-Iglesias, A. Sato, T. M. Hermans, *Nature Communications* **2017**, *8*, 15899.
- (42) D. Görl, X. Zhang, F. Würthner, *Angewandte Chemie International Edition* **2012**, *51*, 6328-6348.
- (43) F. Würthner, C. R. Saha-Möller, B. Fimmel, S. Ogi, P. Leowanawat, D. Schmidt, *Chemical Reviews* **2016**, *116*, 962-1052.
- (44) M. J. Webber, C. J. Newcomb, R. Bitton, S. I. Stupp, *Soft Matter* **2011**, *7*, 9665-9672.
- (45) Z. Yang, G. Liang, L. Wang, B. Xu, *Journal of the American Chemical Society* **2006**, *128*, 3038-3043.
- (46) T.-H. Ku, M.-P. Chien, M. P. Thompson, R. S. Sinkovits, N. H. Olson, T. S. Baker, N. C. Gianneschi, *Journal of the American Chemical Society* **2011**, *133*, 8392-8395.
- (47) M. Tena-Solsona, B. Rieß, R. K. Grötsch, F. C. Löhner, C. Wanzke, B. Käsdorf, A. R. Bausch, P. Müller-Buschbaum, O. Lieleg, J. Boekhoven, *Nature Communications* **2017**, *8*, 15895.
- (48) L. S. Kariyawasam, C. S. Hartley, *Journal of the American Chemical Society* **2017**, *139*, 11949-11955.
- (49) M. de Loos, B. L. Feringa, J. H. van Esch, *European Journal of Organic Chemistry* **2005**, *2005*, 3615-3631.
- (50) R. J. Macfarlane, B. Lee, M. R. Jones, N. Harris, G. C. Schatz, C. A. Mirkin, *Science* **2011**, *334*, 204-208.
- (51) P. W. K. Rothmund, *Nature* **2006**, *440*, 297-302.

-
- (52) R. N. Shah, N. A. Shah, M. M. Del Rosario Lim, C. Hsieh, G. Nuber, S. I. Stupp, *Proceedings of the National Academy of Sciences* **2010**, *107*, 3293-3298.
- (53) J. H. van Esch, *Langmuir* **2009**, *25*, 8392-8394.
- (54) P. Yin, H. M. T. Choi, C. R. Calvert, N. A. Pierce, *Nature* **2008**, *451*, 318-322.
- (55) M. Zelzer, R. V. Ulijn, *Chemical Society Reviews* **2010**, *39*, 3351-3357.
- (56) J.-C. Loudet, P. Barois, P. Poulin, *Nature* **2000**, *407*, 611-613.
- (57) L. Zhang, A. Eisenberg, *Science* **1995**, *268*, 1728-1731.
- (58) B. Jeong, Y. H. Bae, D. S. Lee, S. W. Kim, *Nature* **1997**, *388*, 860-862.
- (59) K. T. Oh, T. K. Bronich, A. V. Kabanov, *Journal of Controlled Release* **2004**, *94*, 411-422.
- (60) G. A. Silva, C. Czeisler, K. L. Niece, E. Beniash, D. A. Harrington, J. A. Kessler, S. I. Stupp, *Science* **2004**, *303*, 1352-1355.
- (61) R. Merindol, A. Walther, *Chemical Society Reviews* **2017**, *46*, 5588-5619.
- (62) H. J. Borg, R. v. Woudenberg, *Journal of Magnetism and Magnetic Materials* **1999**, *193*, 519-525.
- (63) F. Jedema, *Nature Materials* **2007**, *6*, 90-91.
- (64) B. Rieß, J. Boekhoven, *ChemNanoMat* **2018**, *4*, 710-719.
- (65) M. Häckel, L. Kador, D. Kropp, H.-W. Schmidt, *Advanced Materials* **2007**, *19*, 227-231.
- (66) F. Li, J. Zhuang, G. Jiang, H. Tang, A. Xia, L. Jiang, Y. Song, Y. Li, D. Zhu, *Chemistry of Materials* **2008**, *20*, 1194-1196.
- (67) S.-J. Lim, B.-K. An, S. D. Jung, M.-A. Chung, S. Y. Park, *Angewandte Chemie International Edition* **2004**, *43*, 6346-6350.
- (68) S. Kobatake, S. Takami, H. Muto, T. Ishikawa, M. Irie, *Nature* **2007**, *446*, 778-781.
- (69) R. Del Vecchio, N. V. Blough, *Marine Chemistry* **2002**, *78*, 231-253.
- (70) R. Klajn, K. J. M. Bishop, B. A. Grzybowski, *Proceedings of the National Academy of Sciences* **2007**, *104*, 10305-10309.
- (71) R. Klajn, K. J. M. Bishop, M. Fialkowski, M. Paszewski, C. J. Campbell, T. P. Gray, B. A. Grzybowski, *Science* **2007**, *316*, 261-264.
- (72) R. Klajn, T. P. Gray, P. J. Wesson, B. D. Myers, V. P. Dravid, S. K. Smoukov, B. A. Grzybowski, *Advanced Functional Materials* **2008**, *18*, 2763-2769.
- (73) R. Klajn, A. O. Pinchuk, G. C. Schatz, B. A. Grzybowski, *Angewandte Chemie International Edition* **2007**, *46*, 8363-8367.
- (74) T. Yasumoto, M. Murata, *Chemical Reviews* **1993**, *93*, 1897-1909.
- (75) P. Nissen, J. Hansen, N. Ban, P. B. Moore, T. A. Steitz, *Science* **2000**, *289*, 920-930.
- (76) Y. J. Hong, D. J. Tantillo, *Journal of the American Chemical Society* **2009**, *131*, 7999-8015.
- (77) B. C. Tripp, K. Smith, J. G. Ferry, *Journal of Biological Chemistry* **2001**, *276*, 48615-48618.
- (78) H. J. Forman, I. Fridovich, *Archives of Biochemistry and Biophysics* **1973**, *158*, 396-400.
- (79) L. B. Poole, P. A. Karplus, A. Claiborne, *Annual Review of Pharmacology and Toxicology* **2004**, *44*, 325-347.
- (80) M. W. Kanan, M. M. Rozenman, K. Sakurai, T. M. Snyder, D. R. Liu, *Nature* **2004**, *431*, 545-549.
- (81) X. Li, D. R. Liu, *Angewandte Chemie International Edition* **2004**, *43*, 4848-4870.
- (82) M. Movassaghi, E. N. Jacobsen, *Science* **2002**, *298*, 1904-1905.
- (83) T. M. Penning, J. M. Jez, *Chemical Reviews* **2001**, *101*, 3027-3046.

-
- (84) H. Zhao, S. Sen, T. Udayabhaskararao, M. Sawczyk, K. Kučanda, D. Manna, P. K. Kundu, J.-W. Lee, P. Král, R. Klajn, *Nature Nanotechnology* **2016**, *11*, 82-88.
- (85) P. K. Kundu, G. L. Olsen, V. Kiss, R. Klajn, *Nature Communications* **2014**, *5*, 3588.
- (86) Y.-S. Wei, M. Zhang, P.-Q. Liao, R.-B. Lin, T.-Y. Li, G. Shao, J.-P. Zhang, X.-M. Chen, *Nature Communications* **2015**, *6*, 8348.
- (87) A. Fallah-Araghi, K. Meguellati, J.-C. Baret, A. E. Harrak, T. Mangeat, M. Karplus, S. Ladame, C. M. Marques, A. D. Griffiths, *Physical Review Letters* **2014**, *112*, 028301.
- (88) D. Yang, S. Peng, M. R. Hartman, T. Gupton-Campolongo, E. J. Rice, A. K. Chang, Z. Gu, G. Q. Lu, D. Luo, *Scientific Reports* **2013**, *3*, 3165.
- (89) J. Crosby, T. Treadwell, M. Hammerton, K. Vasilakis, M. P. Crump, D. S. Williams, S. Mann, *Chemical Communications* **2012**, *48*, 11832-11834.
- (90) C. Pezzato, L. J. Prins, *Nature Communications* **2015**, *6*, 7790.
- (91) J. M. Rosiak, F. Yoshii, *Nuclear Instruments and Methods in Physics Research Section B: Beam Interactions with Materials and Atoms* **1999**, *151*, 56-64.
- (92) M. R. Singh, S. Patel, D. Singh, in *Nanobiomaterials in Soft Tissue Engineering* (Ed.: A. M. Grumezescu), William Andrew Publishing, **2016**, pp. 231-260.
- (93) E. M. Ahmed, *Journal of Advanced Research* **2015**, *6*, 105-121.
- (94) N. A. Peppas, J. Z. Hilt, A. Khademhosseini, R. Langer, *Advanced Materials* **2006**, *18*, 1345-1360.
- (95) J. L. Drury, D. J. Mooney, *Biomaterials* **2003**, *24*, 4337-4351.
- (96) V. Pertici, C. Pin-Barre, C. Rivera, C. Pellegrino, J. Laurin, D. Gigmes, T. Trimaille, *Biomacromolecules* **2019**, *20*, 149-163.
- (97) J. Li, D. J. Mooney, *Nature Reviews Materials* **2016**, *1*, 16071.
- (98) T. R. Hoare, D. S. Kohane, *Polymer* **2008**, *49*, 1993-2007.
- (99) A. K. Azad, N. Sermsintham, S. Chandkrachang, W. F. Stevens, *Journal of Biomedical Materials Research Part B: Applied Biomaterials* **2004**, *69B*, 216-222.
- (100) V. Compañ, A. Andrio, A. López-Aleman, E. Riande, M. F. Refojo, *Biomaterials* **2002**, *23*, 2767-2772.
- (101) P. Chakma, D. Konkolewicz, *Angewandte Chemie International Edition* **2019**, *58*, 9682-9695.
- (102) C. G. Pappas, I. R. Sasselli, R. V. Ulijn, *Angewandte Chemie International Edition* **2015**, *54*, 8119-8123.
- (103) C. M. Rufo, Y. S. Moroz, O. V. Moroz, J. Stöhr, T. A. Smith, X. Hu, W. F. DeGrado, I. V. Korendovych, *Nature Chemistry* **2014**, *6*, 303-309.
- (104) P. W. J. M. Frederix, G. G. Scott, Y. M. Abul-Haija, D. Kalafatovic, C. G. Pappas, N. Javid, N. T. Hunt, R. V. Ulijn, T. Tuttle, *Nature Chemistry* **2015**, *7*, 30-37.
- (105) M. Reches, E. Gazit, *Science* **2003**, *300*, 625-627.
- (106) J. Naskar, G. Palui, A. Banerjee, *The Journal of Physical Chemistry B* **2009**, *113*, 11787-11792.
- (107) J. M. Slocik, R. R. Naik, *Chemical Society Reviews* **2010**, *39*, 3454-3463.
- (108) S. Marchesan, C. D. Easton, F. Kushkaki, L. Waddington, P. G. Hartley, *Chemical Communications* **2012**, *48*, 2195-2197.
- (109) S. Marchesan, L. Waddington, C. D. Easton, D. A. Winkler, L. Goodall, J. Forsythe, P. G. Hartley, *Nanoscale* **2012**, *4*, 6752-6760.
- (110) J. Fastrez, A. R. Fersht, *Biochemistry* **1973**, *12*, 2025-2034.
- (111) X. Qin, W. Xie, S. Tian, J. Cai, H. Yuan, Z. Yu, G. L. Butterfoss, A. C. Khuong, R. A. Gross, *Chemical Communications* **2013**, *49*, 4839-4841.

-
- (112) B. Zhang, I. M. Jayalath, J. Ke, J. L. Sparks, C. S. Hartley, D. Konkolewicz, *Chemical Communications* **2019**, 55, 2086-2089.
- (113) C. T. Huynh, D. S. Lee, in *Encyclopedia of Polymeric Nanomaterials* (Eds.: S. Kobayashi, K. Müllen), Springer Berlin Heidelberg, Berlin, Heidelberg, **2015**, pp. 439-449.
- (114) H. O. Tbompsont, C. O. Lee, *Journal of the American Pharmaceutical Association* **1945**, 34, 135-138.
- (115) W. H. Helfand, D. L. Cowen, *Pharm Hist* **1983**, 25, 3-18.
- (116) D. M. Yebra, S. Kiil, K. Dam-Johansen, *Progress in Organic Coatings* **2004**, 50, 75-104.
- (117) A. Shaviv, R. L. Mikkelsen, *Fertilizer research* **1993**, 35, 1-12.
- (118) A. Shaviv, in *Advances in Agronomy, Vol. 71*, Academic Press, **2001**, pp. 1-49.
- (119) J. Ge, R. Wu, X. Shi, H. Yu, M. Wang, W. Li, *Journal of Applied Polymer Science* **2002**, 86, 2948-2952.
- (120) X. Han, S. Chen, X. Hu, *Desalination* **2009**, 240, 21-26.
- (121) T. Heuser, E. Weyandt, A. Walther, *Angewandte Chemie International Edition* **2015**, 54, 13258-13262.
- (122) N. A. Peppas, *Current Opinion in Colloid & Interface Science* **1997**, 2, 531-537.
- (123) K. E. Uhrich, S. M. Cannizzaro, R. S. Langer, K. M. Shakesheff, *Chemical Reviews* **1999**, 99, 3181-3198.
- (124) J. Wang, B. M. Wang, S. P. Schwendeman, *Journal of Controlled Release* **2002**, 82, 289-307.
- (125) L. Z. Benet, *Journal of Pharmaceutical Sciences* **2013**, 102, 34-42.
- (126) L. C. Collins-Gold, R. T. Lyons, L. C. Bartholow, *Advanced Drug Delivery Reviews* **1990**, 5, 189-208.
- (127) A. S. Narang, D. Delmarre, D. Gao, *International Journal of Pharmaceutics* **2007**, 345, 9-25.
- (128) S. S. Davis, C. Washington, P. West, L. Illum, G. Liversidge, L. Sternson, R. Kirsh, *Annals of the New York Academy of Sciences* **1987**, 507, 75-88.
- (129) Y.-N. Zhao, X. Xu, N. Wen, R. Song, Q. Meng, Y. Guan, S. Cheng, D. Cao, Y. Dong, J. Qie, K. Liu, Y. Zhang, *Scientific Reports* **2017**, 7, 5524.
- (130) F. van de Manacker, K. Braeckmans, N. e. Morabit, S. C. De Smedt, C. F. van Nostrum, W. E. Hennink, *Advanced Functional Materials* **2009**, 19, 2992-3001.
- (131) A. Gokhale, *Pharmaceutical Technology* **2014**, 38.
- (132) R. Langer, *Nature* **1998**, 392, 5-10.
- (133) D. S. T. Hsieh, W. D. Rhine, R. Langer, *Journal of Pharmaceutical Sciences* **1983**, 72, 17-22.
- (134) A. Abramson, E. Caffarel-Salvador, M. Khang, D. Dellal, D. Silverstein, Y. Gao, M. R. Frederiksen, A. Vegge, F. Hubálek, J. J. Water, A. V. Friderichsen, J. Fels, R. K. Kirk, C. Cleveland, J. Collins, S. Tamang, A. Hayward, T. Landh, S. T. Buckley, N. Roxhed, U. Rahbek, R. Langer, G. Traverso, *Science* **2019**, 363, 611-615.
- (135) O. S. Fenton, K. N. Olafson, P. S. Pillai, M. J. Mitchell, R. Langer, *Advanced Materials* **2018**, 30, 1705328.
- (136) A. R. Kirtane, O. Abouzid, D. Minahan, T. Bensele, A. L. Hill, C. Selinger, A. Bershteyn, M. Craig, S. S. Mo, H. Mazdiyasn, C. Cleveland, J. Rogner, Y.-A. L. Lee, L. Booth, F. Javid, S. J. Wu, T. Grant, A. M. Bellinger, B. Nikolic, A. Hayward, L. Wood, P. A. Eckhoff, M. A. Nowak, R. Langer, G. Traverso, *Nature Communications* **2018**, 9, 2.
- (137) J. Weidner, *Drug Discovery Today* **2002**, 7, 632.

-
- (138) M. Ali, S. Horikawa, S. Venkatesh, J. Saha, J. W. Hong, M. E. Byrne, *Journal of Controlled Release* **2007**, *124*, 154-162.
- (139) C. Celia, S. Ferrati, S. Bansal, A. L. van de Ven, B. Ruozi, E. Zabre, S. Hosali, D. Paolino, M. G. Sarpietro, D. Fine, M. Fresta, M. Ferrari, A. Grattoni, *Advanced Healthcare Materials* **2014**, *3*, 230-238.
- (140) L. Lei, X. Liu, Y.-Y. Shen, J.-Y. Liu, M.-F. Tang, Z.-M. Wang, S.-R. Guo, L. Cheng, *European Journal of Pharmaceutics and Biopharmaceutics* **2011**, *78*, 49-57.
- (141) H. Zhang, R. Hao, X. Ren, L. Yu, H. Yang, H. Yu, *RSC Advances* **2013**, *3*, 22927-22930.
- (142) L. Zhang, J. Alfano, D. Race, R. N. Davé, *European Journal of Pharmaceutical Sciences* **2018**, *117*, 245-254.
- (143) D. Fine, A. Grattoni, S. Hosali, A. Ziemys, E. De Rosa, J. Gill, R. Medema, L. Hudson, M. Kojic, M. Milosevic, L. Brousseau lii, R. Goodall, M. Ferrari, X. Liu, *Lab Chip* **2010**, *10*, 3074-3083.
- (144) C. S. Brazel, N. A. Peppas, *Eur J Pharm Biopharm* **2000**, *49*, 47-58.
- (145) Q. Wang, J. Wang, Q. Lu, M. S. Detamore, C. Berkland, *Biomaterials* **2010**, *31*, 4980-4986.
- (146) M. Tena-Solsona, C. Wanzke, B. Riess, A. R. Bausch, J. Boekhoven, *Nature Communications* **2018**, *9*, 2044.